STRUCTURAL ANALYSIS OF THE BENKAR FAULT ZONE, A CROSS STRUCTURE IN THE HIGHER HIMALAYA OF THE KHUMBU REGION, EASTERN NEPAL

by

Neil Jordan Seifert

A thesis submitted in partial fulfillment
of the requirements for the degree

of

Master of Science

in

Earth Sciences

MONTANA STATE UNIVERSITY
Bozeman, Montana

April 2019

©COPYRIGHT

by

Neil Jordan Seifert

2019

All Rights Reserved

ACKNOWLEDGEMENTS

I would like to thank Dr. Mary Hubbard as my supervisor for the direction of this project, long hours spent in the field teaching me structural geology and guiding me through the entire duration of this project. I am very grateful to have been your student and memories from Nepal and Bozeman will last me a lifetime. I would also like to acknowledge Dr. David Lageson, Dr. Drew Laskowski, and Dr. Madison Myers as my committee members and their continued help and fruitful discussions.

Dr. Colin Shaw generously shared his time at the Imaging and Chemical Analysis Laboratory at Montana State University, thus enabling me to perform EBSD imaging of quartz grains. Dr. Kip Hodges shared his lab at the Arizona State University and performed $^{40}Ar/^{39}Ar$ geochronology analysis.

I would like to thank Dr. Ananta Prasad Gajurel for his help as a Nepali collaborator and valuable time spent together in the field. In addition, I would like to thank Drs. John Cottle, Kyle Larson, Malay Mukul, Jean-Phillipe Avouac, Sudhir Rajaure, and Devon Orme for valuable discussions on cross structures and their role in the Himalaya. This project would not have been possible without the support of Mr. Jiban Ghimire and Shangri La Nepal Trek for assistance with logistics and Gopal Magar, Kumar Magar, and Sunit Sherpa for their support in the field.

This project was undertaken with financial support from the Geological Society of America, the Barry C. Bishop and Donald L. Smith Scholarships at Montana State University Earth Science Department, Graduate School Travel Award, College of Letters and Sciences Student Research Travel Grant, Rolf Seifert and Astrid Seifert-Moritsch.

TABLE OF CONTENTS

1. INTRODUCTION 1

2. TECTONIC SETTING 3

The Himalaya 3
Himalayan Cross Structures 6
The Khumbu Region 8
The Benkar Fault Zone 12

3. METHODS 13

4. RESULTS 15

Structural Geometry 15
Petrography 20
Lithology 20
Metamorphic Assemblage 26
Quartz Petrofabric 30
Structural Relationships 34
Kinematics 40
Quartz Crystallographic Fabrics 46
Geochronology, Thermochronology, and Thermobarometry 50

5. INTERPRETATION AND DISCUSSION 56

Interpretation 56
Tectonic Implications 59

6. FUTURE WORK 63

7. CONCLUSION 64

REFERENCES CITED 66

APPENDICES 77

APPENDIX A: Geochronologic, Thermochronologic, and Thermobarometric Map of the Khumbu Region 78
APPENDIX B: Geologic Map of the Khumbu Region and Benkar Fault Zone 81

TABLE OF CONTENTS CONTINUED

APPENDIX C: Petrographic and Microstructural Descriptions of Thin Sections.....84

LIST OF TABLES

Table Page

1. Key to mineral abbreviations used herein 21

2. $^{40}Ar/^{39}Ar$ ages of Greater Himalaya samples 52

LIST OF FIGURES

Figure Page

1. Geologic map of the Himalaya 5

2. Cross fault models 8

3. Field photographs showing foliation and lineation orientation 17

4. Summary of foliation and lineation measurements 19

5. Major lithologies in the Khumbu region 23

6. Metamorphic assemblage of the Greater Himalayan sequence 28

7. Photomicrographs of quartz petrofabrics 32

8. Map of quartz petrofabric regimes 33

9. Brittle faults cross-cutting metamorphic foliation 36

10. Crosscutting relationships within the Benkar Fault Zone 38

11. Kinematics within the Benkar Fault Zone 42

12. Tangent lineation diagram 45

13. EBSD maps and representative pole figures 48

ABSTRACT

The Himalaya are dominated by laterally continuous, range-parallel thrust faults and less frequent extensional structures such as the South Tibetan Detachment system. Recent discovery of range-perpendicular strike-slip and extensional fault zones (cross structures) in the Himalaya has raised questions regarding the significance of these structures in the collisional process. I have analyzed a newly-recognized cross structure in the Khumbu region of eastern Nepal, the Benkar Fault Zone. Structural mapping, petrographic observation, and analytical evidence reveals a zone of consistently NE-striking, SE-dipping metamorphic foliation from the villages of Phakding to Gorak Shep along the Dudh Kosi valley. Deformation within this zone is restricted to foliation-parallel, nonpenetrative, anastomosing sillimanite- and mica-bearing shear zones that wrap around poorly deformed quartz and feldspar enclaves. Kinematics of these shear zones from thin sections and outcrop observations are consistent with normal, right-lateral oblique slip and some local zones of purely extensional displacement. Quartz crystallographic fabric orientation suggests crystal plastic deformation under upper greenschist to lower amphibolite facies conditions. Outcrop observations show evidence for isolated brittle-ductile deformation, suggesting short-lived brittle events that punctuated a history of predominantly plastic deformation. Benkar Fault Zone fabric crosscuts older, thrust-related foliation and suggests that deformation within the zone postdates peak metamorphism and occurred while rocks were on the retrograde path. Crosscutting relationships between Benkar Fault Zone fabric and leucogranites constraints the timing of deformation to be younger than 20.5-21.3 Ma. The Benkar Fault Zone is interpreted to represent a tear fault within the Greater Himalayan sequence associated with differential displacement along a structurally deeper thrust.

INTRODUCTION

In the last 30 years, geologic research in the Himalayan collisional mountain belt has revealed strike-slip and extensional structures that occurred contemporaneous with compression. These fault systems have led geologists to new insight into the tectonic evolution of collisional mountain belts around the globe. The South Tibetan detachment system (STDS) was the first range-parallel extensional structure to be discovered (Burchfield and Royden, 1985; Burg et al., 1984; Caby, 1983). This discovery was followed by the mapping of widely distributed normal faults within the Tibetan Himalaya (Burchfiel et al., 1992; Burchfield and Royden, 1985). These structures, however, are not restricted to this region and have been discovered within the Lesser Himalaya (Steck et al., 1998), Greater Himalaya (Nakata, 1989), and Indus-Tsangpo suture zone (Guillot et al., 1997). The discovery of strike-slip faults within Tibet dates back to 1975 (Molnar and Tapponnier, 1975) and has played a major role in understanding the tectonic history of this region. Few strike-slip faults, however, have been recognized south of this region. The ongoing research of strike-slip and extensional structures within the Himalaya has shown that collisional mountain belts are complex systems not restricted to contractional tectonics.

Much of the discussion surrounding extension within the Himalaya has focused on structures related to north-south divergence, therefore, range parallel, east-west oriented faults and specifically, the STDS. Within Tibet the focus of extensional research has included the north-south graben systems (Molnar and Tapponnier, 1975; Ni and York, 1978). In the last two decades, the focus has started to include range perpendicular,

roughly north-south trending structures within the Himalaya with some structures relating to east-west extension (e.g. Bordet, 1971; Jessup et al., 2008b; Mukul et al., 2009; Thiede et al., 2006; Wu et al., 1998) and some to strike-slip displacements (e.g. Sahoo et al., 2000; Silver et al., 2015). These features are hereafter referred to as cross structures and include brittle faults and ductile shear zones.

While cross structures have been recognized in Tibet and in the Sub-Himalaya, there has only been recognition of one cross fault exposed in the Greater Himalaya, the Western Nepal Fault system, (Silver et al., 2015). I present structural mapping, field evidence, and analytical results of a regionally extensive cross structure that is a NE-striking, SE-dipping zone of brittle-ductile shear. This structure exhibits right-lateral and normal displacement. The deformation zone is located within the Greater Himalayan sequence, the highest-grade metamorphic rocks exposed within the range. This system of shear zones is herein referred to as the Benkar Fault Zone (BFZ). The BFZ is the first recognized cross fault in the Greater Himalaya of eastern Nepal. Therefore, understanding its role in the evolution of Himalayan tectonics is significant for advancing our knowledge in the region. Here I place the BFZ into broader context by explaining its role in the formation of the Himalayan range and comparing it to other cross structures that have been previously described. Comprehension of the role that cross structures play in Himalayan tectonics will help to decipher the complex geologic history of this mountain belt and advance our understanding of orogenic processes in general.

TECTONIC SETTING

The Himalaya

The main India-Eurasia collision initiated between 58-61 Ma (DeCelles et al., 2014; Ding et al., 2005; Hu et al., 2016; Orme et al., 2015). The present structural framework of the Himalaya is the result of approximately 2900 ± 600 km of convergence (Dupont-Nivet et al., 2010) and the subsequent imbrication and deformation of the Indian plate. This continuous process of deformation, controlled by the underthrusting of the Indian plate underneath Eurasia, has exposed the former sedimentary wedge of the Indian plate and its basement as the exhumed metamorphic rocks of the Himalayan orogen. Rocks within the Himalaya are generally subdivided into four major lithotectonic units (Figure 1). It is important, however, to understand the synchronicity and continuity of events that lead to the present structural makeup of the Himalayan orogen and not to regard any of these four units as stand-alone systems.

The four lithotectonic units are described from south to north: (1) The Subhimalaya is located geographically furthest south (Figure 1). It represents the deformed foreland basin of the orogen and is separated from sedimentary deposits of the Indo-Gangetic Plain, encompassing the northern regions of the Indian subcontinent, by the youngest and most foreland-ward thrust; the Main Frontal thrust (Gansser, 1964). (2) The Lesser Himalayan sequence was emplaced above Subhimalayan rocks along the Main Boundary thrust and consist of middle Proterozoic metasedimentary rocks, typically greenschist to amphibolite facies (Figure 1; Brasier and Singh, 1987; Brookfield, 1993; Gansser, 1964).

The Lesser Himalayan sequence is bound by the Main Central thrust (MCT) to the north which separates it from the Greater Himalayan sequence (Figure 1; Gansser, 1964). (3) The Greater Himalayan sequence consists of late Proterozoic to Paleozoic metasediments, granites, gneisses, volcanic rocks, amphibolites and calcareous rocks, typically upper amphibolite facies to lower granulite facies (Le Fort, 1994). (4) The Tethyan Himalayan sequence, located in southern Tibet, consists of late Precambrian to lower Paleozoic sedimentary and metasedimentary rocks (Figure 1; Gaetani and Garzanti, 1991). These rocks were juxtaposed against the high-grade metamorphic rocks of the Greater Himalayan sequence along a series of normal faults as part of the STDS (Burg et al., 1984; Caby, 1983).

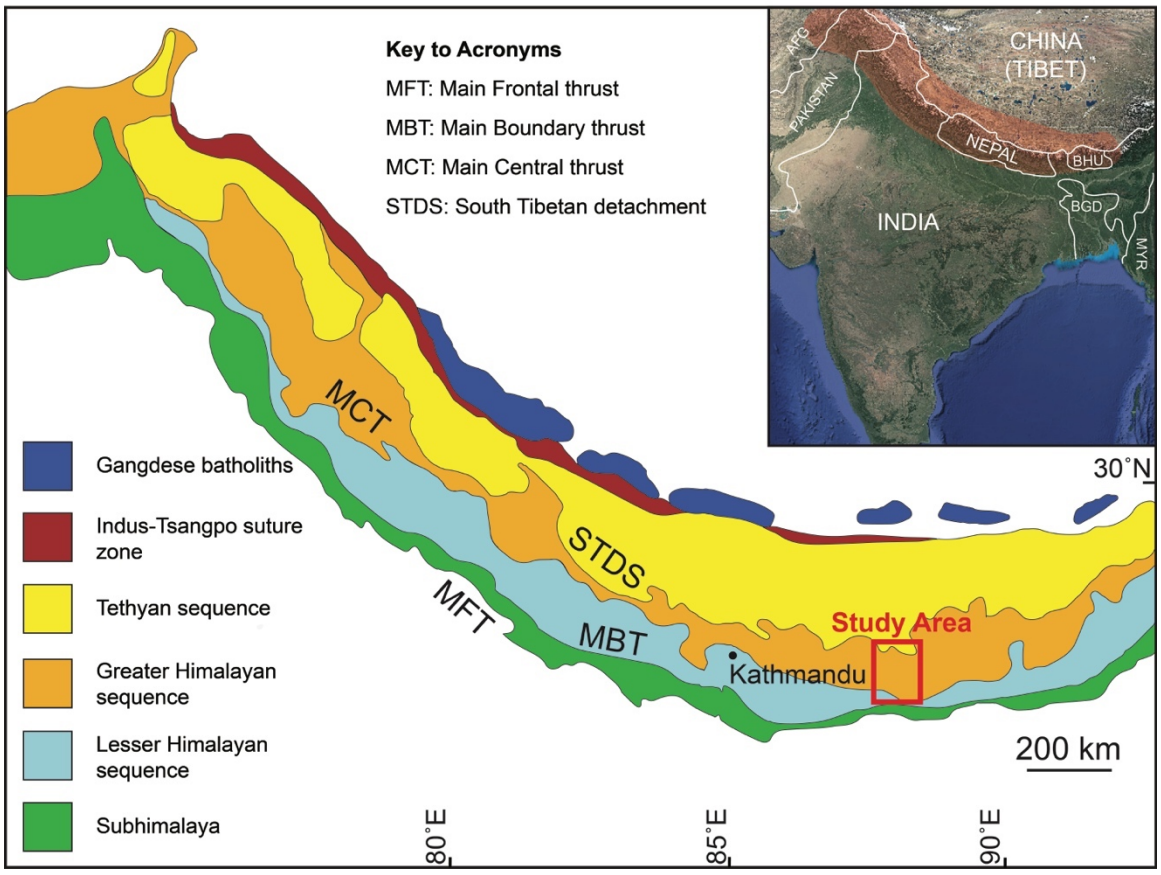


Figure 1. Geologic map of the Himalaya. Modified from Najman et al. (2017). Inset: map location shaded in red. Abbreviations: AFG = Afghanistan; BHU = Bhutan; BGD = Bangladesh; MYR = Myanmar.

The Tethyan Himalayan sequence is separated from what was formerly the Eurasian plate by the Great Counter thrust, located along the Indus-Tsangpo suture zone (Yin et al., 1999). Structurally, all major thrusts and the STDS are broadly parallel north-dipping faults and are thought to merge with the Main Himalayan thrust at depth, the basal décollement of the orogen (Gansser, 1964). These major fault systems are impressively consistent throughout the orogen and can be traced ~2,000 km along strike (Gansser, 1964).

Tectonic models for the emplacement of rocks within the Himalaya during convergence have continuously evolved over the past 50 years and are currently still debated. One major unresolved discussion is whether the high grade rocks of the Greater Himalaya have been extruded southward along a midcrustal channel (Beaumont et al., 2004; Godin et al., 2006) or emplaced through in-sequence thrusting related to the expanding foreland thrust wedge, referred to as critical taper model (Kohn, 2008). More recently, a combined model has become popular (Larson et al., 2010). Although the mechanism for emplacement is still up for debate, the Greater Himalaya exposes a sequence of rocks that have undergone metamorphism, deformation, anatexis, and intrusion. This location is therefore an ideal natural laboratory to study continental collisional processes.

Himalayan Cross Structures

Much of the discussion surrounding the structural geology of the Himalaya has focused on thrust faults, the extensional and strike-slip faults of Tibet, which are related to both north-south extension (e.g. STDS) and east-west extension (e.g. graben systems of Tibet). Recent studies have led to the discovery of cross faults in southern Tibet, the Greater Himalaya, and Lesser Himalaya, which are strike-slip and extensional faults and that are highly oblique/perpendicular to the strike of the major thrusts and STDS. The following is a summary of cross structures contained within these lithotectonic units: Previous workers have discussed the significance of the Kosi, Gish (Mukul, 2010; Mukul et al., 2018; Mukul et al., 2009), and Yadong faults (Wu et al., 1998) in the region of

Sikkim and Bhutan. In the central and western Himalaya, the bounding faults of the Thakkhola graben (Bordet, 1971; Colchen et al., 1980; Hagen, 1968; Hurtado Jr et al., 2001), Leo Pargil dome (Thiede et al., 2006), and Ama Drime Massif (Burchfiel et al., 1992; Jessup et al., 2008b) have been documented as extensional structures that are also orthogonal to the range. Further west, the Western Nepal Fault System (Silver et al., 2015) and the Ganga and Yamuna tear faults (Sahoo et al., 2000) are examples of young or possibly active, strike-slip faults that cut obliquely across the range. Cross structures have been interpreted to represent tear faults (Figure 2A; Hurtado Jr et al., 2001; Sahoo et al., 2000), lateral ramps (Figure 2B; Wu et al., 1998), or have been formed by seismic partitioning (Mukul et al., 2018), oblique convergence (Silver et al., 2015), orogen-parallel extension (Figure 2C; Jessup et al., 2008b; Thiede et al., 2006), or NE-striking basement structures (Godin and Harris, 2014). Although recent work (e.g. Bordet, 1971; Jessup et al., 2008b; Mukul et al., 2009; Sahoo et al., 2000; Silver et al., 2015; Thiede et al., 2006; Wu et al., 1998) has focused on the individual tectonic implications of cross faults, their overall significance and role in the mountain building process of the Himalaya remains largely unexplored.

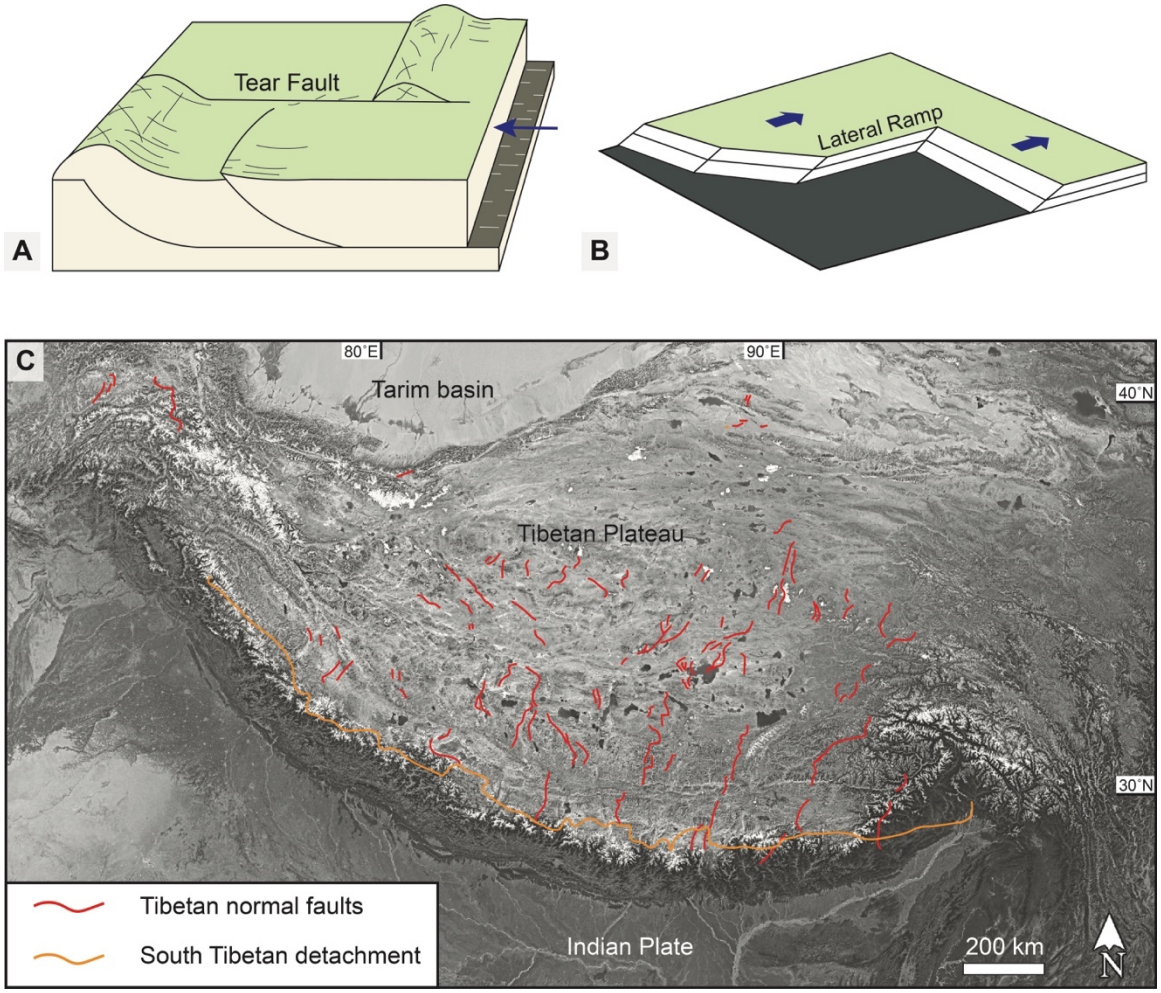


Figure 2. Graphic representation of potential models for cross faults. (A) Schematic representation of a tear fault. Modified from Fossen (2016). Arrow is pointing in the direction of thrust fault propagation. (B) Schematic representation of a lateral ramp. Modified from Fossen (2016). The hangingwall has been removed for clarity. Arrows are pointing in the direction of thrust fault propagation. (C) Map showing NS-trending normal faults of the Tibetan Plateau and extent of the South Tibetan detachment system. Modified from Jessup (2013). Orogen-parallel extension could lead to Tibetan normal faults extending southwards into the Greater Himalaya.

The Khumbu Region

The Khumbu region of the Himalaya (Appendix A) is located in eastern Nepal, south of Mt. Everest and includes the Dudh Khosi and Imja Khola river valleys. The

geology of the Khumbu region is dominated by the Greater Himalayan sequence, which is bound by the STDS above and MCT below. The MCT is located ~7 km south of the village of Lukla and is a 3- to 5-km-thick, north-dipping shear zone composed of augen gneiss, banded biotite gneiss, amphibolite, slate, phyllite, quartzite, talc-schist, pelitic-schist, and calc-silicates with a top-to-the-south sense of shear (Hubbard, 1988). The base of the MCT is a contact between augen gneiss and chlorite-muscovite schist of the Lesser Himalayan sequence, whereas the top of the shear zone is found within less deformed biotite gneiss (Barun gneiss) of the Greater Himalayan sequence (Hubbard, 1988). Peak metamorphic temperatures show an increasing trend from ~460 to 650 ˚C from the base of the MCT to the core of the Greater Himalayan sequence, respectively, therefore representing an inverted thermal sequence (Hubbard, 1989; Searle et al., 2003; Simpson, 2002). Geobarometric calculations yield pressure estimates across the shear zone from ~6 to 8 kbar (Hubbard, 1989; Searle et al., 2003; Simpson, 2002). Timing of MCT movement in the Khumbu was first constrained by Hubbard and Harrison (1989) to ~21 Ma based on $^{40}Ar/^{39}Ar$ thermochronology of hornblende. This timing is a constraint on the initiation of movement along the MCT. With the advent of improved geochronologic techniques Catlos et al. (2002) used in situ ion microprobe Th-Pb analyses of monazite to suggest that MCT deformation and metamorphism was active as early as 14.5 ± 0.1 Ma. A sample collected beneath the MCT in the Garhwal region yields an age of 5.9 ± 0.2 Ma from in situ ion microprobe Th-Pb analyses of monazite grains, which suggests MCT movement continued into the Late Miocene (Catlos et al., 2002).

The Greater Himalayan sequence in the Khumbu region is a 15- to 20-km-thick sequence of sillimanite-grade metasedimentary rocks, variably migmatized orthogneiss, and leucogranite (Hubbard, 1988; Searle et al., 2006; Searle et al., 2003) (Appendix A). It is generally mapped as one continuous, undivided unit due to the difficulty in detailed lithologic and structural mapping. This approach allows for an easier interpretation of the tectonic evolution of the area, however, it misses the intricate small-scale structures within the Greater Himalayan sequence that could prove essential in advancing our understanding of the structural evolution of the Khumbu region. Thus far, workers have agreed on two episodes of metamorphism within the Greater Himalayan rocks of the Khumbu region, which produced an earlier (S1) fabric that was overprinted by a dominant (S2) fabric (Jessup et al., 2006). For instance, Jessup et al. (2006) report an outcrop on the lower section of the Nuptse-Lhotse wall that shows isoclinal folds representing S1 foliation with an orientation of N15E,35NW and isoclinal folds that were refolded to produce the S2 foliation with orientation of N50W,64NE. The first Eohimalayan metamorphic event is associated with prograde metamorphism during crustal thickening and has been constrained between 38.9 ± 0.9 and 32.2 ± 0.4 Ma (Cottle et al., 2009; Searle et al., 2003). P-T conditions of this metamorphic event are estimated to be between 550-680 ˚C and 8-10 kbar (Pognante and Benna, 1993; Searle et al., 2003). The second Neohimalayan metamorphic event is associated with migmatization and leucogranite emplacement and has been constrained between 28.0 ± 1.2 and 22.7 ± 0.2 Ma (Cottle et al., 2009; Simpson et al., 2000). P-T conditions are estimated between 650-750 ˚C and ~3 kbar (Jessup et al., 2008a; Pognante and Benna, 1993; Searle et al., 2003;

Simpson et al., 2000). Available geochronologic, thermochronologic and thermobarometric data for the Greater Himalayan sequence of the Khumbu region has been summarized in Appendix A.

The STDS of the Khumbu region is exposed on the Mount Everest massif (Appendix A) and has been recognized as two distinct-north dipping detachments: a top-down-to-the-northeast ductile shear zone, referred to as the Lhotse shear zone (Carosi et al., 1998; Lombardo et al., 1993; Searle, 1999; Searle et al., 2003) and a structurally higher brittle Qomolangma detachment (Searle, 1999; Searle et al., 2003). The Lhotse shear zone represents a distinct contact between upper amphibolite facies sillimanite gneiss and leucogranite of the Greater Himalayan sequence and middle- to upper-greenschist-facies schist and calcsilicates of the Everest series (Searle, 1999). The Qomolangma detachment on the other hand separates the Yellow Band, predominantly calcsilicates, of the Everest series from the Qomolangma Formation, made up of Tethyan limestone (Searle, 1999). Geothermobarometric data for the deformational temperatures of the STDS in the Khumbu region are sparse due to the lack of garnet bearing assemblages. Deformation is estimated at 630 ˚C and 4.6 kbar (Hodges et al., 1992), from a garnet-bearing sample collected in the Rongbuk Valley, north of Mount Everest. This data is supplemented with quartz c-axis fabric opening angles that suggest a deformational temperature of 450˚C at 10-20 m below the Qomolangma detachment, up to 625 ˚C at ~600 m below the Lhotse shear zone (Law et al., 2004). Although geobarometric estimates have been limited, timing constraints for the movement along the STDS are available through several geochronological investigations (Murphy and

Mark Harrison, 1999; Searle et al., 2003; Searle et al., 2002). It has been estimated most precisely by Cottle et al. (2015) through U/Th-Pb systems of leucogranite samples, constraining the ductile shearing of the Lhotse Shear zone at 16.4-15.6 Ma, and the brittle faulting of the Qomolangma detachment to be younger than 15.4 Ma. Movement along the MCT and STDS are coeval in the Khumbu region.

The Benkar Fault Zone

This project originated from an investigation of satellite imagery of the Khumbu region. Dr. Mary Hubbard identified a NE-striking topographic lineament between the towns of Benkar and Namche Bazar (Appendix A). In between the two villages, NE-trending topographic features resemble fault scarps. I undertook a preliminary field season in December 2017 in order to investigate this topographic lineament and found that this feature is an expression of shear fabric. Between Benkar and Namche Bazar, this fabric is NE-striking and SE-dipping and locally has a shallow SE-plunging lineation. Preliminary field work suggested that this fabric orientation extends northward as well as southward from this area. These original observations prompted further investigation and detailed structural mapping in order to properly identify the Benkar Fault Zone and to identify if it represents a cross structure.

METHODS

Fieldwork was undertaken in December 2017 and May 2018 with a total of 35 days spent in the field. Refer to Appendix B for locations of samples collected in the field and Appendix C for exact GPS coordinates sample locations. Structural and lithologic mapping is shown in the geologic map of Appendix B. Structural measurements were taken primarily with a Brunton compass and supplementary data was collected using the application FieldMove on a hand-held iPad. Field photographs herein commonly use a lens cap for scale which has a diameter of 67 mm. 38 samples were collected for petrologic evaluation, which were cut normal to the foliation and parallel to the lineation for petrographic study. Descriptions of metamorphic fabric, petrography, structural relationships and kinematics are reported from thin sections and field observations, found in Appendix C. Photomicrographs of all thin sections include sample name and sample location and are taken under cross polarized light, unless specified otherwise. Stereonet contour, line, and point plots of foliation and lineation measurements of samples and outcrops are presented in lower hemisphere, equal area projections using the Stereonet (v10.0) software package of R. Allmendinger.

Quartz lattice-preferred orientations were measured on a scanning electron microscope Zeiss SUPRA 55VP by electron backscatter diffraction (EBSD) techniques at the Montana State University Imaging and Chemical Analysis Laboratory. Rock sample billets were cut normal to the foliation and parallel to the lineation, with a diameter no larger than 27 x 46 mm. In order to capture quality diffraction patterns, samples were ground through a sequence of 125, 52, 22, 10, and 5-μm SiC grid paper and cumulated

using 6-μm Dia-grid paper. Sample billets were then fine-polished in four stages using 6, 3 and 1 -μm diamond suspension polish for 6 min each, and 0.05 μm colloidal silica suspension polish for 8 hours. In order to avoid charging effects in the SEM samples were coated with strips of carbon. EBSD images of the entire billet were acquired at an accelerating voltage of 15 kV, a working distance of 40 mm, and using a step size of 1.25 μm for sample 17N3a and 2.0 μm for sample 18N8f. Using the SEM, crystal orientation is determined by comparing Kikuchi band patterns with simulated pre-defined crystallographic structure. The EBSD output consists of an orientation contrast map which assigns a different color to the measured crystal orientation. Data was reduced by only displaying quartz grains that had a mean diameter of at least four times the grid spacing and applying a noise reduction to reduce wild spikes and systematic misindexing.

$^{40}Ar/^{39}Ar$ dating of muscovite (for samples 18N10a, 18N5d, and 18N11e) is being carried out at the Noble Gas Geochronology and Geochemistry Laboratories at Arizona State University in Tempe, Arizona. This work is ongoing, and results have not been obtained and are not presented here. I rely instead on the geochronologic, thermochronologic, and thermobarometric results presented in Hubbard (1989); Hubbard and Harrison (1989), Simpson et al. (2000), Catlos et al. (2002), Searle et al. (2003), and Jessup et al. (2008a) to determine the age, thermal and pressure history of the rocks within the BFZ in an effort to constrain the timing of deformation.

RESULTS

Structural Geometry

I present a map of the NE-striking shear fabric within the Khumbu region from the village of Phakding in the Dudh Kosi valley to Gorak Shep along the Khumbu glacier (Appendix B). This area is dominated by a zone of NE-striking, SE-dipping foliation (Figure 3A), referred herein to as the BFZ. The BFZ shows a sharp contact with adjacent foliation, which is generally EW-striking and N-dipping, or flat lying (Figure 3B). The lateral extent and width of the BFZ has been verified predominantly by the presence of this NE-striking, SE-dipping fabric (Figure 3E). Where exposure is poor or difficult to attain its extent has been inferred from field photographs and satellite imagery. It is important to recognize that the proposed outline for the BFZ presented here is an approximation of its full location. To the north, in the Khumbu glacier area, the zone has a topographic expression of approximately 11 km in width (Appendix B). To the south, between the villages of Phakding and Namche the zone narrows to a topographic width of 1-2 km (Appendix B). The NS-extent of the BFZ has been mapped along a distance of approximately 30 km. Its full extent remains to be explored.

Foliation measurements for the BFZ are summarized in Figure 4A using poles to planes, Kamb contours, and mean vectors on lower hemisphere equal area plots. The mean orientation of foliation in the northern part of the zone has a strike of N37E and a dip of 43SE (Figure 4A-1). The central part is characterized by a mean foliation striking N27E and dipping 42SE (Figure 4A-2). The southern part of the zone shows a mean

foliation striking N12W and dipping 40NE (Figure 4A-3). BFZ fabric is consistently NE-striking, SE-dipping in the northern part of the zone and becomes more isolated and irregular in the southern extent of the BFZ around the village of Benkar (Appendix B) with strikes locally trending NW.

Lineation in the BFZ is predominantly recognized as a ductile mineral stretching lineation (Figure 3C). Some foliation planes are exposed as slickenside-like surfaces and show striations (Figure 3D). These striations are commonly defined by a preferred orientation of elongated sillimanite minerals. In these cases, they are referred to as mineral lineation. There are two distinct groups of lineations, plunging SW and NE respectively (Figure 4C).

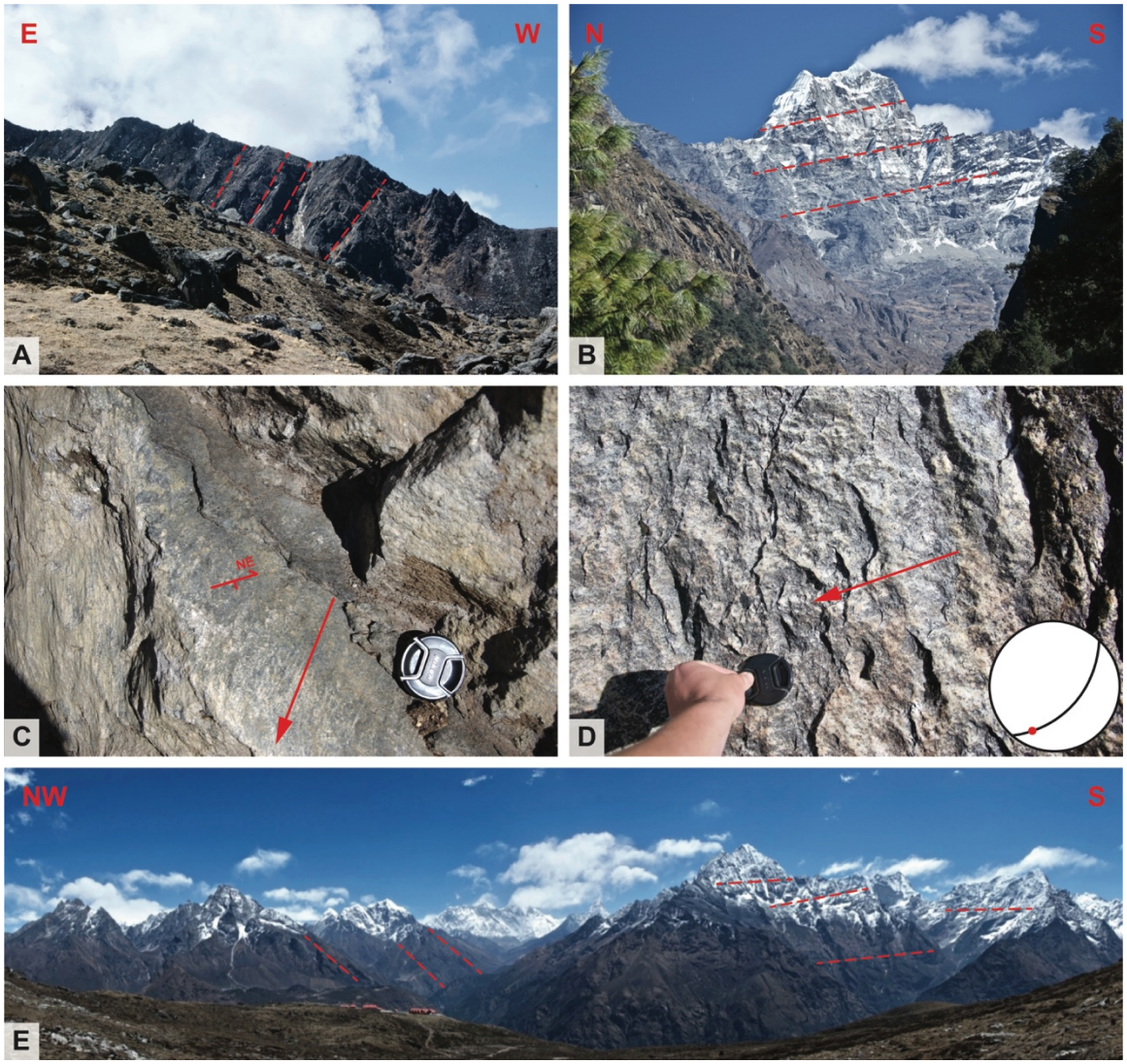


Figure 3. Field photographs showing foliation and lineation orientation. (A) View looking south from Gokyo valley at a flank of Taboche, showing SE-dipping shear fabric. Dashed lines represent trace of foliation planes. Approximate location of photograph: 27˚55'10.26"N, 86˚43'19.60"E. (B) View looking east towards Thamserku from the village of Benkar showing shallow, N-dipping shear fabric that is outside of the BFZ. Dashed lines represent trace of foliation planes. Approximate location of photograph: 27˚46'16.14"N, 86˚43'29.24". (C) Outcrop photo of SW-plunging stretching lineation on NE striking surface at sample location 9. Red arrow is indicating orientation of mineral stretching lineation. Approximate location of photograph: 27˚50'46.31"N, 86˚45'43.91E. (D) Outcrop photograph showing slickenside striations with a mineral lineation defined by sillimanite. Stepped slickenside indicates right-lateral sense of shear. Foliation and lineation are displayed in a lower hemisphere, equal area plot. Red arrow is indicating orientation of mineral lineation near sample location 38. Approximate location of photograph: 27˚57'30.33"N, 86˚45'31.72E. (E) Panorama looking northeast from the

Kongde Ri hotel towards the Everest Massif in the center of the image. Dashed lines indicate approximate trace of foliation planes, showing relationship of NE-striking, SE-dipping fabric and near flat-lying, EW-striking fabric. Approximate location of photograph: 27˚46’39.61”N, 86˚41’55.14”E.

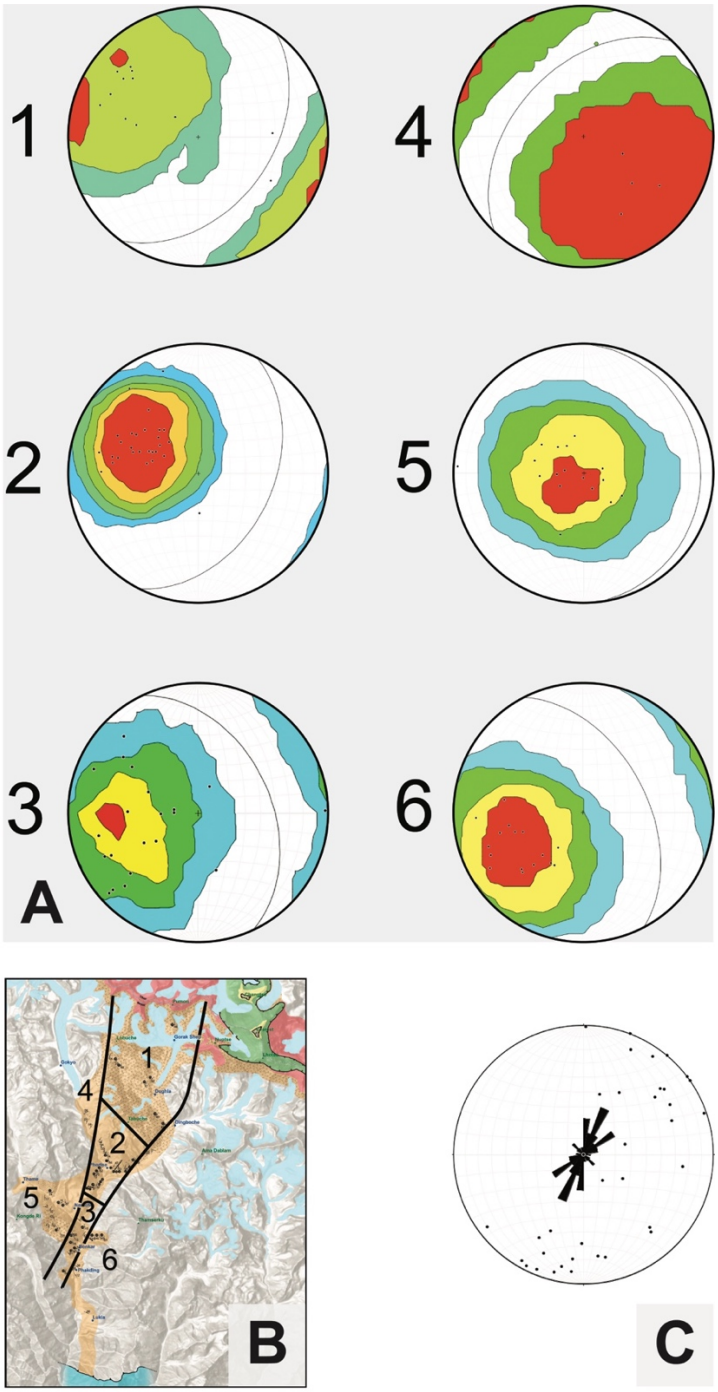


Figure 4. Summary of foliation and lineation measurements taken in the field. (A) Kamb contoured poles to planes and mean vector of metamorphic foliation. Portrayed on lower hemisphere, equal area plots. Plots 1, 2, and 3 are within the BFZ. (B) Map showing where foliation measurements in A were collected. (C) Lower hemisphere, equal area stereonet with rose diagram portraying lineation measurements of rock samples collected in the field.

Petrography

Lithology:

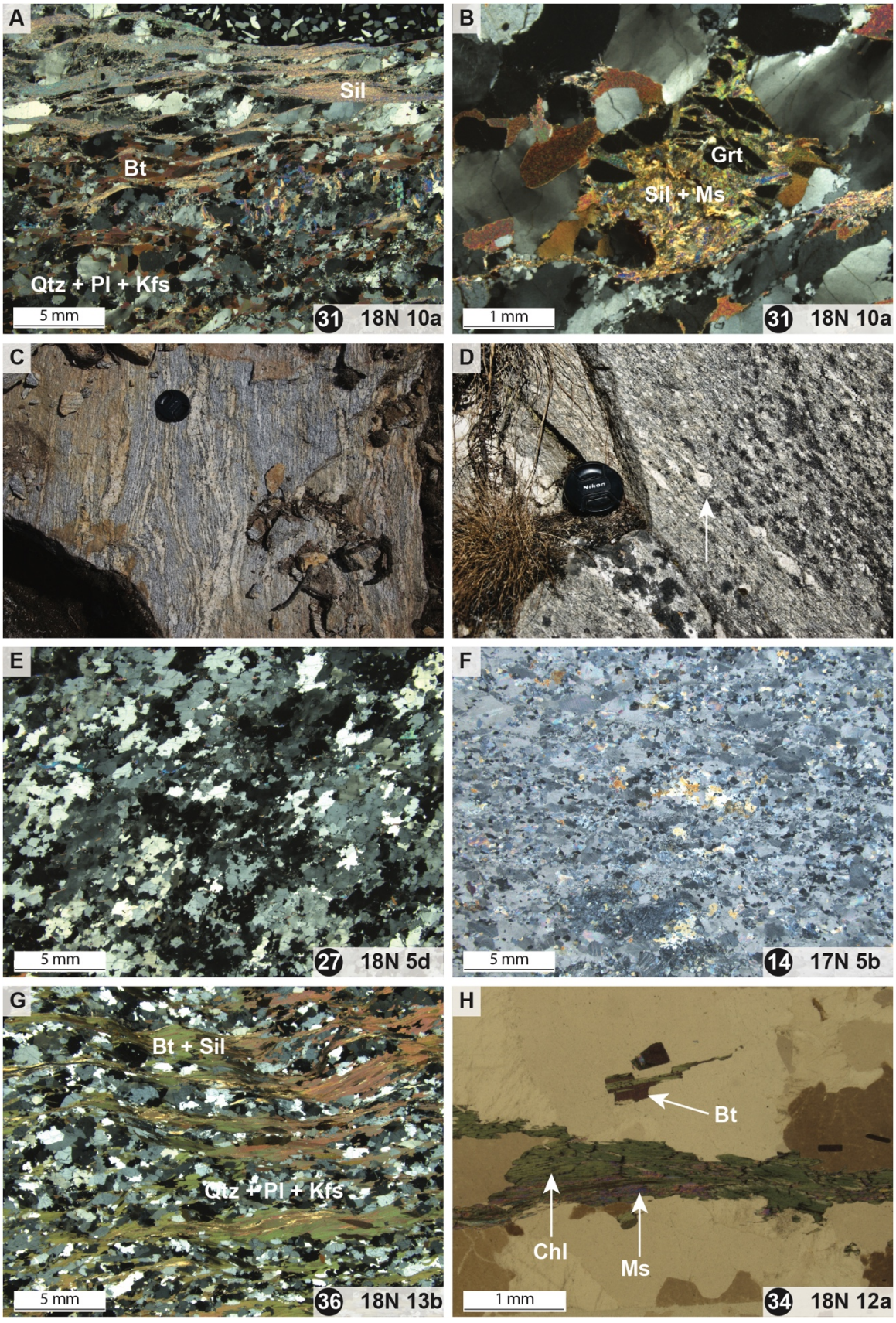
To determine the makeup of the BFZ and to determine variation in lithologies within and across the zone, I have mapped the major lithologies within the BFZ and surrounding areas. The resultant geologic map in Appendix B provides structural fabric measurements, but overall the map is a simplification of the true complexity of lithologic variability of these high-grade metamorphic rocks. The lithology of the Greater Himalayan sequence in the Khumbu area from Phakding to Gorak Shep varies surprisingly little and is commonly mapped as a continuous unit of sillimanite gneiss (Hubbard, 1988; Jessup et al., 2008a; Searle et al., 2003). Difficulty in attaining consistent exposure throughout the area, due to the rugged terrain and high elevation, make it difficult to map individual rock units. The following is a detailed petrographic description of the major lithologies within the BFZ. Mineral abbreviations used herein after Siivola and Schmid (2007) and are summarized in Table 1.

Abbreviation	Mineral
Qtz	quartz
Pl	plagioclase
Kfs	K-feldspar
Bt	biotite
Grt	garnet
Sil	sillimanite
Ms	muscovite
Crd	cordierite
Chl	chlorite
Wmca	white mica
Cal	calcite
Hbl	hornblende
Tur	tourmaline
Hyp	hypersthene
St	staurolite

Table 1. Key to mineral abbreviations used herein. After Siivola and Schmid (2007).

Structurally above the MCT lies a unit of quartzofeldspathic gneiss which is often referred to as Namche orthogneiss, Namche migmatites, or Namche augen gneiss (Bordet, 1961; Hubbard, 1988; Searle et al., 2003). The assemblage generally consists of: Qtz + Pl + Kfs + Bt ± Grt ± Sil ± Ms ± Crd (Figure 5A). This quartzofeldspathic gneiss is migmatitic in some outcrops and shows stromatic texture and banded leucosomes (Figure 5C). Some outcrops show beautiful augen gneiss texture (Figure 5D). This unit varies gradationally between migmatite and augen gneiss, therefore I refer to this lithology as quartzofeldspathic gneiss. The quartzofeldspathic gneiss generally exhibits an equigranular texture of course grained, subhedral crystals with embayed grain boundaries. Enclaves and layers consisting of Bt ± Sil ± Ms surrounded by Qtz + Pl + Kfs is common. These layers are generally sheared, whereas the surrounding Qtz + Pl + Kfs

is less deformed, indicating an apparent strain variation. Quartz grain size has been reduced in some thin sections and some exhibit myrmekitic intergrowth of quartz and feldspar. Sillimanite is fibrolitic and garnets are typically anhedral and have been fractures and replaced (Figure 5B).


A
Sil
Bt
Qtz + Pl + Kfs
5 mm
31 18N 10a
B
Grt
Sil + Ms
1 mm
31 18N 10a
C
D
E
5 mm
27 18N 5d
F
5 mm
14 17N 5b
G
Bt + Sil
Qtz + Pl + Kfs
5 mm
36 18N 13b
H
Bt
Chl
Ms
1 mm
34 18N 12a

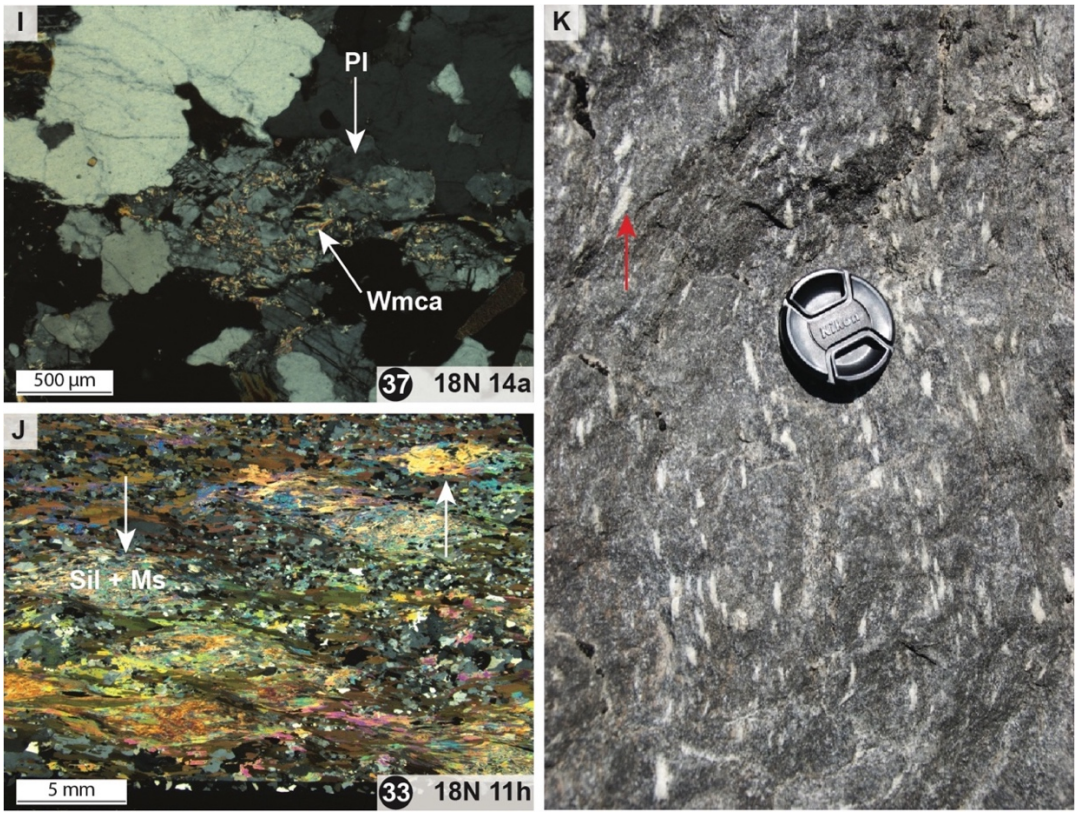


Figure 5. Photomicrographs and outcrop photos of the major lithologies in the Khumbu region. Photomicrographs include sample name and sample location. Refer to Appendix B for sample locations and Appendix C for exact GPS coordinates. (A) Photomicrograph of a quartzofeldspathic gneiss. Thin section shows strain variation between Bt + Sil layers and surrounding Qtz + Pl + Kfs layers. (B) Anhedral garnet that has been fractured and replaced by sillimanite and muscovite. (C) Outcrop photo showing stromatic texture and banded leucosomes of a quartzofeldspathic gneiss near the village of Namche Bazar. Approximate location of photograph: 27˚48’38.83”N, 86˚41’52.56”E. (D) Outcrop photo showing an example of augen gneiss (Namche augen gneiss) near the village of Phortse. Arrow points to a large augen. Approximate location of photograph: 27˚50’46.02”N, 86˚46’11.09”E. (E) Photomicrograph of a quartzite. Foliation is difficult to discern in thin section. Quartz grains show undulatory extinction and subgrains. (F) Photomicrograph of a calc-silicate. (G) Photomicrograph of a biotite gneiss. Biotite and sillimanite are arranged into thicker units and show more strain compared to the quartz, plagioclase, and K-feldspar layers. A strong strain variation is visible. (H) Photomicrograph of a biotite gneiss under plane polarized light. Thin section shows secondary mineral alteration of chlorite. (I) Photomicrograph of a biotite gneiss. Sericitic alteration of plagioclase feldspar into a fine-grained white mica. (J) Photomicrograph of a biotite gneiss. Arrows point to fibrolitic sillimanite occurring in symmetrical clasts oriented along the foliation plane. (K) Outcrop photo of fibrolitic sillimanite clasts. Arrow is pointing to one of the clasts. Near sample location 38. Approximate location of photograph: 27˚57’30.33”N, 86˚45’31.72E.

Quartzite occurs intermittently surrounding the area of Namche Bazar with a large outcrop east of Thame. The assemblage is generally: Qtz + Pl + Kfs + Bt + Ms ± Sil (Figure 5E). Embayed grain boundaries are common and quartz grains are irregular showing undulatory extinction and subgrains. K-feldspar grains are commonly sericitized. Small outcrops of calc-silicate rock occur east of Phortse. The mineralogy consists of: Qtz + Pl + Kfs + Cal ± Ms ± Sil (Figure 5F).

In the central Khumbu there is a greater percentage of biotite gneiss. The assemblage is generally: Qtz + Pl + Kfs + Bt ± Sil ± Ms ± Chl ± Hbl ± Grt ± Crd (Figure 5G). Garnet is less common in the northern part of the Khumbu, but fibrolitic sillimanite occurs in various percentages and chlorite is present as a secondary alteration mineral (Figure 5H). The biotite gneiss shows a stronger strain variation compared to the quartzofeldspathic gneiss with thicker layers and enclaves of Bt ± Ms ± Sil. Quartz grain size has been reduced in some thins section with myrmekite present and k-feldspars grains are sericitized in many samples (Figure 5I). Modal percentage, especially the amount of biotite and sillimanite, varies throughout this lithologic unit from biotite schist to leucocratic gneiss.

The biotite gneisses have been intruded by leucogranite sills and dykes at the highest structural level below the STDS. Significant volumes of leucogranitic rock are observed around the village of Phortse and become more common in the area surrounding the Khumbu glacier on the flanks of Tabuche, Lobuche, Ama Dablam, and the Everest Massif (Appendix B). The largest intrusive body is visible on the south face of Nuptse, though a significant amount of leucogranite is exposed on the southwest side

of Taboche. Leucogranite mineralogy is reported to be Qtz + Pl + Kfs + Bt + Ms + Tur (Hubbard, 1988).

In the northern Khumbu, near the village of Dughla, fibrolitic sillimanite commonly occurs in symmetrical clasts the size of approximately 6 mm by 2 mm (Figure 5J). In outcrop these clasts are lighter grey in color embedded in a darker biotite rich matrix (Figure 5K). They occur along the foliation plane and show a preferred orientation along the lineation. Biotite and muscovite are commonly dragged into these sillimanite clasts and an apparent strain variation is visible between Sil ± Bt ± Ms and the surrounding Qtz ± Pl ± Kfs grains. Although amphibolites (hornblende-bearing) have been reported to occur in the upper part of the Khumbu valley around Gokyo (Hubbard, 1988), this lithology was not observed in the BFZ and adjacent areas.

Metamorphic Assemblage

Metamorphic assemblages and petrological textures are discussed to give insight into possible variations in pressure and temperature conditions of metamorphism across or along the BFZ. Samples from the Greater Himalayan sequence in the Khumbu region generally show cuspate-lobate grain boundaries between quartz and feldspar suggesting high-grade metamorphic conditions (Passchier and Trouw, 2005) and the presence of sillimanite suggests upper amphibolite to lower granulite phases metamorphism of > 500 ˚C. Quartzofeldspathic gneiss samples commonly contain the metamorphic assemblage of: Qtz + Pl + Kfs + Bt ± Grt ± Sil ± Ms ± Crd. The presence of coexisting Grt + Sil + Crd + Qtz suggests a limited P-T range over which these minerals can occur in equilibrium (Hensen and Green, 1973). For instance, Hensen and Green (1973) have

shown, through experimental studies, that the $Mg/Mg + Fe^{2+}$ ratio of the coexisting cordierite and garnet phases are determined by pressure and temperature. The reactions of:

$$Crd = Grt + Sil + Qtz \text{ and} \quad (1)$$

$$Crd + Hyp = Grt + Qtz \quad (2)$$

are used to obtain a pressure-temperature estimate of 700-850 ˚C and 5-10 kbar for this system. Comparing geothermobarometric results from previous researchers (Appendix A) suggests that these experimental values might either be a slight overestimate, that vapor-absent partial melting might contribute to the lower values provided by other researchers or suggests that re-equilibrium occurred at lower temperature and pressure conditions.

Several prograde metamorphic reactions are evident within rocks of the Greater Himalayan sequence in the Khumbu region. Anhedral garnet poikiloblasts with a diameter of 2-3 mm contain abundant inclusions of biotite, plagioclase, quartz, and less commonly sillimanite (Figure 6A). Biotite commonly wraps around the garnets. Pressure shadows around some garnets suggest pre- or syn-tectonic garnet growth (Figure 6B). Most grains are highly replaced and only remnant grains remain. This assemblage and the fact that muscovite and staurolite occur at lower grade than these samples (not present in collected samples), suggests that they formed through a prograde reaction such as:

$$Ms + St + Qtz = Sil + Bt + Grt + H_2O \quad (3)$$

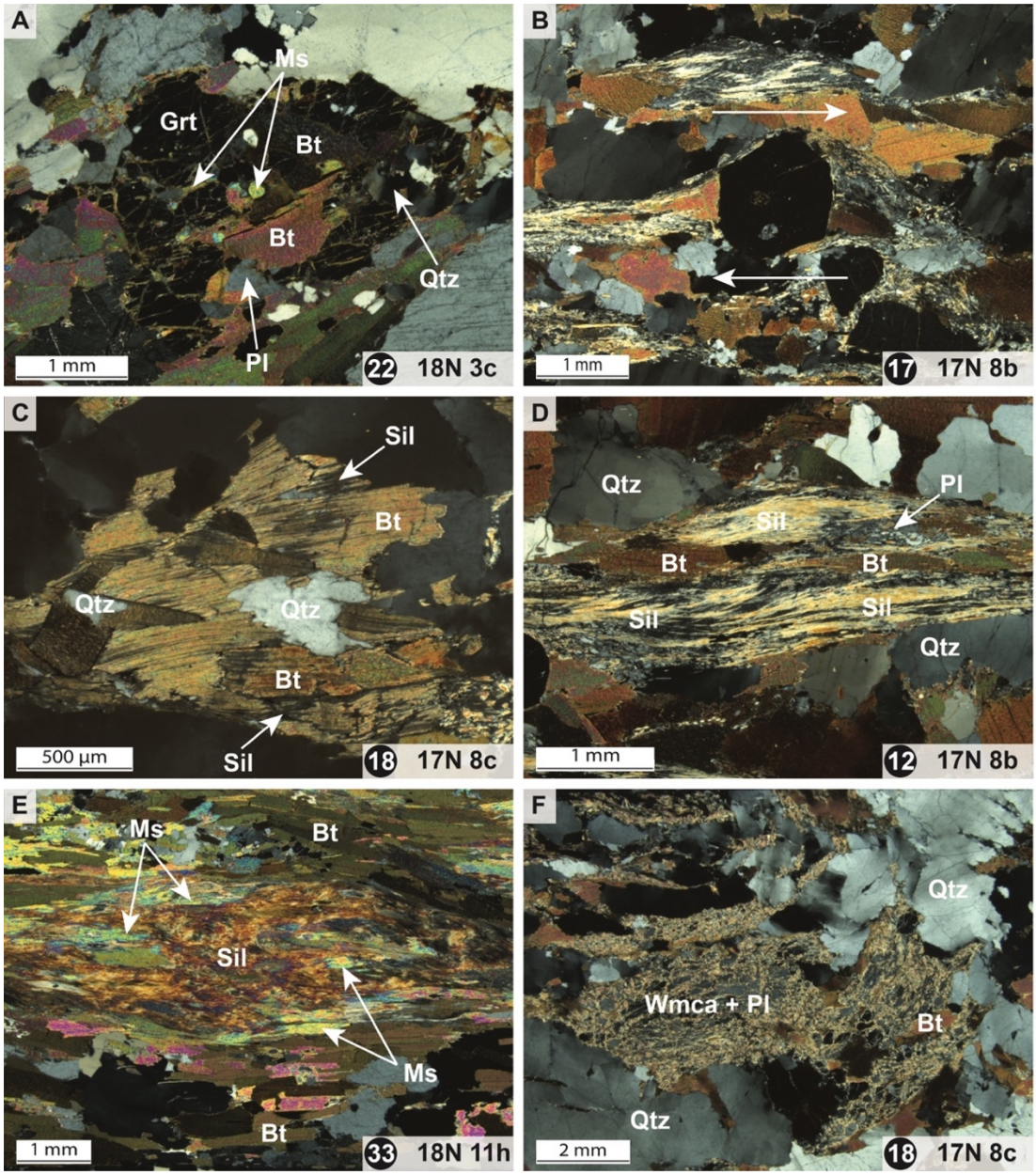


Figure 6. Photomicrographs of mineral relationships giving important insight into the metamorphic assemblage of the Greater Himalayan sequence in the Khumbu region. Photomicrographs include sample name and sample location. Refer to Appendix B for sample locations and Appendix C for exact GPS coordinates. (A) Garnet poikiloblasts with inclusions of muscovite, biotite, plagioclase, and quartz. (B) Rotated garnet porphyroblast with strain shadows indicating top-to-the right sense of shear and pre- or syn-tectonic garnet growth. (C) Fibrolitic sillimanite growing along biotite margins. (D) Fibrolitic sillimanite growing along biotite and feldspar margins. Biotite and sillimanite layers are clearly sheared. (E) Fibrolitic sillimanite clast showing intergrowth texture with muscovite. (F) Sericitic alteration of plagioclase.

Fibrolitic sillimanite occurs throughout the gneisses of the Khumbu region and commonly grows along biotite and feldspar margins (Figure 6C-D). Fibrolitic sillimanite occurs as clasts in the upper part of the Greater Himalayan sequence and commonly show inclusions of relict muscovite grains (Figure 6E). Musumeci (2002) has proposed a metasomatic origin of sillimanite in BFZ lithologies of the Khumbu region by replacement of K-feldspar, biotite, and plagioclase. The samples collected in this study do not rule out that sillimanite nucleated and grew by a discontinuous prograde reaction:

$$St + Ms + Qtz = Sil + Bt + Grt + H_2O \quad (4)$$

Either case is a possibility and more petrographic work has to be undertaken to precisely determine the origin of sillimanite, which is important in understanding the complete deformational history of sillimanite.

In some biotite gneiss samples biotite replaces chlorite as a solid-fluid mineral reaction (Figure 5H), a general prograde reaction sequence in pelitic rocks of clay minerals → chlorites → micas → anhydrous silicates. Sericitic alteration of feldspar is evidence for hydrothermal alteration (Figure 6F). Additionally, Searle et al. (2003) suggests that the presence of cordierite indicates partial melting under high-temperature, low-pressure conditions when in the presence of sillimanite. The high H^+ concentration, during hydrogen metasomatism, relative to other major elements removes Na, K, Ca, Mg, and Fe in feldspars, which causes white micas ± clay minerals to stabilize according to the reaction (Best, 2013):

$$2KAlSi_3O_8 + 2H^+ + H_2O = Al_2Si_2O_5(OH)_4 + 4SiO_2 + 2K^+ \quad (5)$$

Quartz Petrofabric

I analyzed microstructures and petrofabric of quartz grains in order to compare deformational temperatures of samples to each other and identify any pattern that might be related to offset along the BFZ. This work was also conducted to see if deformation associated with the BFZ affected the quartz petrofabric in samples collected within the zone, or if quartz grains record an inherited fabric from older thrust-related metamorphism. Hirth and Tullis (1992) have determined three regimes of dislocation creep in experimentally deformed quartz aggregates and showed that the dislocations and distinctive types of microstructures that result are a product of temperature and strain rate, including: (1) at lower temperatures and faster strain rate dislocation recovery is controlled by strain-induced grain boundary migration, commonly referred to as bulging (BLG) recrystallization. (2) an increase in temperature, or lower strain rate will result in progressive subgrain rotation (SGR) recrystallization. (3) with further increase in temperature or decrease in strain rate recrystallization occurs by both grain boundary migration and subgrain rotation, resulting in fully recrystallized quartz grains, referred to as high-temperature grain boundary migration (GBM) recrystallization. Stipp et al. (2002b) have, in turn, related the three regimes from Hirth and Tullis (1992) to temperature ranges. BLG recrystallization occurs under conditions of 280-390 ˚C, where the transition from BLG to SGR recrystallization occurs from 390-420 ˚C, SGR recrystallization occurs from 420-490 ˚C, the transition from SGR to GBM recrystallization occurs from 490-530 ˚C, and GBM recrystallization occurs > 530 ˚C. Since quartz recrystallization microstructures are related to both temperature and strain

rate this method has to be used carefully as a thermometer. I suggest using the three textural regimes to compare samples relative to each other and not as an absolute determination for deformational temperature.

I have categorized all 38 samples using Hirth and Tullis (1992) regimes. Generally, quartz grains show undulatory extinction, bulging grain boundaries, subgrains exhibiting polygonal texture, or completely strain-free recrystallized grains (Figure 7). This suggests deformation conditions in a transitional regime between SGR and GBM recrystallization with deformational temperatures of at least 420 ˚C and > 500 ˚C for most samples. This is likely not a reflection of peak metamorphic temperatures since strain rate is unknown and a later retrograde thermal event could have deformed quartz grains at a lower temperature. More interestingly, however, samples collected north of Taboche, mainly biotite gneiss, show predominantly GBM recrystallization (Figure 7C-D; Figure 8). Samples collected around the village of Phortse show both SGR and GBM recrystallization (Figure 7B) and samples south of Namche Bazar show predominantly SGR recrystallization (Figure 7A; Figure 8). This indicates that there is a clear increasing trend in deformational temperature or decreasing trend in strain rate from structurally lower to higher levels within the Greater Himalayan sequence of the Khumbu region (Figure 8).

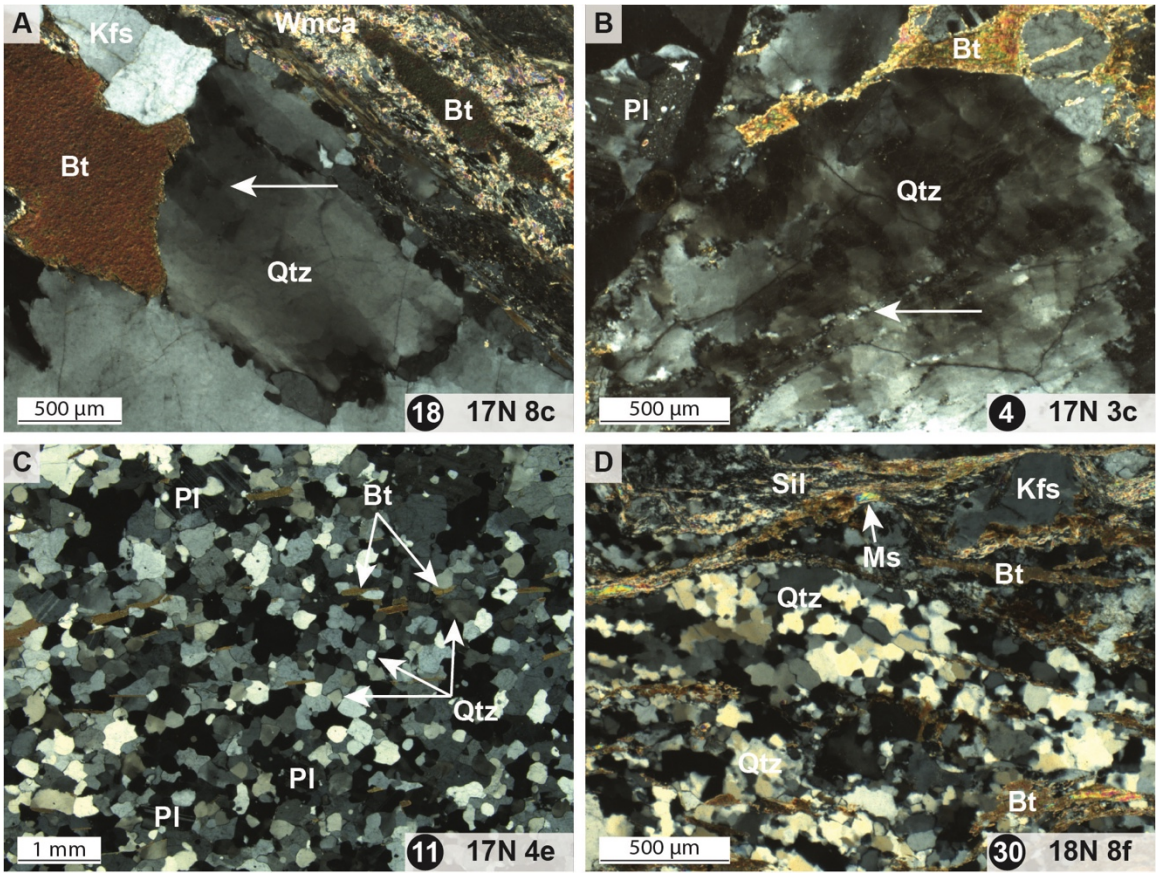


Figure 7. Photomicrographs of quartz petrofabrics. Photomicrographs include sample name and sample location. Refer to Appendix B for sample locations and Appendix C for exact GPS coordinates. (A) Quartz grains exhibiting SGR recrystallization. Quartz grains show undulose extinction, subgrains exhibiting polygonal texture, and strong deformation lamellae. Arrow is point to a group of subgrains. (B) Quartz grains exhibiting both SGR and GBM recrystallization. Quartz grains show undulose extinction, subgrains exhibiting polygonal texture, however, there are also some completely recrystallized grains. Arrow is pointing to a group of fully recrystallized grains. (C) Quartz grains exhibiting GBM recrystallization. Quartz grains are completely recrystallized, no deformation lamellae or undulose extinction visible, grains have lobate and straight grain boundaries. Quartz appears randomly scattered. (D) Quartz grains exhibiting GBM recrystallization. Quartz grains are completely recrystallized, no deformation lamellae or undulose extinction visible, grains have lobate and straight grain boundaries. Quartz grains are located in groups and layers.

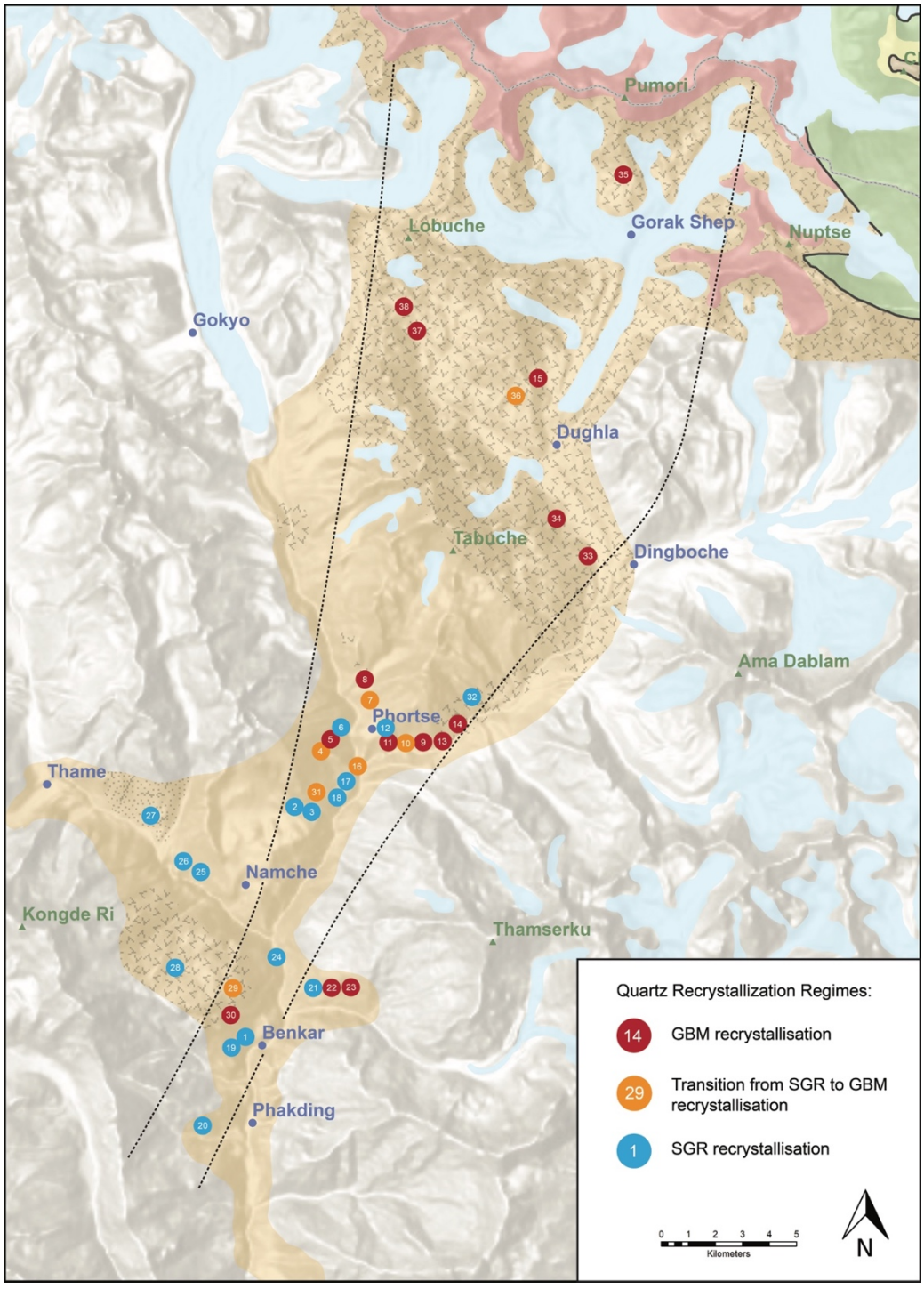


Figure 8. Map showing all 38 collected samples and their dominant quartz petrofabric regime, after (Hirth and Tullis, 1992). The base map is an exert from Appendix B and the stippled lines represent the extent of the BFZ. Numbers inside the colored circles are a reference to sample location.

Structural Relationships

Several cross-cutting relationships have been documented in the Khumbu region and are presented here in order to constrain the timing of BFZ fabric development. I have mapped three low-angle, brittle, normal and right-lateral faults that cross cut metamorphic foliation (Figure 9; Appendix B): (1) The first fault is located NE of Benkar towards Thamserku peak and strikes N51W and dips 28SW. (2) The second fault is located between the towns of Namche Bazar and Phortse and strikes N60W and dips 44NE (Figure 9A). This fault has first been recognized by Hubbard (1988), mapped by Carosi et al. (1999), and subsequently reinterpreted by Hubbard et al. (2017). (3) The third structure lies east of Phortse and strikes N44E and dips 37NW (Figure 7B). It also has previously been mapped by Carosi et al. (1999). These faults are within the central and southern mapped extent of the BFZ. The length of these three brittle faults has not been constrained, however, field mapping indicates that they are at least several hundred meters long and field photographs suggests a length of up to 1-2 kilometers. Fault surfaces are up to three meters wide and characterized by brittle slickensides and slickenline striations and made up of fault breccia and fault gouge (Figure 9C). Fault kinematics has been determined from slickenline striations, stepped mineral fibers, drag of metamorphic foliation, as well as thin section analysis. Fault one shows a normal, right-lateral sense of shear with a lineation plunging 24˚ and trending S2W (Figure 9D). Fault two kinematics indicate a normal sense of shear with a lineation plunging 44˚ and trending N30E (Figure 9E). Fault three shows a right-lateral sense of shear on a lineation plunging 0˚ and trending S64W (Figure 9F). The faults between Namche Bazar and

Phortse, as well as east of Phortse, have been attributed to southward migration of orogenic collapse in the Himalaya in response to southward propagation of the Main Frontal Thrust system as India continues to underthrust Eurasia (Hubbard et al., 2017). These brittle faults have also been interpreted to be related to isostatic reequilibration within the footwall of the STDS (Carosi et al., 1999). In either case, these structures are clearly younger, isolated, entirely brittle faults and their orientation suggests that they are unrelated to the formation of the BFZ.



Figure 9. Photographs and photomicrograph of brittle faults cross-cutting metamorphic foliation. Photomicrograph includes sample name and sample location. Refer to Appendix B for sample location and Appendix C for exact GPS coordinates. (A) Brittle fault between the villages of Namche Bazar and Phortse. Red arrow is pointing towards drag on the metamorphic foliation indicating normal sense of shear. Note that some of the stair steps are float rocks. The arrow is pointing to a stair step that is in place. Kumar Magar is posing for scale. Approximate location of photograph: 27˚49'36.07"N, 86˚43'52.62"E. (B) Approximately 1m-wide brittle fault zone made up of fault gauge and fault breccia. Located east of Phortse. Arrow is pointing towards fault surface. Approximate location of photograph: 27˚50'49.56"N, 86˚45'34.49"E. (C) Example of fault breccia found within these brittle faults. Approximate location of photograph: 27˚50'47.70"N, 86˚45'29.17"E. (D) Exposed stepped slickenside surface of fault located

east of Benkar. Arrow is pointing in the direction of lineation. Kinematics are interpreted to be normal, right-lateral. Foliation and lineation are displayed in a lower hemisphere, equal area plot. Approximate location of photograph: 27˚46’20.57”N, 86˚43’50.25”E. (E) Photomicrograph of a sample collected from the fault between the villages of Namche Bazar and Phortse. Sense of shear is interpreted as normal. Foliation and lineation are displayed in a lower hemisphere, equal area plot. (F) Stepped slickenside surface of fault located east of Phortse. Arrow is pointing in the direction of lineation. Sense of shear is interpreted to be right-lateral. Foliation and lineation are displayed in a lower hemisphere, equal area plot. Approximate location of photograph: 27˚50’49.56”N, 86˚45’34.49”E.

North of Namche Bazar, within the mapped area of the BFZ, the dominant shear fabric strikes consistently NE, dipping SE. Key overprinting relationships exposed throughout this zone provide critical insight into the structural evolution of this fabric. One such exposure is located on the southern flank of Taboche peak. A NE-striking, SE-dipping brittle-ductile shear zone has cut more or less flat-lying fabric, which has been dragged into the shear zone (Figure 10A). Drag clearly shows a normal component of shear. Due to the two-dimensional exposure of this outcrop it is unclear if there is a strike-slip component to movement as well. Unfortunately, sampling of this structure is unrealistic due to the inaccessibility of this wall. Another such exposure is located on a flank of Kangchung peak, located west of Lobuche peak. Steep fabric on an eastern limb of the mountain appears to cut the more or less flat-lying fabric of Kangchung peak (Figure 10B). I interpret this to be part of the western edge of the BFZ.

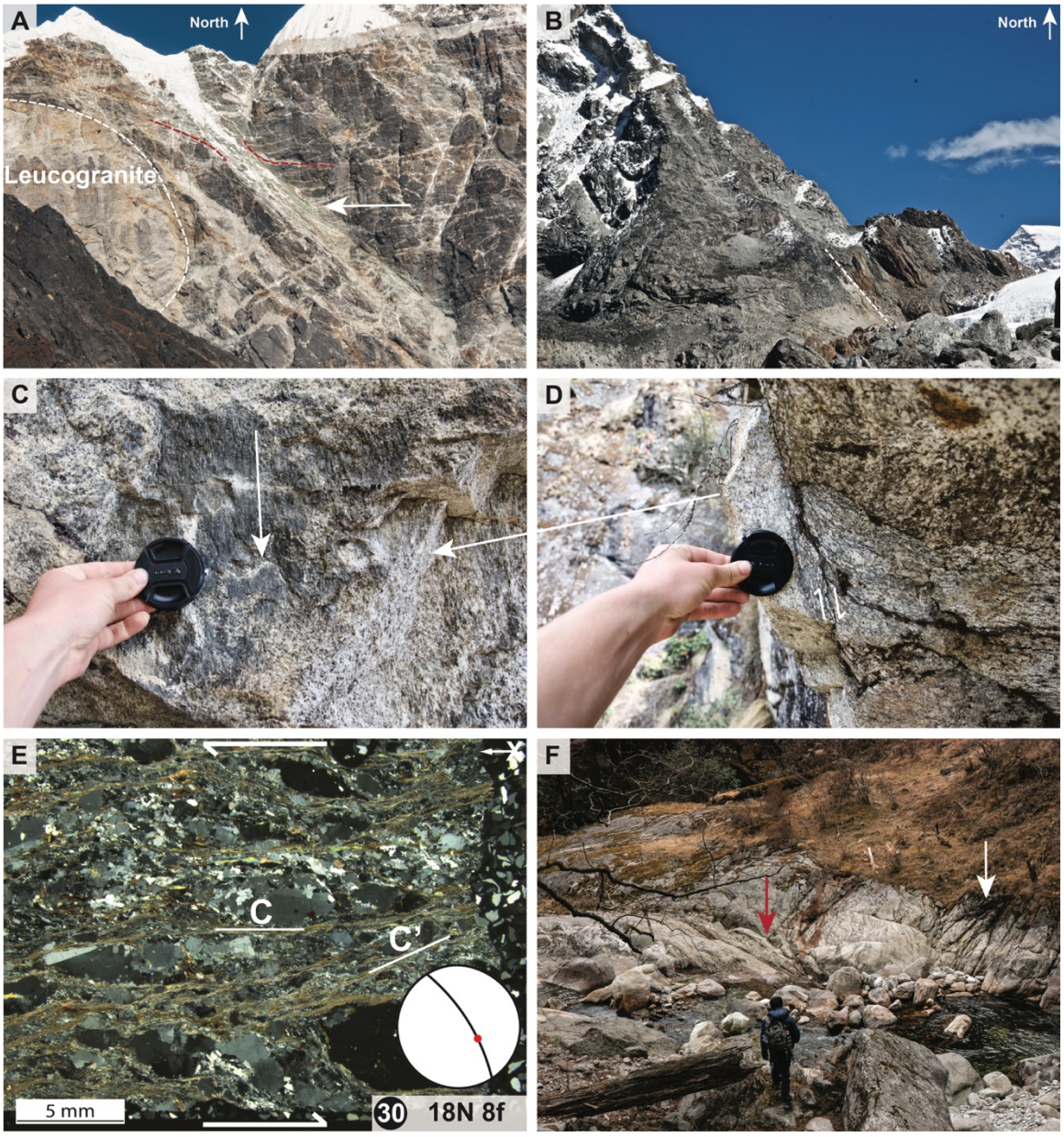


Figure 10. Photographs and photomicrograph of crosscutting relationships within the BFZ. Photomicrograph includes sample name and sample location. Refer to Appendix B for sample location and Appendix C for exact GPS coordinates. (A) Photograph of the south side of Taboche peak, taken from Phortse looking north. Arrow is pointing towards a ductile shear zone. Red dashed lines represent drag of flat lying fabric into the shear zone. The white dashed line outlines an intrusive leucogranite body. Photo courtesy of Mary Hubbard. Approximate location of photograph: 27˚50'24.17"N, 86˚44'13.28"E. (B) Photograph of a flank of Kangchung peak, taken from the base of Cho La pass looking north. White dashed line represents the contact between flat lying fabric to the west and steep NE-striking, SE-dipping fabric to the east. Approximate location of photograph:

27˚57’22.07”N, 86˚44’41.85”E. (C) Photograph of a slickenside with stepped mineral fibers indicating extension. Arrow is pointing in the direction of lineation. Approximate location of photograph: 27˚46’4.23”N, 86˚42’30.24”E. (D) Photograph taken perpendicular to the shear surface showing ductile drag on the older fabric with evidence for a normal sense of shear. The white arrow connecting C and D shows from what perspective photograph D was taken from. Approximate location of photograph: 27˚46’04.23”N, 86˚42’30.24”E. (E) Photomicrograph of a thin section created from a sample taken from the outcrop displayed in C and D. Deformation is concentrated on mica and sillimanite-rich planes. Sense of shear is interpreted as normal. Foliation and lineation are displayed in a lower hemisphere, equal area plot. (F) Photograph of an outcrop east of Phakding towards Kongde Ri basecamp, near the village of Sano Gumela. White arrow is pointing to a set of brittle joints and fractures with an average orientation of N41E,71SE. Red arrow is pointing to a spot where these fracturs are crosscutting foliation, which have an average orientation of N30W,47NE. Bibek Giri for scale. Photo courtesy of Mary Hubbard. Approximate location of photograph: 27˚44’15.26”N, 86˚41’33.87”E.

South of Namche Bazar foliation is more complex. Steeper NE, sometimes NW striking fabric is more isolated within EW, shallow N-dipping fabric. This steeper foliation appears to be anastomosing and constricted to small regions. An outcrop near the village of Toktok shows that low-angle fabric is cut by a steep, NE-dipping shear zone with evidence for extension in both stepped mineral stretching lineation and ductile drag on the older fabric (Figure 10C-D). Thin section analysis of a sample collected at this location shows that deformation is concentrated on mica and sillimanite-rich planes. Mica fish and orientation of shear bands are consistent with an interpretation for a normal sense of shear (Figure 10E). Many outcrops south of Namche Bazar show sets of joints and fractures striking NW to NE and dipping steeply towards the SE and NE, respectively, that crosscut low-angle foliation. One such exposure is located near the village of Sano Gumela, west of Phakding towards Kongde Ri basecamp where a set of joints and fractures that, on average, strikes N41E and dips 71SE, cuts a foliation with an

average strike of N30W and dip of 47NE (Figure 10F). Crosscutting structural relationships throughout the Khumbu region show that BFZ fabric crosscuts older, low-angle fabric.

Kinematics

Detailed thin section analysis and outcrop observations have led to important insights into the kinematics of rocks within the BFZ. Throughout the BFZ metamorphic foliation strikes consistently NE and dips SE. Thin section analysis shows that deformation and shear is restricted to high strain zones within this NE-striking, SE-dipping foliation. For instance, some samples show no asymmetric clasts and evidence for shear (Figure 11A), whereas other samples show high-strain zones with asymmetric clasts and shear-sense indicators. In these strongly deformed samples biotite, muscovite and sillimanite are arranged in layers with a strong preferred orientation and separated from quartz, plagioclase, and K-feldspar domains (Figure 11B). These biotite, muscovite, and sillimanite layers range in thickness from millimeters to centimeters and in length from tens of centimeters to meters in scale. They are arranged parallel to foliation and fine-grained sillimanite grains and fibers define the lineation. They are generally arranged in anastomosing patterns. Sillimanite is present in the form of fibrolite with minor amounts of white mica at grain boundaries. Mica fish, foliation fish, asymmetric boudinage, asymmetric clasts, and deformation bands within the biotite, muscovite and sillimanite layers are evidence for shear along these layers. Such asymmetric structures are absent within quartz, plagioclase, and K-feldspar domains. Only 10 samples show a

strong lattice preferred orientation (LPO) of quartz grains. All this suggests a strain variation between the two domains, where shear is located and focused along sillimanite and mica grains.

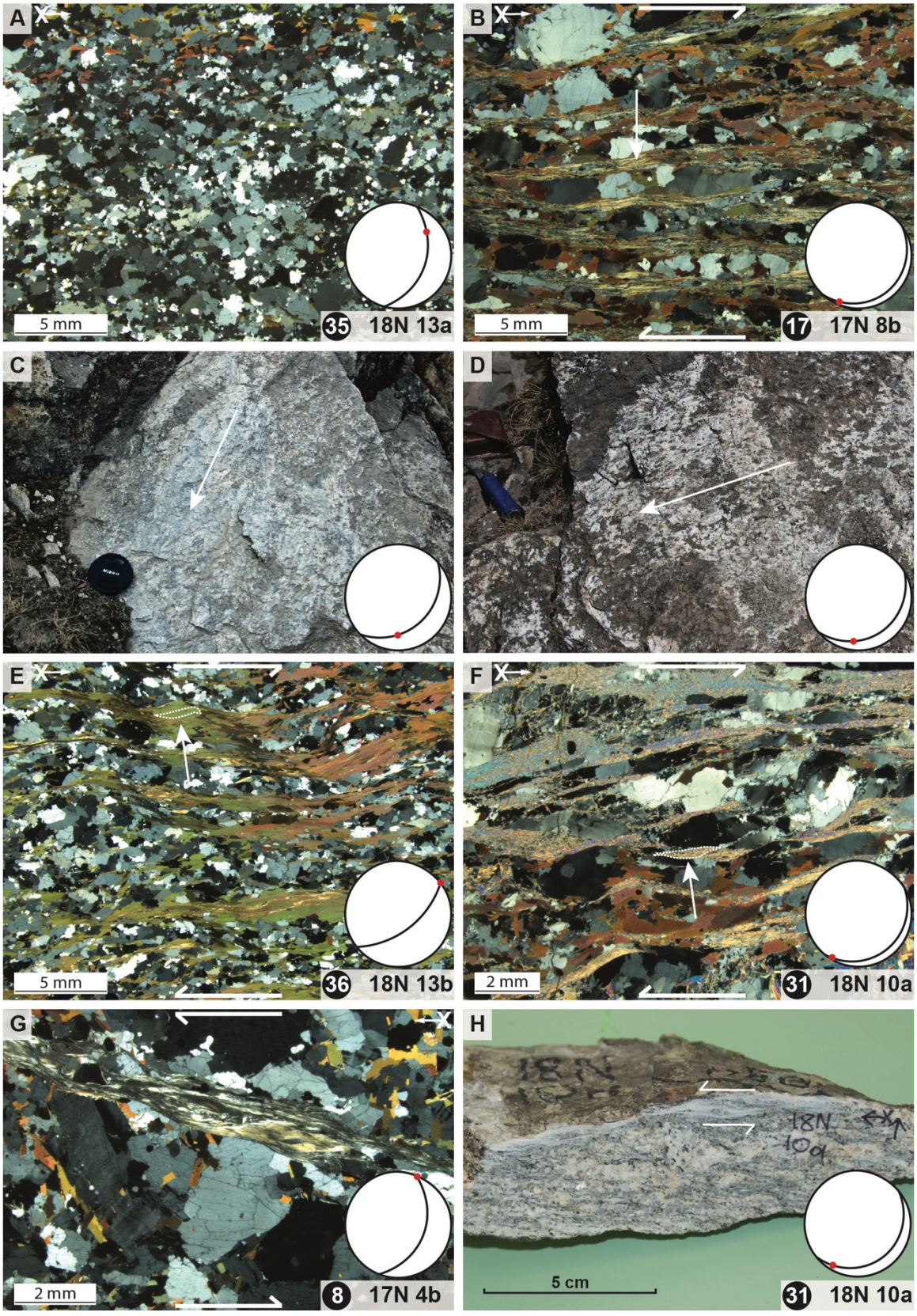

A
5 mm
35 18N 13a
B
5 mm
17 17N 8b
C
D
E
5 mm
36 18N 13b
F
2 mm
31 18N 10a
G
2 mm
8 17N 4b
H
5 cm
31 18N 10a

Figure 11. Photomicrographs and outcrop photos portraying kinematics within the BFZ. Photomicrographs include sample name and sample location. Refer to Appendix B for sample locations and Appendix C for exact GPS coordinates. (A) Thin section displaying weak metamorphic foliation with no evidence for localized shear. Foliation and lineation are displayed in a lower hemisphere, equal area plot. (B) Sillimanite and mica aligned in layers parallel to foliation and separated from quartz, plagioclase, and K-feldspar domains. Arrow is pointing to a sillimanite and mica layer. Sense of shear is interpreted as normal, right-lateral oblique slip. Foliation and lineation are displayed in a lower hemisphere, equal area plot. (C) Outcrop photo of a stepped slickenside made up predominantly of sillimanite. Arrow is pointing in the direction of lineation. Outcrop location near the village of Sanasa. Sense of shear is interpreted as normal, right-lateral oblique slip. Foliation and lineation are displayed in a lower hemisphere, equal area plot. Approximate location of photograph: 27˚49’35.14”N, 86˚43’56.03”E. (D) Outcrop photo of a stepped sillimanite slickenside. Arrow is pointing in the direction of lineation. Sense of shear is interpreted as normal, right-lateral oblique slip. Sample 18N11e has been collected at this outcrop and thin section analysis of this sample is consistent with the outcrop interpretation for the sense of shear. Foliation and lineation are displayed in a lower hemisphere, equal area plot. Approximate location of photograph: 27˚51’11.08”N, 86˚46’53.54”E. (E) Photomicrograph of sample 18N13b, biotite with small amounts of sillimanite define the foliation planes. Arrow is pointing to a mica fish that has been outlined with a stippled line. Sense of shear is interpreted as right-lateral. Foliation and lineation are displayed in a lower hemisphere, equal area plot. (F) Photomicrograph portraying a strong foliation dominated by sillimanite, muscovite, and white mica. Arrow is pointing to a foliation fish that has been outlines with a stippled line. Sense of shear is interpreted as normal, right-lateral oblique slip. Foliation and lineation are displayed in a lower hemisphere, equal area plot. (G) Photomicrograph of sample 17N4b. A thick sillimanite layer is present that has been internally sheared. Sense of shear is interpreted to be left-lateral. Foliation and lineation are displayed in a lower hemisphere, equal area plot. (H) Photograph of sample 18N10a. It has been cut parallel to lineation and perpendicular to foliation. The top of the sample shows a stepped slickenside surface with a strong lineation made up of fibrolitic sillimanite. The cross-section view shows ductile shearing of sillimanite layers. Sense of shear is interpreted to be normal, right-lateral oblique slip, which is consistent with thin section observations, as seen in F. Foliation and lineation are displayed in a lower hemisphere, equal area plot.

In outcrop these sillimanite and mica layers are commonly exposed in the form of slabs. These slabs represent foliation surfaces with slickenside-like appearance. They show a defined mineral lineation made up of fine-grained, elongated sillimanite grains or fibers (Figure 11C-D). The mineral lineation indicates ductile to semi-brittle deformation.

Steps in mineral lineation on these exposed foliation surfaces were used to make kinematic interpretations at the outcrop. I have observed sillimanite and mica layers, in outcrop exposure, that exhibit extensional, dip-slip sense of shear, places that exhibit right-lateral sense of shear, and exposures with evidence for normal, right-lateral oblique-slip. For example, three outcrops near the village of Phortse show normal, right-lateral oblique slip with a foliation of N24E,34SE, N48E,37SE, and N11E,57SE and a lineation of 22,S8E, 32,S1W, and 7,S14W respectively.

Petrographic observation of thin sections yields more insight into the ductile sense of shear of these sillimanite and mica layers (Figure 11E-G). Ten samples yield a kinematic interpretation: Samples 17N4b (Figure 11G) and 17N4f show mica fish, foliation fish, and asymmetric sillimanite clasts that have been interpreted as left-lateral sense of shear. Mica fish in sample 18N2c and 18N5a suggest a predominantly normal sense of shear. Mica fish, delta clasts, and foliation fish in samples 18N3g and 18N13b (Figure 11E) suggest a right-lateral sense of shear. Samples 17N8b (Figure 11B), 18N8f (Figure 10E), 18N10a (Figure 11F), and 18N11e all indicate normal, right-lateral oblique slip. A garnet pressure shadow yields a strong kinematic interpretation in sample 17N8b (Figure 6B). Shear bands are present in both 18N2c and 18N8f (Figure 10E). Kinematic interpretations of thin sections and outcrop have been summarized in a tangent-lineation diagram in Figure 12. Poles to foliation planes plot predominantly in the NE quadrant and sense of shear is most dominant as normal, right-lateral oblique slip. The exposed sillimanite and mica foliation planes with a defined mineral lineation are evidence for ductile to semi-brittle deformation. In thin section, shear on sillimanite layers, with

deformation being absent in quartz and feldspar layers, are evidence for ductile nonpenetrative deformation. Hand sample 18N10a shows both ductile deformation in the form of asymmetric sillimanite clasts and ductile to semi-brittle deformation in the form of steps in mineral lineation on the exposed foliation surface (Figure 11H).

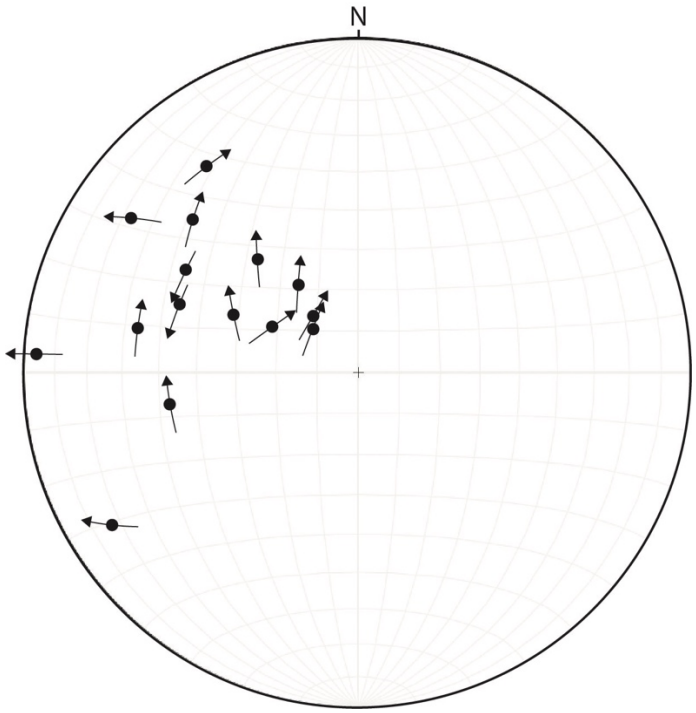


Figure 12. Tangent lineation diagram of samples and outcrop measurements collected within the BFZ. Plotted in a lower hemisphere equal-area projection. The points are poles to foliation planes. The arrows are tangent to the plane containing both the pole and lineation on the foliation surface and point in the direction of motion of the footwall block. Note the prevalence of poles in the NE quadrant and arrows displaying normal, right-lateral oblique slip (i.e. arrows pointing north).

Quartz Crystallographic Fabrics

Previous workers have employed quartz crystallographic fabrics in areas surrounding the Khumbu to examine the strain history of quartz rich rocks (e.g. Larson et al., 2017; Larson and Cottle, 2014). The orientation of lattice preferred quartz grains can provide information on flow stress from grain size (e.g. Stipp et al., 2010; Twiss, 1977), deformation temperatures (e.g. Kruhl, 1998; Law et al., 2011; Law et al., 2004; Law et al., 2013), shear parameters including vorticity, kinematics, and active slip systems (e.g. Law, 1990). Samples 18N8f and 17N3a were selected for measuring quartz crystallographic orientations. A lattice preferred orientation (LPO) of quartz grains in rocks within the BFZ is uncommon, however, both samples 18N8f and 17N3a are quartz rich and display a LPO of quartz, observed in thin section through inserting the accessory plate in cross polarized light. Therefore, these two samples were selected for quartz crystallographic analyses. 18N8f is a quartzofeldspathic gneiss with shear along sillimanite and mica layers. 17N3a is a sample collected from a brittle fault between Namche Bazar and the village of Phortse.

Quartz crystallographic orientations were measured in samples 18N8f and 17N3a by EBSD as described in detail in the methods section. Four EBSD maps were analyzed for sample 18N8f and one EBSD map was determined for 17N3a. Two EBSD maps of sample 18N8f yielded low quartz grain counts, due to improper selection of the mapping area, and were excluded from this compilation. Lower and upper hemisphere, equal-area pole figures were created for the remaining three maps and contoured using the post-processing software HKL Channel 5. For each sample, the crystallographic directions of

the [0001] (c axes) plane were plotted on a lower hemisphere, equal-area pole figure. The crystallographic directions of the <$2\bar{1}10$> (a axes) plane were also plotted on lower and upper hemisphere, equal-area pole figures in the rock fabric (XYZ) reference frame. Therefore, foliation is presented as an E-W-trending vertical plane (X-axis) and lineation as a horizontal line. All EBSD maps, corresponding pole figures of crystallographic directions and contour maps are displayed in Figure 13.

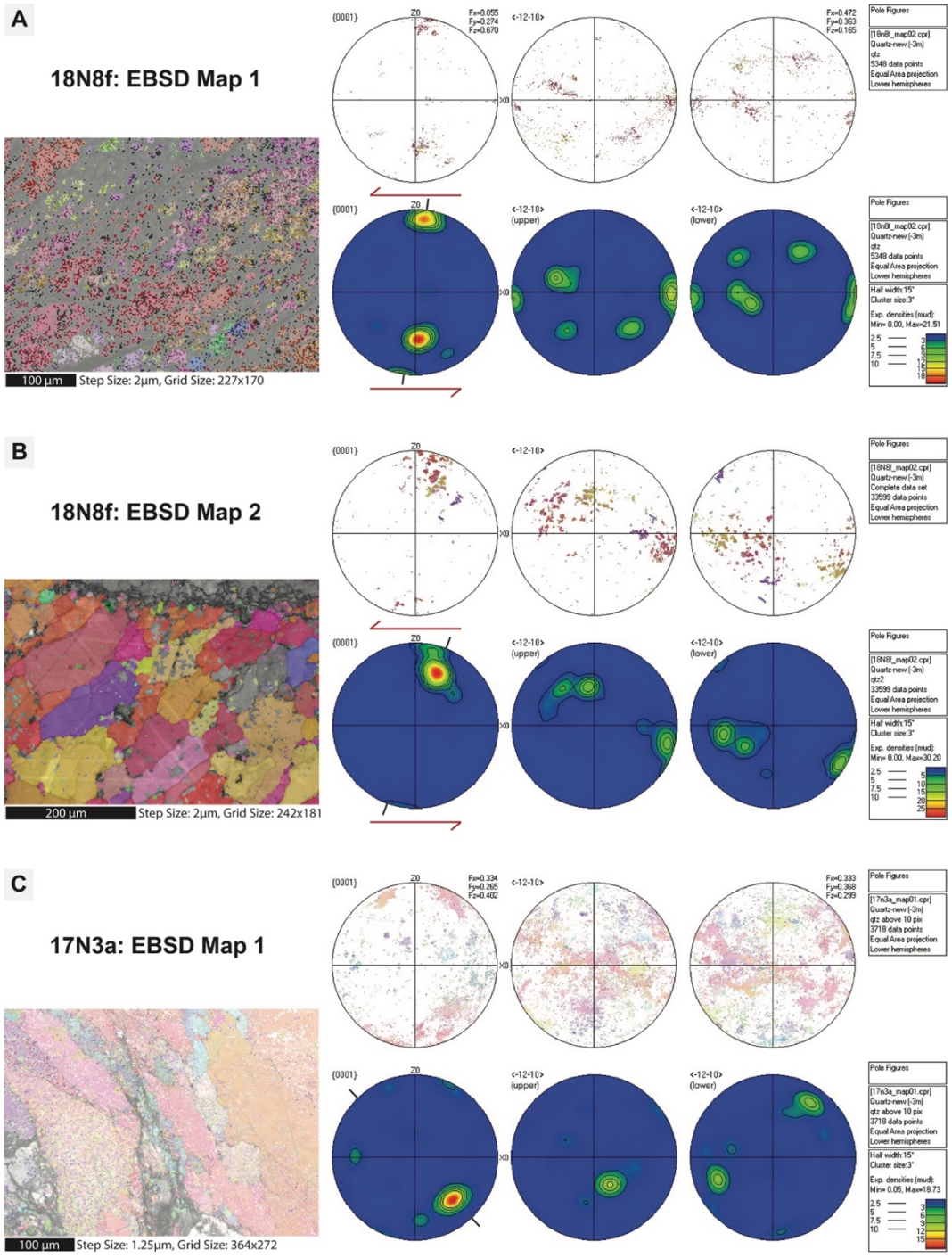


Figure 13. EBSD maps and representative pole figures of quartz crystallographic fabric orientation of samples 18N8f and 17N3a. From left to right: (1) EBSD map with scale, step size, and grid size labelled. (2) Crystallographic directions of the [0001] (c axes) plane plotted on a lower hemisphere, equal-area pole figure. [c] axes orientations plotted as lineations on top and contoured below. The contoured [c] axes pole figures show outer

tick marks of each peripheral maximum in [c] axes. Interpretation of sense of slip is indicated with red arrows. (3) Crystallographic directions of the <$2\bar{1}10$> (a axes) plane plotted in upper hemisphere, equal-area pole figures. <a> axes orientations plotted as lineations on top and contoured below. (4) Crystallographic directions of the <$2\bar{1}10$> (a axes) plane plotted in lower hemisphere, equal-area pole figures. <a> axes orientations plotted as lineations on top and contoured below. (5) Information on EBSD analysis and parameters for contouring. (A) EBSD Map 1 and representative pole figures of sample 18N8f. (B) EBSD Map 2 and representative pole figures of sample 18N8f. (C) EBSD Map 1 and representative pole figures of sample 17N3a.

EBSD maps of sample 18N8f show a strong LPO with a vertical [c] axes concentration parallel to Y with no defined opening angles and girdles (Figure 13A-B). LPO shows a strong peripheral maximum of [c] axes concentration in the XZ plane with a small angle to Z. In addition, they show <a> axes concentration perpendicular to the [c] axes concentration with an <a> axis maximum at small angle to X. LPO's are asymmetrical with respect to foliation, defined by an acute angle between [c] axes concentration and X. These crystallographic fabric patterns are consistent with predominantly basal- <a> slip with minor amounts of slip on $\{r\}$ <a>, $\{z\}$ <a>, and prism- <a> slip (Keller and Stipp, 2011; Law, 1990; Lister and Dornsiepen, 1982; Wilson, 1975). This indicates non-coaxial progressive plane strain deformation under upper greenschist to lower amphibolite facies conditions, with dislocation creep being the dominant deformation mechanism (Blumenfeld et al., 1985; Kruhl, 1998; Lister and Dornsiepen, 1982; Mainprice et al., 1986; Stipp et al., 2002a). Kinematic interpretation from asymmetry in [c] axes and <a> axes patterns are consistent with asymmetric clasts and orientation of shear bands as observed in thin section and suggests normal displacement. Kinematic interpretation from these pole figures, however, is ambiguous

due to the small angle between [c] axes concentration and Z and has to be interpreted with caution.

EBSD map of sample 17N3a shows quartz grain orientations with no distinct LPO (Figure 13C). The contoured pole figure, however, shows a strong preferred orientation. This is likely due to a high number of point-count indexing of several larger grains. Therefore, the [c] axes concentration in the contoured pole figure represents several larger grains and is not representative of the overall LPO of sample 17N3a. The weak LPO in this sample suggests no crystal plastic deformation associated with this fabric orientation. The preferred orientation of several larger grains, as observed in the contoured pole figures, is likely a representation of inherited quartz grains and not representing fabric development in sample 17N3a.

Geochronology, Thermochronology, and Thermobarometry

Here I summarized available geochronologic, thermochronologic and thermobarometric data for the Khumbu region taken from the literature in order to establish pressure, temperature, and timing constraints associated with BFZ deformation. Geochronologic, thermochronologic and thermobarometric data of Greater Himalayan rocks in the Khumbu region is available from six studies (Catlos et al., 2002; Hubbard, 1989; Hubbard and Harrison, 1989; Jessup et al., 2008a; Searle et al., 2003; Simpson et al., 2000). Geochronologic data is available as U-Th-Pb ages (Appendix A). Catlos et al. (2002) obtained Th-Pb monazite ages, Simpson et al. (2000) obtained U-Pb monazite ages, and Jessup et al. (2008a) analyzed U(-Th)-Pb monazite ages. Thermochronologic

data is available as $^{40}Ar/^{39}Ar$ ages, however, data is sparse (Appendix A). Hubbard and Harrison (1989) collected samples at three locations within the Greater Himalaya and used K-feldspar, biotite, muscovite, and hornblende in order to determine cooling ages (Table 2). P-T conditions across the Greater Himalaya have also been investigated using garnet-biotite cation exchange thermobarometry and the computer program THERMOCALC for average P-T calculations (Appendix A; Hubbard, 1989; Jessup et al., 2008a; Searle et al., 2003; Simpson, 2002). Where full analysis of garnet-biotite was unavailable garnet-cordierite thermometry was used (Searle et al., 2003). Because data from Hubbard (1989) was acquired without the compositional maps of garnet it was subsequently reprocessed by Simpson (2002) using more modern calibrations. U-Th-Pb ages are interpreted to represent crystallization ages and used to constrain the minimum timing of metamorphism, and fabric development (Jessup et al., 2008a). $^{40}Ar/^{39}Ar$ ages represent retrograde cooling ages at a closure temperature of 220±15 ˚C for K-feldspar, 300±50 ˚C for biotite, 350±50 ˚C for muscovite, and 500±50 ˚C for hornblende (McDougall and Harrison, 1999). The garnet-biotite exchange thermobarometry and resulting P-T estimates represent temperature and pressure of last equilibration (Holland and Powell, 1998).

Sample Location	Sample	Mineral	Age
Ghat	87H21C	K-feldspar	3.6±0.2 Ma
	87H21C	biotite	9.1±0.2 Ma
	87H21D	K-feldspar	6.4±0.8 Ma
	87H21D	biotite	7.5±0.6 Ma
	87H21D	muscovite	7.7±0.4 Ma
Na	87H19B	biotite	20.2±0.2 Ma
	87H19A	hornblende	22.7±4.4 Ma
Ngozumba	87H18A	K-feldspar	18.7±0.8 Ma
	87H18A	biotite	17.2±0.8 Ma
	87H18B	K-feldspar	21.7±0.8 Ma
	87H18B	biotite	16.8±1.4 Ma
	87H18B	muscovite	17.0±0.4 Ma
	87H18C	K-feldspar	15.5±1.8 Ma
	87H18C	muscovite	16.6±0.4 Ma

Table 2. Summary of $^{40}Ar/^{39}Ar$ ages of Greater Himalaya samples in the Khumbu region. Data collected by Hubbard and Harrison (1989). Sample locations can be found in Appendix A.

The following summary is meant as a background for interpreting how geochronologic, thermochronologic and thermobarometric data relate to the BFZ. For a full review of the P-T-t-D path for rocks in the Khumbu region refer to work done by Jessup et al. (2008a) and Searle et al. (2003). For crystallization age dates, U-Th-Pb results for the Greater Himalayan rocks in the Khumbu range from 20.3±0.3 Ma to 32.2±0.4 Ma (samples E13 and E137 repsectively; Simpson et al., 2000). The U-Pb monazite age of 32.2±0.4 Ma is interpreted to represent peak Barrovian metamorphism and younger crystallization ages at 20.5-21.3 Ma are interpreted to represent timing of leucogranite emplacement (Simpson et al., 2000). An outlier of 533±13 Ma of a monazite

inclusion in garnet, north of the village of Benkar, is interpreted to represent remnant evidence of Cambro-Ordovician suturing of India to Gondwana (sample ET19; Catlos et al., 2002). $^{40}Ar/^{39}Ar$ ages within the Greater Himalaya yields muscovite, biotite, and K-feldspar ages of 7.7±0.4 Ma, 7.5±0.6 Ma, and 6.4±0.8 Ma respectively, which are interpreted to represent deformation within the Greater Himalaya that postdates major movement on the MCT (Table 2; Ghat samples; Hubbard and Harrison, 1989). In the upper region of the Greater Himalayan sequence $^{40}Ar/^{39}Ar$ biotite and muscovite analysis yield average ages of 17.0±1.4 Ma and 16.6±0.2 Ma respectively, which are interpreted to represent timing of exhumation (Table 2; Ngozumba samples; Hubbard and Harrison, 1989). Garnet-biotite cation exchange thermobarometry yields estimates for the P-T conditions in the Khumbu which range from temperatures of 508±85 ˚C (sample 85H23; Hubbard, 1989) to 826±150 ˚C (sample E214; Searle et al., 2003) and pressures of 3.9±1.2 kbar (sample E187; Searle et al., 2003) to 8.0±2.4 kbar (sample E214; Searle et al., 2003). Jessup et al. (2008a) have interpreted the higher-pressure, moderate-temperature metamorphic conditions and record of prograde compositional zoning of garnet in their samples ET-70E, L-8, and L-13 to represent a record of Eohimalayan metamorphism at the margins of the Greater Himalayan sequence. Record of lower-pressure, high-temperature metamorphic conditions and evidence for staurolite with cordierite overgrowths in the core of the Greater Himalayan sequence point to Neohimalayan metamorphism (Jessup et al., 2008a). This relationship of Eohimalayan metamorphism at the margins and Neohimalayan metamorphism in the core of the

Greater Himalayan sequence is interpreted as evidence for partitioning of deformation into the margins of a mid-crustal channel (Jessup et al., 2008a).

Using $^{40}Ar/^{39}Ar$ thermochronology of muscovite across the Greater Himalayan sequence of the Kali Gandaki valley of central Nepal Godin et al. (2001) constrained exhumation of the Himalayan metamorphic core between 15 and 13 Ma. Hubbard and Harrison (1989) have sampled for $^{40}Ar/^{39}Ar$ geochronology at three outcrop locations (Appendix A). Two sample locations are located in the Gokyo valley, NE of the BFZ and one location originates south of Phakding in the village of Ghat, in close proximity to the BFZ. Samples 87H21C and 87H21D collected in Ghat are biotite gneiss and a pegmatite, respectively, with the assemblage: Qtz + Pl + Bt + Kfs. Both samples show evidence for deformation in thin section and are interpreted as ductile shear zones (Hubbard and Harrison, 1989). Analysis of several mineral phases of samples 87H21C and 87H21D yield a muscovite cooling age of 7.7±0.4 Ma; biotite cooling ages of 9.1±0.2 Ma and 7.5±0.6 Ma respectively; and K-feldspar cooling ages of 3.6±0.2 Ma and 6.4±0.8 Ma respectively (Table 2; Hubbard and Harrison, 1989). These cooling ages collected by Hubbard and Harrison (1989) postdates the proposed timing of exhumation of the Greater Himalayan sequence between 15 and 13 Ma (Godin et al., 2001) and all other $^{40}Ar/^{39}Ar$ ages in the Khumbu region (Table 2). Because these samples were collected in close proximity to the mapped extent of the BFZ, they have potential for informing on the timing of movement along the BFZ. In order to test this hypothesis, three samples (18N10a, 18N5d, and 18N11e) were selected for $^{40}Ar/^{39}Ar$ analysis that represent a transect across the BFZ approximately at the village of Phortse. Although these ages will

shed more light on the timing of deformation across the BFZ, results have not been determined yet.

INTERPRETATION AND DISCUSSION

Interpretation

Field, petrographic, and analytical evidence has been presented, supporting evidence for shear on a NE-striking, SE-dipping zone of deformation from the villages of Phakding to Gorak Shep along the Dudh Kosi valley in the Khumbu region. I found that shear is restricted to sillimanite and mica rich domains that are parallel to foliation and range in thickness from millimeters to centimeters and in length from tens of centimeters to meters in scale. These sillimanite and mica layers represent a network of anastomosing shear zones. Strong stretching lineation in hand samples combined with thin section analysis showing strongly deformed networks and layers of sillimanite and mica wrapping around poorly deformed quartz and feldspar enclaves is evidence for nonpenetrative ductile deformation. Exposed slickenside-like foliation surfaces with mineral lineations of elongated sillimanite and biotite, however, suggests semi-brittle deformation in some outcrops. Quartz crystallographic fabric orientation in sample 18N8f shows a strong LPO with predominantly basal- <a> slip indicating upper greenschist to lower amphibolite-facies crystal plastic deformation and shear along the foliation plane and is consistent with an interpretation for high strain zones within the zone of NE-striking, SE-dipping fabric. Deformation is thus interpreted to be nonpenetrative semi-brittle to ductile.

Kinematics from thin sections and outcrop show predominantly normal, right-lateral oblique slip with localized zones showing purely extensional movement. Two

samples of the 38 analyzed, both collected near the village of Phortse in approximation to each other, suggest left-lateral displacement. Due to the limited amount of data I suggest that these two samples are outliers in this dataset and do not represent the overall kinematic interpretation, which is predominantly normal, right-lateral oblique slip.

Structural crosscutting relationships on a flank of Taboche peak and Kangchung peak, and outcrops near the village of Toktok and Sano Gumela show that this NE-striking, SE-dipping fabric crosscuts older fabric. This suggests that deformation associated with these sillimanite and mica shear zones postdates the predominant S2 metamorphic fabric development that created the general EW-striking, N-dipping fabric of the Greater Himalayan sequence in the Khumbu region.

To the north, in the Khumbu glacier area, the metamorphic foliation has a continuous NE-striking, SE-dipping orientation with a 11 km width. To the south, between the villages of Phakding and Namche the zone narrows to a width of 1-2 km and NE-striking, SE-dipping foliation is more isolated. The increased volume of leucogranite intrusions, moving south to north, coincides with the widening of the BFZ. The widening geometry to the north could be explained with the presence of leucogranite bodies that force the zone of deformation to widen.

An outlier $^{40}Ar/^{39}Ar$ age collected by Hubbard and Harrison (1989), which coincides with this zone, represents supplementary evidence of deformation postdating the metamorphic event associated with S2 formation, however, more data is required to augment this argument.

I have mapped three low-angle, brittle, normal and right-lateral faults that cross cut metamorphic foliation in the central and southern portion of the BFZ. Movement on these brittle faults postdates shearing of the BFZ and their orientation suggests that they are unrelated to movement on the BFZ. Quartz crystallographic fabric orientation in sample 17N3a, collected from the fault between the villages of Namche Bazar and Phortse, further suggests no component of crystal plastic deformation. The interpretation of Hubbard et al. (2017) that these brittle faults are related to southward migration of orogenic collapse fits well with the observations made here. Dating these structures in the future will allow testing of this interpretation.

Analysis of quartz petrofabric of all 38 samples collected in the field show an increasing trend in deformational temperature, or a decreasing trend in strain rate, from structurally lower to higher levels within the Greater Himalayan sequence of the Khumbu region. This trend is interpreted to be related to thermal events associated with migmatization and leucogranite emplacement that are focused towards the top of the Greater Himalayan sequence. Since deformation associated with the BFZ is localized to sillimanite and mica domains and wrapped around quartz and feldspar enclaves it is likely that quartz petrofabrics are related to metamorphism associated with the dominant S2 fabric in the Khumbu region and not related to later BFZ deformation.

Overall, the BFZ represents a zone of NE-striking, SE-dipping deformation, which is focused on anastomosing shear zones of sillimanite and mica. I interpret this deformation to be nonpenetrative semi-brittle to ductile under upper greenschist to lower amphibolite facies conditions. Deformation post-dates peak metamorphism and is

occurring while rocks of the Greater Himalayan sequence were on the retrograde path. The development of these lower grade brittle-ductile shear zones lead to deformation and possibly syndeformational growth of pre-existing weak minerals, such as fibrolitic sillimanite and phyllosilicates. Crosscutting relationships between BFZ fabric and thrust-related S2 foliation, as well as leucogranite bodies constrain the timing of deformation to be younger than leucogranite emplacement of 20.5-21.3 Ma.

Tectonic Implications

Musumeci (2002) was the first to identify sillimanite-bearing shear zones in the Khumbu region. He interpreted top-to-the-south extensional kinematics with evidence for ductile deformation and brittle fracturing under amphibolite facies conditions. Observations by Musumeci (2002) of brittle-ductile shear zones under amphibolite facies conditions is consistent with my interpretations of BFZ deformation conditions. Observations by Musumeci (2002) are restricted to outcrops near the village of Phortse and show extensional sillimanite-bearing shear zones in proximity to leucogranite dykes. Due to the proximity to, and kinematics consistent with emplacement of leucogranite dykes, Musumeci (2002) suggests that these sillimanite-bearing shear zones were emplaced during syn-tectonic cooling of leucogranite dykes. Mapping of leucogranite dykes surrounding the village of Phortse is inconsistent with the interpretations presented in Musumeci (2002). My field observations have discovered only a few dykes in the area, and none are closely associated with sillimanite and mica layers. In addition, my kinematic interpretations are for a predominant normal, right-lateral oblique slip on NE-

striking, SE-dipping fabric. The interpretation that sillimanite-bearing shear zones were emplaced during cooling of leucogranite dykes does not explain occurrence of such shear zones south of the village of Phortse where leucogranite dykes are mostly absent. In addition, it does not explain the consistent fabric orientation throughout the BFZ and crosscutting relationships.

The BFZ is a NNE-SSW trending structure with evidence for normal, right-lateral oblique slip and purely extensional displacement that represents a discontinuity to the general E-W striking, N-dipping thrust fabric of the Greater Himalayan sequence in the Khumbu region. Tectonically the BFZ could be an expression of the following: (1) A large scale tear fault resulting from differential displacement of MCT segments (e.g. Hurtado Jr et al., 2001; Sahoo et al., 2000). (2) A lateral ramp in the Greater Himalayan sequence at the edge of a Lesser Himalayan duplex (e.g. Wu et al., 1998). (3) Irregularities in the underthrusting Indian crust resulting in this discontinuity in the overriding Eurasian crust (e.g. Godin and Harris, 2014). (4) Seismic partitioning of MCT movement resulting in segmentation of the Himalayan arc along a transverse fault (e.g. Mukul et al., 2018). (5) Strain partitioning due to oblique convergence of India and Eurasia that results in a transverse fault that separates a strain-partitioned region from a non-strain partitioned region (e.g. Silver et al., 2015). (6) Extension of both Tibet and the Greater Himalaya due to orogenic collapse (e.g. Jessup et al., 2008b; Thiede et al., 2006).

Seismic and strain partitioning (4 & 5), as well as orogenic collapse (6) would result in an expression of predominantly brittle structures. Since there is a clear component of ductile deformation under upper greenschist to lower amphibolite facies

conditions within the BFZ, I suggest these three models are an unlikely explanation. The BFZ, however, could have partitioned older seismic events, meaning it cannot be fully ruled out. Modern modeling of the lower crust does not have the required resolution needed to link BFZ deformation to irregularities within the underthrusting Indian crust (3), so we cannot fully evaluate its applicability here. Although data collected in this study cannot fully rule out any of the above models, my interpretations of the BFZ are most consistent with a tear fault (1) or lateral ramp (2).

A lateral ramp in the Greater Himalayan sequence at the edge of a Lesser Himalayan duplex would result in folding of Greater Himalayan fabric, and explain a NE-striking, SE-dipping orientation of the BFZ. This model, however, is not consistent with a kinematic interpretation of normal, right-lateral oblique slip and does not explain the crosscutting relationships that provide evidence that BFZ deformation postdates formation of the dominant S2 metamorphic fabric. For these reasons, and the fact that, as of now, a duplex edge has not been modeled below the Khumbu region, I suggest that the BFZ is not an expression of a lateral ramp.

Instead, I suggest that this structure represents a tear fault within the Greater Himalayan sequence. Differential displacement of MCT or other thrust segments south of the Khumbu region could explain a zone of NE-striking, SE-dipping metamorphic foliation with localized, nonpenetrative sillimanite and mica-bearing shear zones indicating normal, right-lateral oblique slip kinematics. Deformation was focused on weaker pre-existing zones of fibrolitic sillimanite and mica and possibly led to syndeformational growth of these minerals. Crosscutting relationships indicate that this

zone postdates major thrust fabric development and evidence for brittle-ductile deformation suggests a more prolonged history of plastic deformation that was punctuated by short-lived brittle-ductile events. A tear fault caused by differential displacement along the MCT or other thrusts south of the Khumbu region best explains available data to this date.

FUTURE WORK

To further investigate the interpretation that the BFZ represents a tear fault within the Greater Himalayan sequence, I have selected three samples across the zone for analysis of $^{40}Ar/^{39}Ar$ thermochronology. The goal is to determine the exhumation history of these three samples and see if they represent younger ages compared to the general timing of exhumation of the Greater Himalayan sequence, which would shed light on the timing of movement associated with BFZ deformation. Results are pending and will be included in future publications. In addition, Montana State University Earth Science Department Ph.D. student Bibek Giri will continue structural geologic mapping and thermochronologic work to the south of Lukla. He has proposed to collect samples across three transects: one just north of the MCT zone within Greater Himalayan rocks, a second within the MCT zone, and one to the south within the Lesser Himalayan sequence. The aim of his research is to determine if there is a possible E-W offset through the MCT zone using $^{40}Ar/^{39}Ar$ thermochronology of muscovite grains coupled with cooling ages for all samples. An offset within the MCT zone south of the BFZ would be further evidence for the presence of a tear fault. Lastly, continued research on cross faults within the Himalayan range will shed light on how the BFZ relates to similar structures in the westerns and eastern Himalaya, ultimately informing on the bigger picture of Himalayan orogenesis.

CONCLUSION

Structural mapping, petrographic observation, and EBSD analysis of quartz crystallographic fabrics of the Khumbu region of eastern Nepal reveals a zone of consistently NE-striking, SE-dipping metamorphic foliation from the villages of Phakding to Gorak Shep along the Dudh Kosi valley. Deformation within this zone is restricted to nonpenetrative, anastomosing sillimanite- and mica-bearing shear zones that wrap around poorly deformed quartz and feldspar enclaves. Kinematic indicators within these shear zones are consistent with normal, right-lateral oblique slip and locally, purely extensional movement in some outcrops. A strong stretching lineation throughout the zone and evidence for crystal plastic deformation in thin section suggests a component of ductile deformation. Quartz crystallographic fabric orientation in a sheared sample is consistent with an interpretation of ductile deformation and suggests upper greenschist to lower amphibolite facies deformation. Exposed slickenside-like foliation surfaces with mineral lineations of elongated sillimanite and biotite suggests a component of semi-brittle deformation in some outcrops. Structural relationships show that this NE-striking, SE-dipping fabric crosscuts older, E-W oriented thrust fabric and leucogranite intrusions. This indicates that deformation associated with this zone post-dates peak metamorphism for the Khumbu region and occurred post leucogranite emplacement of 20.5-21.3 Ma, while rocks of the Greater Himalayan sequence were on the retrograde path. Thermochronologic $^{40}Ar/^{39}Ar$ data of two samples collected by Hubbard and Harrison (1989) in proximity to the mapped extent of the zone show muscovite cooling age of 7.7±0.4 Ma; biotite cooling ages of 9.1±0.2 Ma and 7.5±0.6 Ma; and K-feldspar cooling

ages of 3.6±0.2 Ma and 6.4±0.8 Ma. These ages are much younger than general exhumation ages throughout the Greater Himalayan sequence and could represent timing of deformation within the zone. This structure is termed the BFZ and is interpreted to be an expression of a tear fault within the Greater Himalayan sequence caused by differential displacement along the MCT or other thrusts south of the Khumbu region. This is the first tear fault recognized within the metamorphic core of the Himalaya and this project highlights the need for continued detailed structural mapping of the Higher Himalaya coupled with geochronologic, thermochronologic and petrologic work. Future work will focus on how the BFZ fits into the bigger picture of Himalayan orogenesis.

REFERENCES CITED

Amatya, K., and Jnawali, B., 1994, Geological map of Nepal: Department of Mines and Geology: Nepal, scale 1:1000000, 1 sheet.

Beaumont, C., Jamieson, R. A., Nguyen, M. H., and Medvedev, S., 2004, Crustal channel flows: 1. Numerical models with applications to the tectonics of the Himalayan-Tibetan orogen: Journal of Geophysical Research: Solid Earth, v. 109, no. B6.

Best, M. G., 2013, Igneous and metamorphic petrology, John Wiley & Sons.

Blumenfeld, P., Mainprice, D., and Bouchez, J.-L., 1985, Glissement de direction [c] dominant dans le quartz de filons de granite, cisaillés en conditions sub-solidus (Vosges, France): Comptes rendus de l'Académie des sciences. Série 2, Mécanique, Physique, Chimie, Sciences de l'univers, Sciences de la Terre, v. 301, no. 18, p. 1303-1308.

Bordet, P., 1961, Recherches géologiques dans l'Himalaya du Népal, région du Makalu, Paris, Edition du Centre National de la Recherche Scientifique.

Bordet, P., 1971, Recherches géologiques dans l'Himalaya du Népal, région de la Thakkhola, Éd. du Centre Nat. de la Recherche Scientif.

Brasier, M., and Singh, P., 1987, Microfossils and Precambrian–Cambrian boundary stratigraphy at Maldeota, Lesser Himalaya: Geological Magazine, v. 124, no. 4, p. 323-345.

Brookfield, M., 1993, The Himalayan passive margin from Precambrian to Cretaceous times: Sedimentary Geology, v. 84, no. 1-4, p. 1-35.

Burchfiel, B. C., Zhiliang, C., Hodges, K. V., Yuping, L., Royden, L. H., and Changrong, D., 1992, The South Tibetan detachment system, Himalayan orogen: Extension contemporaneous with and parallel to shortening in a collisional mountain belt, Geological Society of America.

Burchfield, B., and Royden, L. H., 1985, North-south extension within the convergent Himalayan region: Geology, v. 13, no. 10, p. 679-682.

Burg, J., Brunel, M., Gapais, D., Chen, G., and Liu, G., 1984, Deformation of leucogranites of the crystalline Main Central Sheet in southern Tibet (China): Journal of Structural Geology, v. 6, no. 5, p. 535-542.

Caby, R., Pêcher, A., and Le Fort, P., 1983, Le grande chevauchement central himalayen: Nouvelles données sure les métamorphisme inverse à la base de la Dalle du Tibet: Revue de Géographie Physiqueau et Géologie Dynamique, v. 24, p. 89-100.

Carosi, R., Lombardo, B., Molli, G., Musumeci, G., and Pertusati, P., 1998, The South Tibetan detachment system in the Rongbuk valley, Everest region. Deformation features and geological implications: Journal of Asian Earth Sciences, v. 16, no. 2-3, p. 299-311.

Carosi, R., Musumeci, G., and Pertusati, P., 1999, Extensional tectonics in the higher Himalayan crystallines of Khumbu Himal, eastern Nepal: Geological Society of America Special Paper, v. 328, p. 211-224.

Catlos, E., Harrison, T. M., Manning, C. E., Grove, M., Rai, S. M., Hubbard, M. S., and Upreti, B., 2002, Records of the evolution of the Himalayan orogen from in situ Th–Pb ion microprobe dating of monazite: Eastern Nepal and western Garhwal: Journal of Asian Earth Sciences, v. 20, no. 5, p. 459-479.

Colchen, M., Fort, M., and Freytet, P., 1980, Evolution paléogéographique et structurale du fossé de la Thakkhola-Mustang (Himalaya du Népal): implications sur l'histoire récente de la chaîne himalayenne: Comptes Rendus des Académie des Sciences, v. 290, p. 311-314.

Cottle, J. M., Searle, M. P., Horstwood, M. S., and Waters, D. J., 2009, Timing of midcrustal metamorphism, melting, and deformation in the Mount Everest region of southern Tibet revealed by U (-Th)-Pb geochronology: The Journal of Geology, v. 117, no. 6, p. 643-664.

Cottle, J. M., Searle, M. P., Jessup, M. J., Crowley, J. L., and Law, R. D., 2015, Rongbuk re-visited: Geochronology of leucogranites in the footwall of the South Tibetan detachment system, Everest region, southern Tibet: Lithos, v. 227, p. 94-106.

DeCelles, P. G., Kapp, P., Gehrels, G. E., and Ding, L., 2014, Paleocene-Eocene foreland basin evolution in the Himalaya of southern Tibet and Nepal: Implications for the age of initial India-Asia collision: Tectonics, v. 33, no. 5, p. 824-849.

Ding, L., Kapp, P., and Wan, X., 2005, Paleocene–Eocene record of ophiolite obduction and initial India-Asia collision, south central Tibet: Tectonics, v. 24, no. 3.

Dupont-Nivet, G., Lippert, P. C., Van Hinsbergen, D. J., Meijers, M. J., and Kapp, P., 2010, Palaeolatitude and age of the Indo–Asia collision: palaeomagnetic constraints: Geophysical Journal International, v. 182, no. 3, p. 1189-1198.

Fossen, H., 2016, Structural geology, Cambridge University Press.

Gaetani, M., and Garzanti, E., 1991, Multicyclic history of the northern India continental margin (northwestern Himalaya)(1): AAPG Bulletin, v. 75, no. 9, p. 1427-1446.

Gansser, A., 1964, Geology of the Himalayas, 289 pp, Wiley-Interscience, New York.

Godin, L., Grujic, D., Law, R., and Searle, M., 2006, Channel flow, ductile extrusion and exhumation in continental collision zones: an introduction, Geological Society of London.

Godin, L., and Harris, L. B., 2014, Tracking basement cross-strike discontinuities in the Indian crust beneath the Himalayan orogen using gravity data–relationship to upper crustal faults: Geophysical Journal International, v. 198, no. 1, p. 198-215.

Godin, L., Parrish, R. R., Brown, R. L., and Hodges, K. V., 2001, Crustal thickening leading to exhumation of the Himalayan metamorphic core of central Nepal: Insight from U-Pb geochronology and 40Ar/39Ar thermochronology: Tectonics, v. 20, no. 5, p. 729-747.

Guillot, S., De Sigoyer, J., Lardeaux, J., and Mascle, G., 1997, Eclogitic metasediments from the Tso Morari area (Ladakh, Himalaya): Evidence for continental subduction during India-Asia convergence: Contributions to Mineralogy and Petrology, v. 128, no. 2-3, p. 197-212.

Hagen, T., 1968, Geology of the Thakkhola: Denkschr. Schweiz. Naturforsch. Ges., v. 86, no. 2, p. 160.

Hensen, B. J., and Green, D., 1973, Experimental study of the stability of cordierite and garnet in pelitic compositions at high pressures and temperatures: Contributions to Mineralogy and Petrology, v. 38, no. 2, p. 151-166.

Hirth, G., and Tullis, J., 1992, Dislocation creep regimes in quartz aggregates: Journal of Structural Geology, v. 14, no. 2, p. 145-159.

Hodges, K., Parrish, R., Housh, T., Lux, D., Burchfiel, B., Royden, L., and Chen, Z., 1992, Simultaneous Miocene extension and shortening in the Himalayan orogen: Science, v. 258, no. 5087, p. 1466-1470.

Holland, T., and Powell, R., 1998, An internally consistent thermodynamic data set for phases of petrological interest: Journal of metamorphic Geology, v. 16, no. 3, p. 309-343.

Hu, X., Wang, J., BouDagher-Fadel, M., Garzanti, E., and An, W., 2016, New insights into the timing of the India–Asia collision from the Paleogene Quxia and Jialazi formations of the Xigaze forearc basin, South Tibet: Gondwana Research, v. 32, p. 76-92.

Hubbard, M. S., 1988, Thermobarometry, ^{40}A r/^{39}Ar geochronology, and structure of the Main Central Thrust zone and Tibetan Slab, eastern Nepal Himalaya: Massachusetts Institute of Technology.

Hubbard, M. S., 1989, Thermobarometric constraints on the thermal history of the Main Central Thrust Zone and Tibetan Slab, eastern Nepal Himalaya: Journal of Metamorphic Geology, v. 7, no. 1, p. 19-30.

Hubbard, M. S., and Harrison, T. M., 1989, 40Ar/39Ar age constraints on deformation and metamorphism in the Main Central Thrust zone and Tibetan Slab, eastern Nepal Himalaya: Tectonics, v. 8, no. 4, p. 865-880.

Hubbard, M. S., Lageson, D., and Bhattarai, R. R., 2017, Reactivated normal-sense shear zones in the core of the Greater Himalayan Sequence, Solukhumbu District, Nepal: Journal of the Nepal Geological Society v. 53, p. 99-105.

Hurtado Jr, J. M., Hodges, K. V., and Whipple, K. X., 2001, Neotectonics of the Thakkhola graben and implications for recent activity on the South Tibetan fault

system in the central Nepal Himalaya: Geological Society of America Bulletin, v. 113, no. 2, p. 222-240.

Jessup, M., Cottle, J., Searle, M., Law, R., Newell, D., Tracy, R., and Waters, D., 2008a, P–T–t–D paths of Everest Series schist, Nepal: Journal of Metamorphic Geology, v. 26, no. 7, p. 717-739.

Jessup, M., Law, R., Searle, M., and Hubbard, M., 2006, Structural evolution and vorticity of flow during extrusion and exhumation of the Greater Himalayan Slab, Mount Everest Massif, Tibet/Nepal: implications for orogen-scale flow partitioning: Geological Society, London, Special Publications, v. 268, no. 1, p. 379-413.

Jessup, M. J., 2013, Mid-crustal processes in the Himalaya: https://geosociety.wordpress.com/2013/08/28/mid-crustal-processesin-the-Himalaya (accessed March 2019).

Jessup, M. J., Newell, D. L., Cottle, J. M., Berger, A. L., and Spotila, J. A., 2008b, Orogen-parallel extension and exhumation enhanced by denudation in the trans-Himalayan Arun River gorge, Ama Drime Massif, Tibet-Nepal: Geology, v. 36, no. 7, p. 587-590.

Keller, L., and Stipp, M., 2011, The single-slip hypothesis revisited: Crystal-preferred orientations of sheared quartz aggregates with increasing strain in nature and numerical simulation: Journal of Structural Geology, v. 33, no. 10, p. 1491-1500.

Kohn, M. J., 2008, PTt data from central Nepal support critical taper and repudiate large-scale channel flow of the Greater Himalayan Sequence: Geological Society of America Bulletin, v. 120, no. 3-4, p. 259-273.

Kruhl, J., 1998, Prism- and basal-plane parallel subgrain boundaries in quartz: A microstructural geothermabarometer: Journal of Metamorphic Petrology, v. 16.

Larson, K., Cottle, J., Lederer, G., and Rai, S., 2017, Defining shear zone boundaries using fabric intensity gradients: An example from the east-central Nepal Himalaya: Geosphere, v. 13, no. 3, p. 771-781.

Larson, K. P., and Cottle, J. M., 2014, Midcrustal discontinuities and the assembly of the Himalayan midcrust: Tectonics, v. 33, no. 5, p. 718-740.

Larson, K. P., Godin, L., and Price, R. A., 2010, Relationships between displacement and distortion in orogens: Linking the Himalayan foreland and hinterland in central Nepal: Bulletin, v. 122, no. 7-8, p. 1116-1134.

Law, R., 1990, Crystallographic fabrics: a selective review of their applications to research in structural geology: Geological Society, London, Special Publications, v. 54, no. 1, p. 335-352.

Law, R., Jessup, M., Searle, M., Francsis, M., Waters, D., and Cottle, J., 2011, Telescoping of isotherms beneath the South Tibetan detachment system, Mount Everest Massif: Journal of Structural Geology, v. 33, no. 11, p. 1569-1594.

Law, R., Searle, M., and Simpson, R., 2004, Strain, deformation temperatures and vorticity of flow at the top of the Greater Himalayan Slab, Everest Massif, Tibet: Journal of the Geological Society, v. 161, no. 2, p. 305-320.

Law, R., Stahr Iii, D., Francsis, M., Ashley, K., Grasemann, B., and Ahmad, T., 2013, Deformation temperatures and flow vorticities near the base of the Greater Himalayan Series, Sutlej Valley and Shimla Klippe, NW India: Journal of Structural Geology, v. 54, p. 21-53.

Le Fort, P., 1994, French earth sciences research in Himalaya regions, Alliance Française.

Lister, G., and Dornsiepen, U., 1982, Fabric transitions in the Saxony granulite terrain: Journal of Structural Geology, v. 4, no. 1, p. 81-92.

Lombardo, B., Pertusati, P., and Borghi, S., 1993, Geology and tectonomagmatic evolution of the eastern Himalaya along the Chomolungma-Makalu transect: Geological Society, London, Special Publications, v. 74, no. 1, p. 341-355.

Mainprice, D., Bouchez, J.-L., Blumenfeld, P., and Tubià, J. M., 1986, Dominant c slip in naturally deformed quartz: Implications for dramatic plastic softening at high temperature: Geology, v. 14, no. 10, p. 819-822.

McDougall, I., and Harrison, T. M., 1999, Geochronology and Thermochronology by the 40Ar/39Ar Method, Oxford University Press on Demand.

Molnar, P., and Tapponnier, P., 1975, Cenozoic tectonics of Asia: effects of a continental collision: science, v. 189, no. 4201, p. 419-426.

Mukul, M., 2010, First-order kinematics of wedge-scale active Himalayan deformation: Insights from Darjiling–Sikkim–Tibet (DaSiT) wedge: Journal of Asian Earth Sciences, v. 39, no. 6, p. 645-657.

Mukul, M., Jade, S., Ansari, K., Matin, A., and Joshi, V., 2018, Structural insights from geodetic Global Positioning System measurements in the Darjiling-Sikkim Himalaya: Journal of Structural Geology.

Mukul, M., Jade, S., and Matin, A., 2009, Active Deformation in the Darjiling-Sikkim Himalaya based on 2000-2004 Geodetic Global Positioning System Measurements: Ghosh, P., Gangopadhyay, S. (Eds.), Numerical Methods and Models in Earth Science, v. Indian Statistical Institute Platinum Jubilee Volumes, no. New India Publishing Agency, New Delhi, p. 1-28.

Murphy, M., and Mark Harrison, T., 1999, Relationship between leucogranites and the Qomolangma detachment in the Rongbuk Valley, south Tibet: Geology, v. 27, no. 9, p. 831-834.

Musumeci, G., 2002, Sillimanite-bearing shear zones in syntectonic leucogranite: fluid-assisted brittle–ductile deformation under amphibolite facies conditions: Journal of Structural Geology, v. 24, no. 9, p. 1491-1505.

Najman, Y., Jenks, D., Godin, L., Boudagher-Fadel, M., Millar, I., Garzanti, E., Horstwood, M., and Bracciali, L., 2017, The Tethyan Himalayan detrital record shows that India–Asia terminal collision occurred by 54 Ma in the Western Himalaya: Earth and Planetary Science Letters, v. 459, p. 301-310.

Nakata, T., 1989, Active faults of the Himalaya of India and Nepal: Geological Society of America Special Paper, v. 232, p. 243-264.

Ni, J., and York, J. E., 1978, Late Cenozoic tectonics of the Tibetan plateau: Journal of Geophysical Research: Solid Earth, v. 83, no. B11, p. 5377-5384.

Orme, D. A., Carrapa, B., and Kapp, P., 2015, Sedimentology, provenance and geochronology of the upper Cretaceous–lower Eocene western Xigaze forearc basin, southernTibet: Basin Research, v. 27, no. 4, p. 387-411.

Passchier, C. W., and Trouw, R. A., 2005, Microtectonics, Springer Science & Business Media.

Pognante, U., and Benna, P., 1993, Metamorphic zonation, migmatization and leucogranites along the Everest transect of eastern Nepal and Tibet: record of an exhumation history: Geological Society, London, Special Publications, v. 74, no. 1, p. 323-340.

Sahoo, P. K., Kumar, S., and Singh, R. P., 2000, Neotectonic study of Ganga and Yamuna tear faults, NW Himalaya, using remote sensing and GIS: International Journal of Remote Sensing, v. 21, no. 3, p. 499-518.

Searle, M., 1999, Extensional and compressional faults in the Everest–Lhotse massif, Khumbu Himalaya, Nepal: Journal of the Geological Society, v. 156, no. 2, p. 227-240.

Searle, M., Law, R., and Jessup, M., 2006, Crustal structure, restoration and evolution of the Greater Himalaya in Nepal-South Tibet: implications for channel flow and ductile extrusion of the middle crust: Geological Society, London, Special Publications, v. 268, no. 1, p. 355-378.

Searle, M., Simpson, R., Law, R., Parrish, R., and Waters, D., 2003, The structural geometry, metamorphic and magmatic evolution of the Everest massif, High Himalaya of Nepal–South Tibet: Journal of the Geological Society, v. 160, no. 3, p. 345-366.

Searle, M. P., Simpson, R. L., Law, R. D., Waters, D. J., and Parrish, R. R., 2002, Quantifying displacement on the South Tibetan detachment normal fault, Everest massif, and the timing of crustal thickening and uplift in the Himalaya and South Tibet: Journal of Nepal Geological Society, v. 26, p. 1-6.

Siivola, J., and Schmid, R., 2007, List of mineral abbreviations, Cambridge University Press: New York, p. 93-110.

Silver, C. R., Murphy, M. A., Taylor, M. H., Gosse, J., and Baltz, T., 2015, Neotectonics of the western Nepal fault system: Implications for Himalayan strain partitioning: Tectonics, v. 34, no. 12, p. 2494-2513.

Simpson, R. L., 2002, Metamorphism, melting and extension at the top of the High Himalayan slab, Mount Everest region, Nepal and Tibet: University of Oxford.

Simpson, R. L., Parrish, R. R., Searle, M. P., and Waters, D. J., 2000, Two episodes of monazite crystallization during metamorphism and crustal melting in the Everest region of the Nepalese Himalaya: Geology, v. 28, no. 5, p. 403-406.

Steck, A., MatthieuGirard, A. M., and Robyr, M., 1998, Geological transect across the Tso Morari and Spiti areas: Thenappe structures of the Tethys Himalaya.

Stipp, M., StuÈnitz, H., Heilbronner, R., and Schmid, S. M., 2002a, The eastern Tonale fault zone: a 'natural laboratory'for crystal plastic deformation of quartz over a temperature range from 250 to 700 C: Journal of Structural Geology, v. 24, no. 12, p. 1861-1884.

Stipp, M., Stünitz, H., Heilbronner, R., and Schmid, S. M., 2002b, Dynamic recrystallization of quartz: correlation between natural and experimental conditions: Geological Society, London, Special Publications, v. 200, no. 1, p. 171-190.

Stipp, M., Tullis, J., Scherwath, M., and Behrmann, J. H., 2010, A new perspective on paleopiezometry: Dynamically recrystallized grain size distributions indicate mechanism changes: Geology, v. 38, no. 8, p. 759-762.

Thiede, R. C., Arrowsmith, J. R., Bookhagen, B., McWilliams, M., Sobel, E. R., and Strecker, M. R., 2006, Dome formation and extension in the Tethyan Himalaya, Leo Pargil, northwest India: Geological Society of America Bulletin, v. 118, no. 5-6, p. 635-650.

Twiss, R. J., 1977, Theory and applicability of a recrystallized grain size paleopiezometer, Stress in the Earth, Springer, p. 227-244.

Wilson, C., 1975, Preferred orientation in quartz ribbon mylonites: Geological Society of America Bulletin, v. 86, no. 7, p. 968-974.

Wu, C., Nelson, K., Wortman, G., Samson, S. D., Yue, Y., Li, J., Kidd, W., and Edwards, M., 1998, Yadong cross structure and South Tibetan Detachment in the east central Himalaya (89–90 E): Tectonics, v. 17, no. 1, p. 28-45.

Yin, A., Harrison, T. M., Murphy, M., Grove, M., Nie, S., Ryerson, F., Xiao Feng, W., and Zeng Le, C., 1999, Tertiary deformation history of southeastern and southwestern Tibet during the Indo-Asian collision: Geological Society of America Bulletin, v. 111, no. 11, p. 1644-1664.

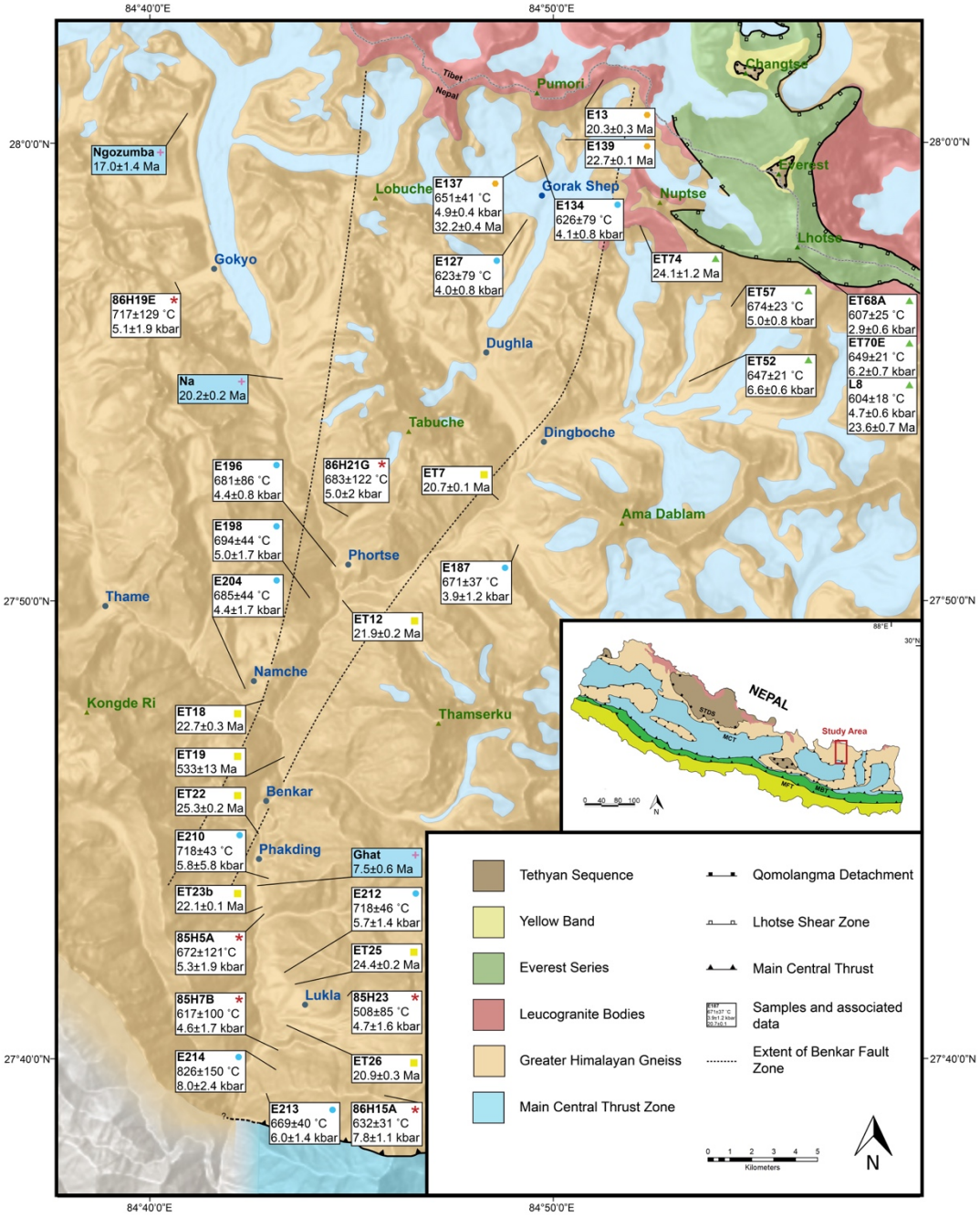
APPENDICES

APPENDIX A

GEOCHRONOLOGIC, THERMOCHRONOLOGIC, AND THERMOBAROMETRIC MAP OF THE KHUMBU REGION

MAP DESCRIPTION

Simplified geologic map and synthesis of geochronologic, thermochronologic, and thermobarometric data of the Khumbu region, Eastern Nepal. A full-scale version of this map is available as Plate 1 of the supplemental materials. Everest area mapping adopted from Searle (2003), MCT zone mapping adopted from Hubbard (1988), and inset map modified from Amatya and Jnawali (1994). The extent of the Benkar Fault Zone is included for reference. U-Th-Pb ages and P-T estimates displayed in white boxes and $^{40}Ar/^{39}Ar$ thermochronologic biotite ages displayed in blue boxes. Samples collected by: Hubbard (1989) and reprocessed by Simpson (2002) , red stars 85H7B-86H21G; Catlos et al. (2002), yellow squares ET7-ET26; Simpson et al. (2000), orange hexagons E13, E137, and E139; Searle et al. (2003), blue circles E127-E214; Jessup et al. (2008), green triangles ET52-ET74 and L8; Hubbard and Harrison (1989), pink crosses Ghat, Na, and Ngozumba.

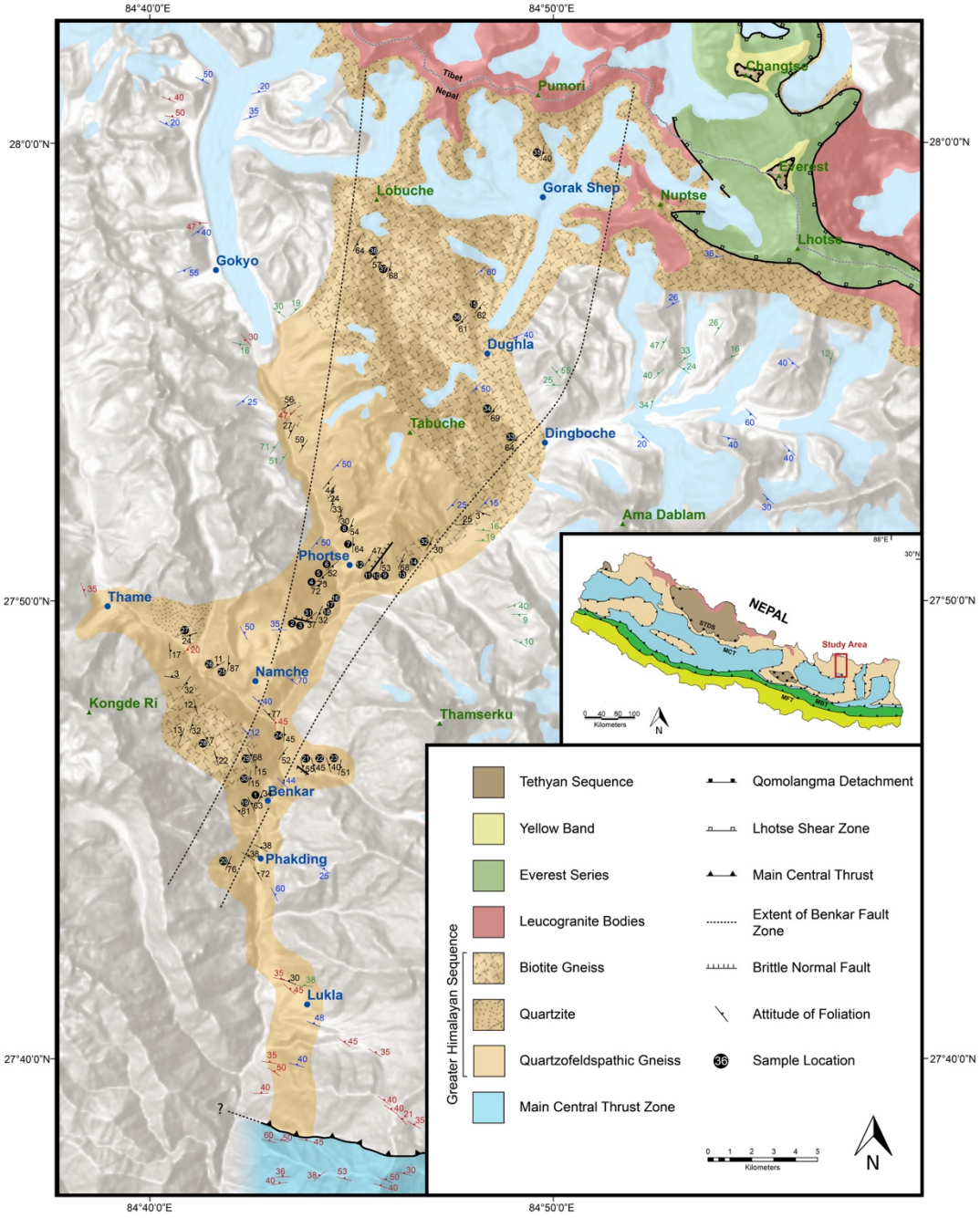

84°40'0"E
84°50'0"E
28°0'0"N
27°50'0"N
27°40'0"N
Tibet
Nepal
Pumori
Changtse
Everest
Lhotse
Nuptse
Lobuche
Gorak Shep
Gokyo
Dughla
Tabuche
Dingboche
Ama Dablam
Phortse
Thame
Namche
Kongde Ri
Thamserku
Benkar
Phakding
Lukla
Ngozumba 17.0±1.4 Ma
E13 20.3±0.3 Ma
E139 22.7±0.1 Ma
E137 651±41 °C 4.9±0.4 kbar 32.2±0.4 Ma
E134 626±79 °C 4.1±0.8 kbar
E127 623±79 °C 4.0±0.8 kbar
ET74 24.1±1.2 Ma
ET57 674±23 °C 5.0±0.8 kbar
ET68A 607±25 °C 2.9±0.6 kbar
ET70E 649±21 °C 6.2±0.7 kbar
ET52 647±21 °C 6.6±0.6 kbar
L8 604±18 °C 4.7±0.6 kbar 23.6±0.7 Ma
86H19E 717±129 °C 5.1±1.9 kbar
Na 20.2±0.2 Ma
E196 681±86 °C 4.4±0.8 kbar
86H21G 683±122 °C 5.0±2 kbar
ET7 20.7±0.1 Ma
E198 694±44 °C 5.0±1.7 kbar
E204 685±44 °C 4.4±1.7 kbar
E187 671±37 °C 3.9±1.2 kbar
ET12 21.9±0.2 Ma
ET18 22.7±0.3 Ma
ET19 533±13 Ma
ET22 25.3±0.2 Ma
E210 718±43 °C 5.8±5.8 kbar
Ghat 7.5±0.6 Ma
ET23b 22.1±0.1 Ma
E212 718±46 °C 5.7±1.4 kbar
85H5A 672±121°C 5.3±1.9 kbar
ET25 24.4±0.2 Ma
85H7B 617±100 °C 4.6±1.7 kbar
85H23 508±85 °C 4.7±1.6 kbar
E214 826±150 °C 8.0±2.4 kbar
ET26 20.9±0.3 Ma
E213 669±40 °C 6.0±1.4 kbar
86H15A 632±31 °C 7.8±1.1 kbar
NEPAL
STDS
MCT
MFT
MBT
Study Area
Tethyan Sequence
Yellow Band
Everest Series
Leucogranite Bodies
Greater Himalayan Gneiss
Main Central Thrust Zone
Qomolangma Detachment
Lhotse Shear Zone
Main Central Thrust
Samples and associated data
Extent of Benkar Fault Zone
Kilometers
N

APPENDIX B

GEOLOGIC MAP OF THE KHUMBU REGION AND BENKAR FAULT ZONE

MAP DESCRIPTION

Simplified geologic map of the Khumbu region, eastern Nepal highlighting the mapped extent of the Benkar Fault Zone. A full-scale version of this map is available as Plate 2 of the supplemental materials. Field mapping was completed over two field seasons in December 2017 and May 2018. Everest area mapping adopted from Searle (2003), MCT zone mapping adopted from Hubbard (1988), and inset map modified from Amatya and Jnawali (1994). Greater Himalayan sequence mapping and structural data marked in black are original to this work. Supplementary structural data by: Carosi et al. (1999), blue color; Jessup et al. (2008), green color; Hubbard (1988), red color.


84°40'0"E
84°50'0"E
28°0'0"N
27°50'0"N
27°40'0"N
Tibet
Nepal
Pumori
Changtse
Everest
Lobuche
Gorak Shep
Nuptse
Lhotse
Gokyo
Dughla
Tabuche
Dingboche
Ama Dablam
Phortse
Thame
Namche
Kongde Ri
Thamserku
Benkar
Phakding
Lukla
NEPAL
Study Area
STDS
MCT
MFT
SNH
Tethyan Sequence
Yellow Band
Everest Series
Leucogranite Bodies
Biotite Gneiss
Quartzite
Quartzofeldspathic Gneiss
Main Central Thrust Zone
Greater Himalayan Sequence
Qomolangma Detachment
Lhotse Shear Zone
Main Central Thrust
Extent of Benkar Fault Zone
Brittle Normal Fault
Attitude of Foliation
Sample Location
Kilometers
N

APPENDIX C

PETROGRAPHIC AND MICROSTRUCTURAL DESCRIPTIONS OF THIN SECTIONS

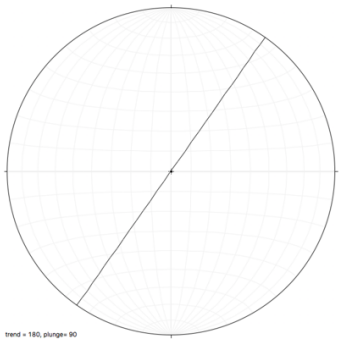
APPENDIX C DESCRIPTION

Petrographic and microstructural descriptions of 39 thin sections from 38 rock samples collected in the Khumbu region, eastern Nepal. All oriented thin sections were cut normal to the foliation and parallel to the lineation. Due to difficulty in obtaining lineation orientation for sample 17N3d two thin section were created. Samples 17N5a and 17N5b were collected without orientation for lithologic description. Map label refers to the sample location in the geologic map of Appendix B. GPS coordinates are given in decimal degrees in the form of northing/easting (e.g. 27.769937/86.714704). Orientation, foliation and lineation measurements are in 360-degree notation using right-hand rule. Foliation and lineation are presented in lower hemisphere, equal area projections using the Stereonet (v10.0) software package of R. Allmendinger. Photomicrographs have been taken in cross polarized light unless specified otherwise. Lineation orientation refers to the orientation of photomicrographs with respect to lineation. Where applicable sense of shear is indicated with red arrows and shear bands are displayed with solid lines.

Sample:	**17N 1a**	Map label: 1	Foliation: 035,90
Location:	Top of Benkar notch		Rake: 90
GPS:	27.769937/86.714704		Lineation: 90,180
Notes:	Strike/dip marking on east side of sample		

Thin Section Description:

Rock Type:	Quartzofeldspathic gneiss
Mineralogy:	Orthoclase, quartz, biotite, muscovite, sillimanite
Microstructure:	Coarse grained, subhedral, mostly equigranular gneissic fabric, alignment of micas along foliation, micaceous enclaves consisting of biotite and muscovite surrounded by orthoclase and quartz, feldspars show myrmekitic texture
Shear Sense:	Small zone of deformed sillimanite indicating shear, sense of shear unclear but suggesting normal sense of shear (Image 2)
LPO:	Weak quartz LPO
Qtz. grains:	Subgrain rotation recrystallization (Image 3), quartz grains show individual subgrains with a polygonal texture



Type of Lineation:
Brittle-ductile mineral lineation

Sense of Shear:
N./A.

Metamorphic grade:
Sillimanite grade, SGR recrystallization

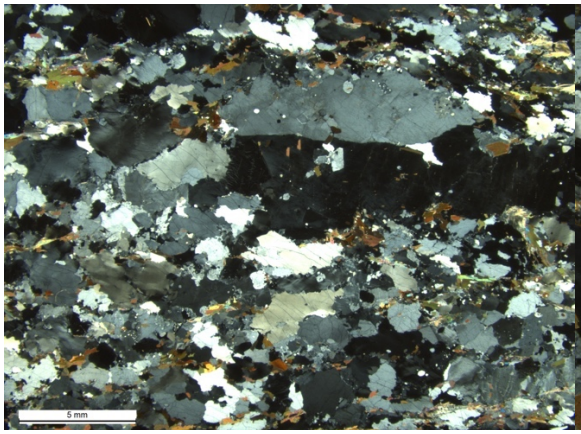


Image 1

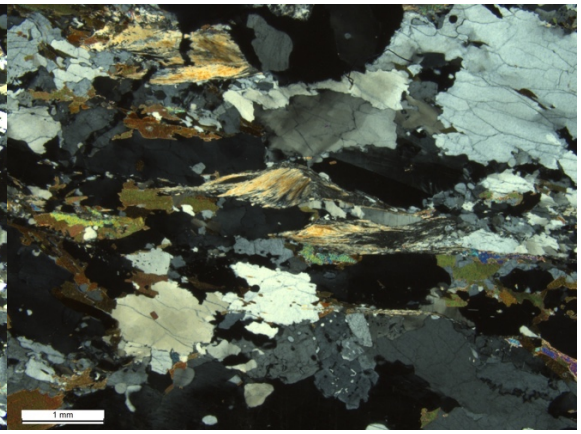


Image 2

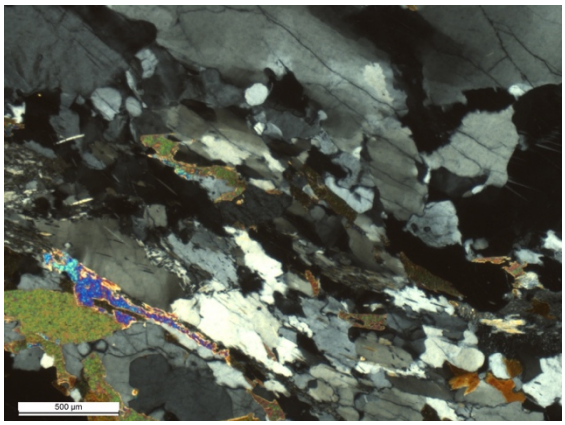


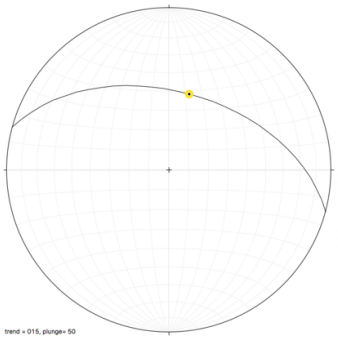
Image 3

Lineation orientation: top right

Sample:	**17N 3a**	Map label: 2	Foliation: 285,50
Location:	Brittle fault above Sanasa		Rake: 90
GPS:	27.826687/86.731283		Lineation: 50,015
Notes:	Oriented sample, normal fault, overturned		

Thin Section Description:

Rock Type:	Quartzofeldspathic gneiss
Mineralogy:	Biotite, muscovite, quartz, orthoclase
Microstructure:	Highly sheared fabric, grain size reduction occurring, protomylonite texture showing, brittle fractures visible as well, apparent strain variation
Shear Sense:	Shear bands (Image 6), mica fish (Image 5), phi clast and rotated clasts (Image 7) indicating normal sense of shear
LPO:	Very strong quartz LPO across entire thin section
Qtz. grains:	Subgrain rotation recrystallization (Image 8), quartz grains show individual subgrains with a polygonal texture



Type of Lineation:
Brittle slickenlines

Sense of Shear:
Normal

Metamorphic grade:
Sillimanite grade, SGR recrystallization

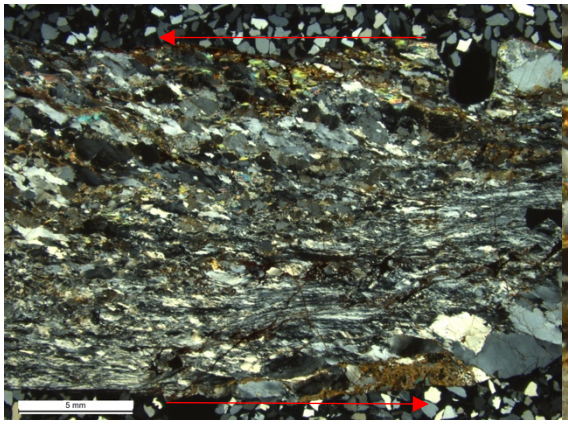


Image 4

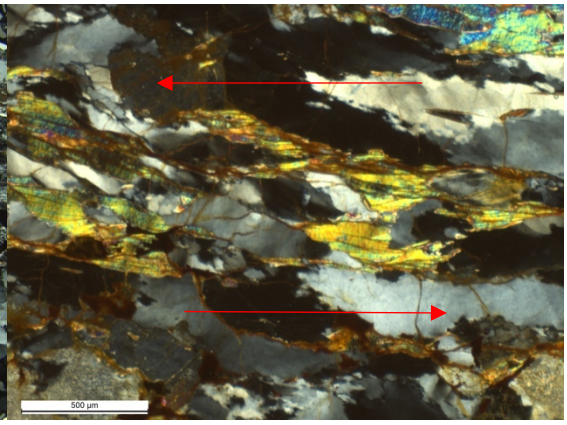


Image 5

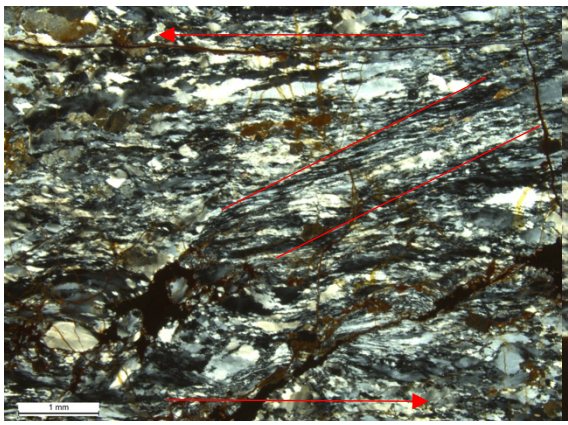


Image 6

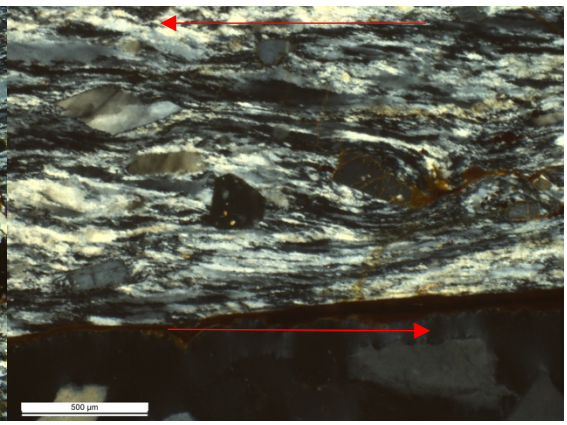


Image 7

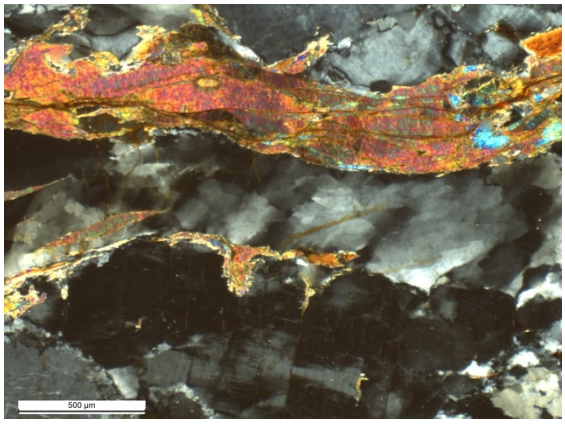


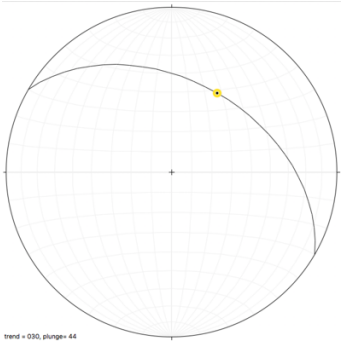
Image 8

Lineation orientation: top right

Sample:	**17N 3b**	Map label: 3	Foliation: 300,44
Location:	Fault cutting a fault, above Sanasa		Rake: 90
GPS:	27.826687/86.731283		Lineation: 44,030
Notes:	Quartz vein in brittle fault, overturned		

Thin Section Description:

Rock Type:	Quartzofeldspathic gneiss
Mineralogy:	Biotite, muscovite, quartz, orthoclase, albite
Microstructure:	Highly sheared fabric, grain size reduction occurring, protomylonite texture showing, apparent strain variation
Shear Sense:	Mica fish (Image 10), sigma clast (Image 11) indicating normal sense of shear
LPO:	Very strong quartz LPO across entire thin section
Qtz. grains:	Subgrain rotation recrystallization (Image 12), quartz grains show individual subgrains with a polygonal texture



Type of Lineation:
Brittle slickenlines

Sense of Shear:
Normal

Metamorphic grade:
Sillimanite grade, SGR recrystallization

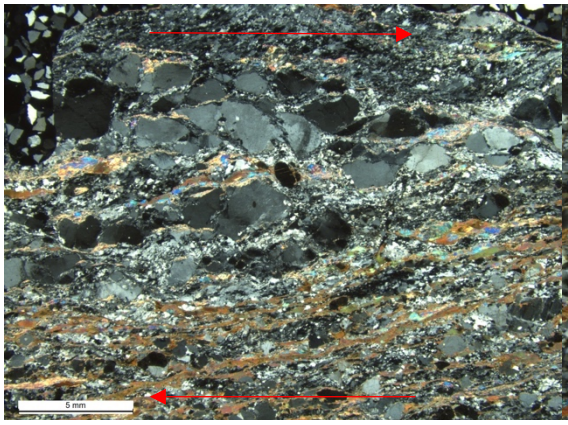


Image 9

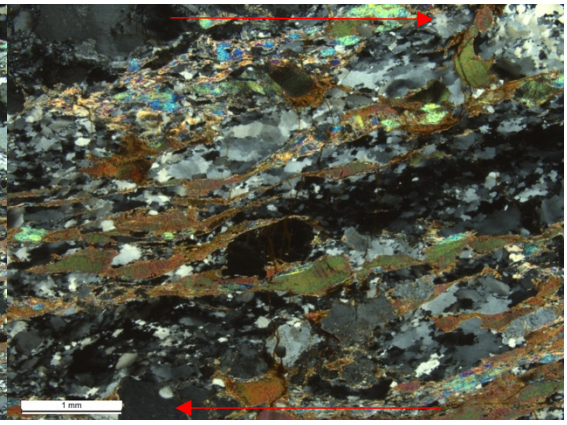


Image 10

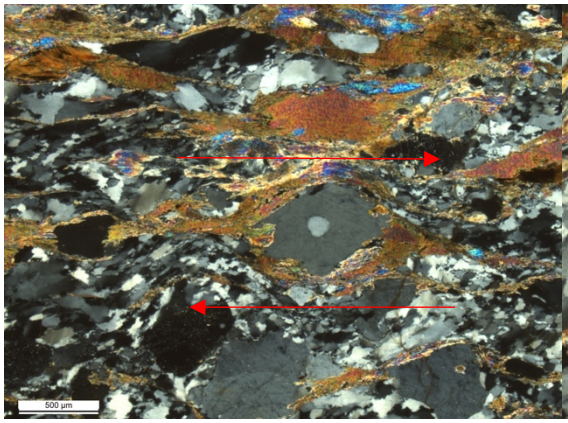


Image 11

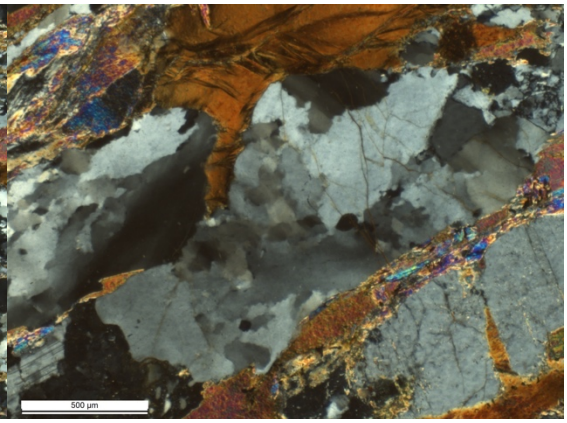


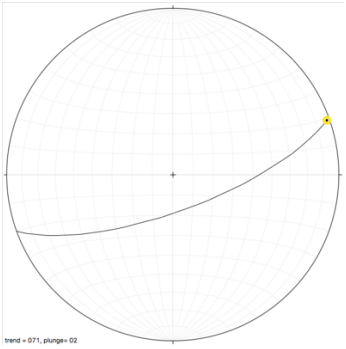
Image 12

Lineation orientation: top left

Sample:	**17N 3c**	Map label:	4	Foliation:	070,72
Location:	Just below Mongla			Rake:	02 NE
GPS:	27.838696/86.734643			Lineation:	02,071
Notes:	Notch on SW end of strike line				

Thin Section Description:

Rock Type:	Biotite gneiss
Mineralogy:	Biotite, albite, quartz, white mica (sericite)
Microstructure:	Mostly equigranular texture, weak foliation, micas randomly organized, brittle plains visible, sericitized feldspars common along brittle fracture (Image 14)
Shear Sense:	None
LPO:	Weak quartz LPO
Qtz. grains:	Subgrain rotation recrystallization, as well as high temperature grain boundary migration (Image 15), quartz shows undulose extinction, subgrains exhibiting polygonal texture, however, there are also some completely recrystallized grains



Type of Lineation:
Weak ductile stretching lineation

Sense of Shear:
N./A.

Metamorphic grade:
Sillimanite grade, SGR and GBM recrystallization

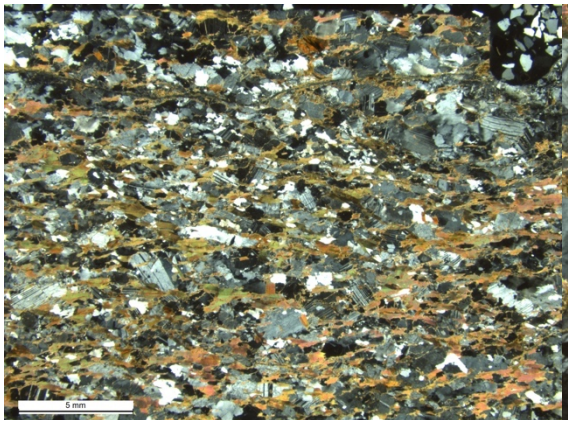


Image 13

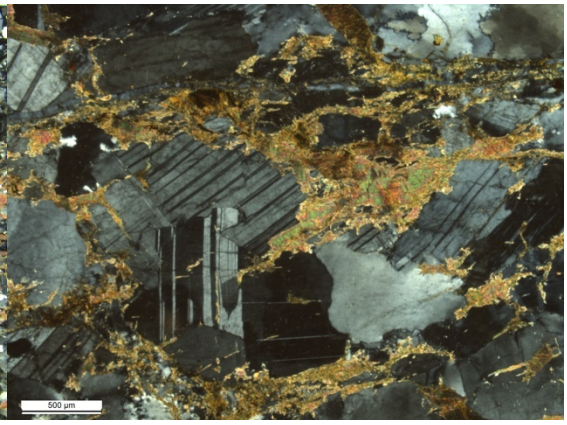


Image 14

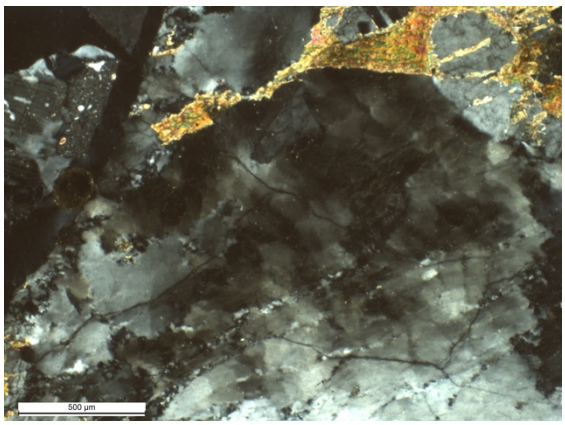


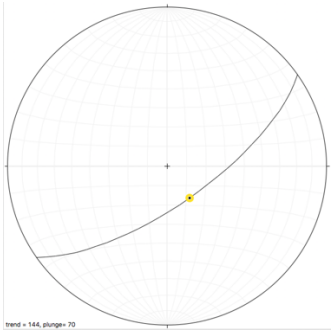
Image 15

Lineation orientation: top right

Sample:	**17N 3d1**	Map label:	5	Foliation:	055,70
Location:	Trail down from Mongla			Rake:	90
GPS:	27.841271/86.736687			Lineation:	70,144
Notes:	No surface lineation visible				

Thin Section Description:

Rock Type:	Biotite gneiss
Mineralogy:	Biotite, muscovite, quartz, feldspars, white mica (sericite), garnet
Microstructure:	Mostly equigranular texture, weak foliation, quartz bands clearly separated from mica rich bands, heavily sericitized thin section (Image 17), altered garnet (Image 18)
Shear Sense:	None
LPO:	No distinguishable LPO
Qtz. grains:	Fully recrystallized quartz, almost no deformation lamellae, subgrains, etc., (Image 19), high temperature grain boundary migration recrystallization



Type of Lineation:
Weak ductile-brittle mineral lineation

Sense of Shear:
N./A.

Metamorphic grade:
Sillimanite grade, GMB recrystallization

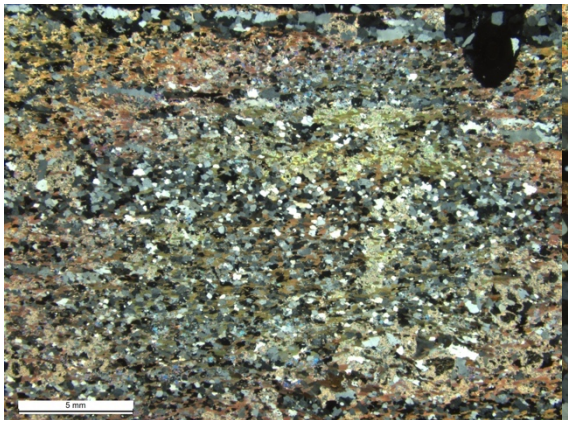


Image 16

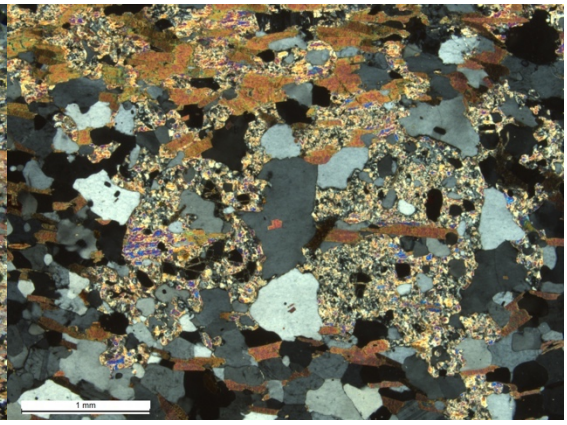


Image 17

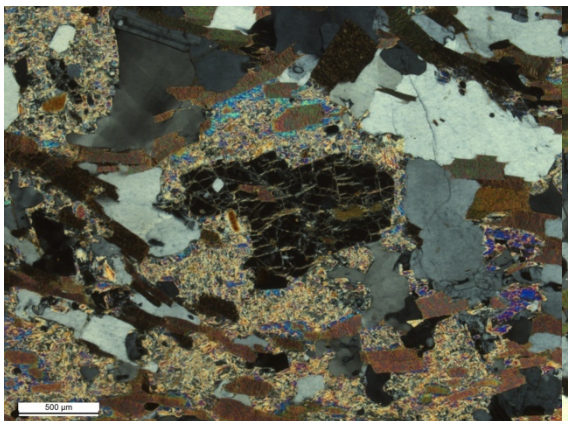


Image 18

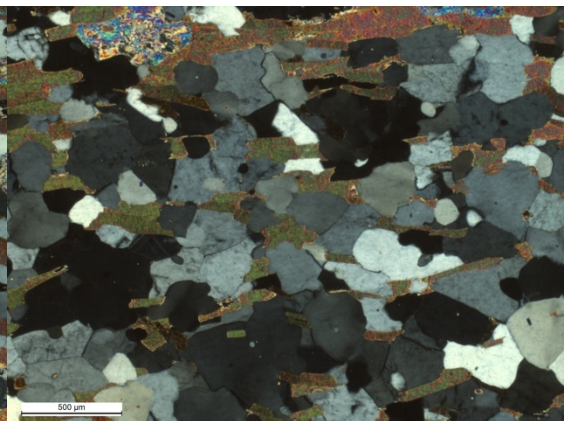


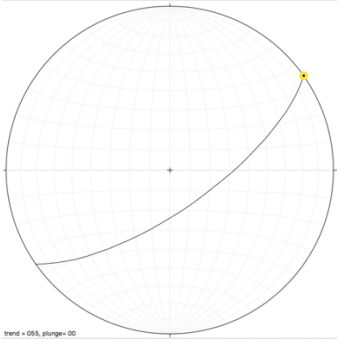
Image 19

Lineation orientation: top right

Sample:	**17N 3d2**	Map label:	5	Foliation:	055,70
Location:	Trail down from Mongla			Rake:	00
GPS:	27.841271/86.736687			Lineation:	00,055
Notes:	No surface lineation visible				

Thin Section Description:

Rock Type:	Biotite gneiss
Mineralogy:	Biotite, muscovite, quartz, feldspars, white mica (sericite), garnet
Microstructure:	Mostly equigranular texture, weak foliation, quartz bands clearly separated from mica rich bands, heavily sericitized thin section, altered garnet
Shear Sense:	None
LPO:	No distinguishable LPO
Qtz. grains:	Fully recrystallized quartz, almost no deformation lamellae, subgrains, etc., high temperature grain boundary migration recrystallization



Type of Lineation:
Weak ductile-brittle mineral lineation

Sense of Shear:
N./A.

Metamorphic grade:
Sillimanite grade, GMB recrystallization

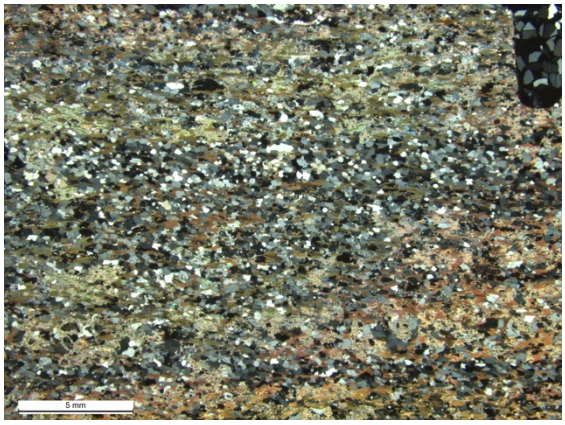


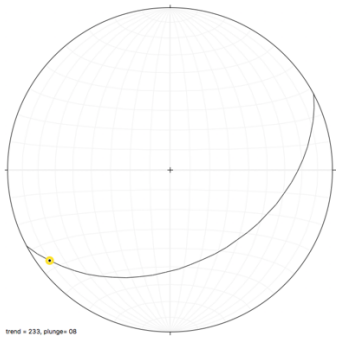
Image 20

Lineation orientation: top right

Sample:	**17N 3e**	Map label: 6	Foliation: 062,41
Location:	Further down the trail from Mongla		Rake: 12SW
GPS:	27.845260/86.740941		Lineation: 08,233
Notes:	Sillimanite growing on fault fabric		

Thin Section Description:

Rock Type:	Biotite, sillimanite gneiss
Mineralogy:	Biotite, sillimanite, orthoclase, quartz, muscovite, white mica (sericite)
Microstructure:	Porphyroblasitc orthoclase band surrounded by equigranular quartz, mica matrix. Sillimanite present within top of thin section (notch side) which has been clearly sheared (Image 22), feldspars exhibit perthitic texture
Shear Sense:	Difficult to determine
LPO:	No distinguishable LPO
Qtz. grains:	Subgrain rotation recrystallization, quartz grains show individual subgrains with a polygonal texture (Image 23)



Type of Lineation:
Weak ductile stretching lineation

Sense of Shear:
N./A.

Metamorphic grade:
Sillimanite grade, SGR recrystallization

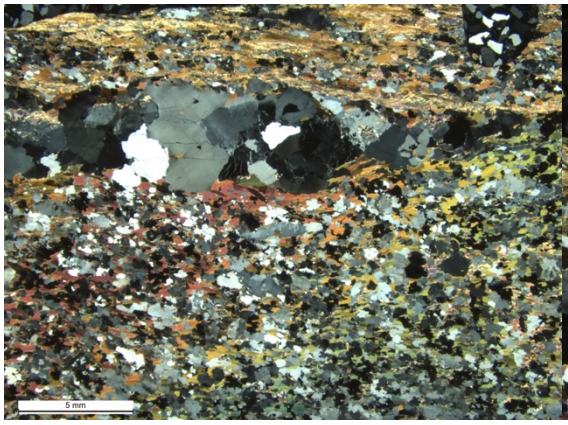


Image 21

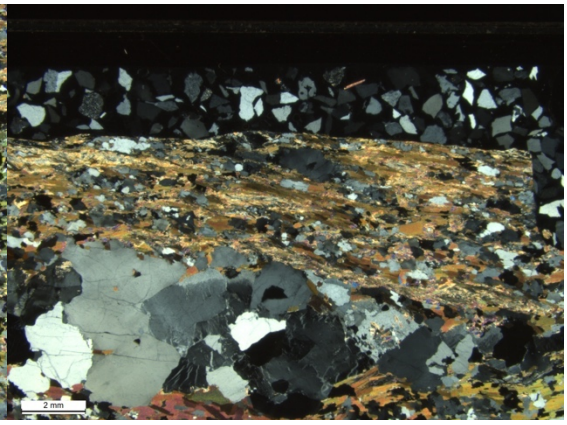


Image 22

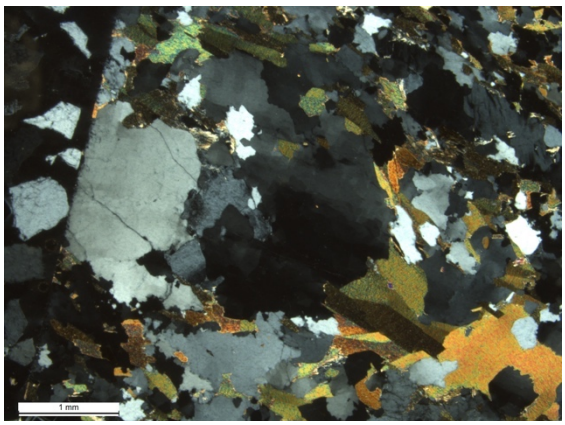


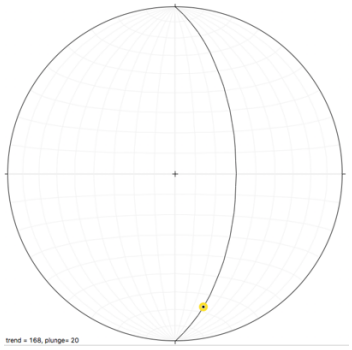
Image 23

Lineation orientation: top right

Sample:	**17N 4a**	Map label: 7	Foliation: 000,60
Location:	Phortse trail to Gokyo		Rake: 23S
GPS:	27.852706/86.750855		Lineation: 20,168
Notes:	Fresh exposure surface showing lineation. Entire outcrop shows highly sheared foliation with areas of higher pegmatite content.		

Thin Section Description:

Rock Type:	Biotite, sillimanite, garnet gneiss
Mineralogy:	Biotite, sillimanite, quartz, albite, garnet, orthoclase
Microstructure:	Equigranular texture with some orthoclase porphyroblasts, garnets being replaced by feldspars and micas (Image 25)
Shear Sense:	Difficult to determine
LPO:	No distinguishable LPO
Qtz. grains:	Subgrain rotation recrystallization, as well as high temperature grain boundary migration (Image 26), quartz shows undulose extinction, subgrains exhibiting polygonal texture, however, there are also some completely recrystallized grains



Type of Lineation:
Weak ductile stretching lineation

Sense of Shear:
N./A.

Metamorphic grade:
Sillimanite grade, SGR and GBM recrystallization

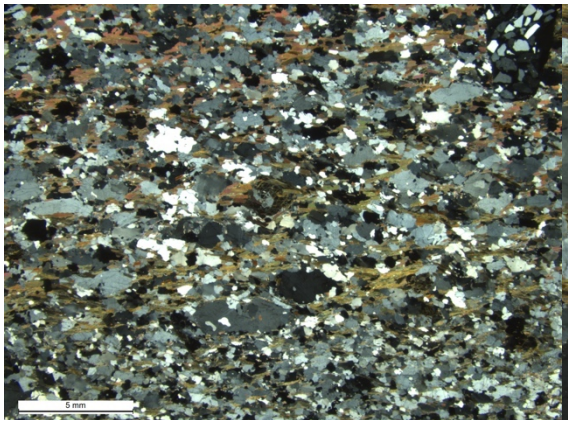


Image 24

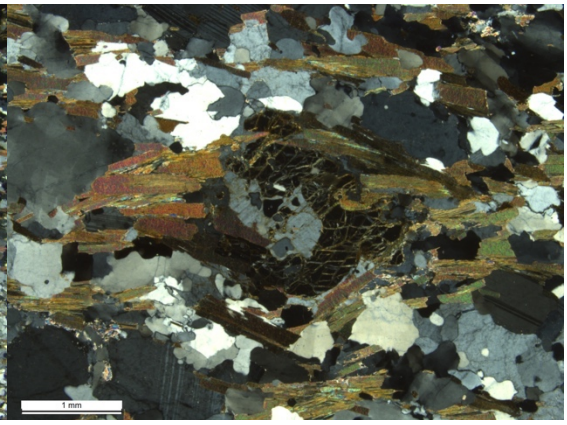


Image 25

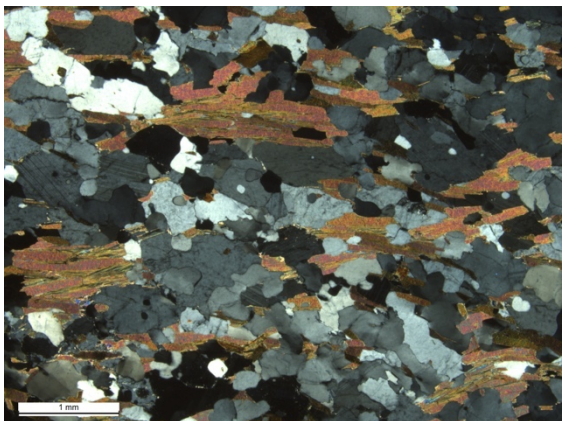


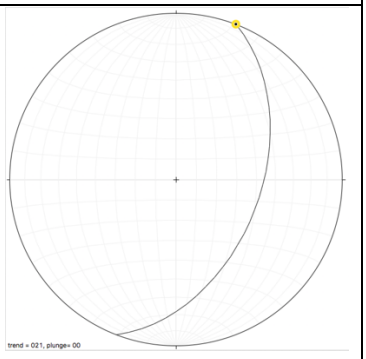
Image 26

Lineation orientation: top right

Sample:	**17N 4b**	Map label: 8	Foliation: 021,48
Location:	Khumbu climbing wall above Phortse		Rake: 0
			Lineation: 00,021
GPS:	27.859561/86.749333		
Notes:	Weathered exposure. Measurement might be inaccurate due to poor exposure of foliation. Large garnets present.		

Thin Section Description:

Rock Type:	Biotite, sillimanite gneiss
Mineralogy:	Biotite, sillimanite, orthoclase, quartz
Microstructure:	Equigranular texture with some coarse-grained orthoclase, sillimanite occurs along distinct bands, micas are randomly oriented, feldspars show perthitic texture
Shear Sense:	Sillimanite is acting as a shear zone, suggesting left-lateral sense of shear, low confidence (Image 28)
LPO:	No distinguishable LPO
Qtz. grains:	Fully recrystallized quartz, almost no deformation lamellae, subgrains, etc., high temperature grain boundary migration recrystallization (Image 29)



Type of Lineation:
Strong ductile stretching lineation

Sense of Shear:
Left-lateral

Metamorphic grade:
Sillimanite grade, GMB recrystallization

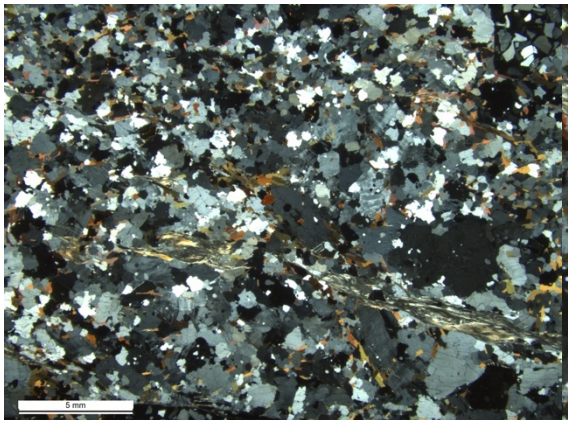


Image 27

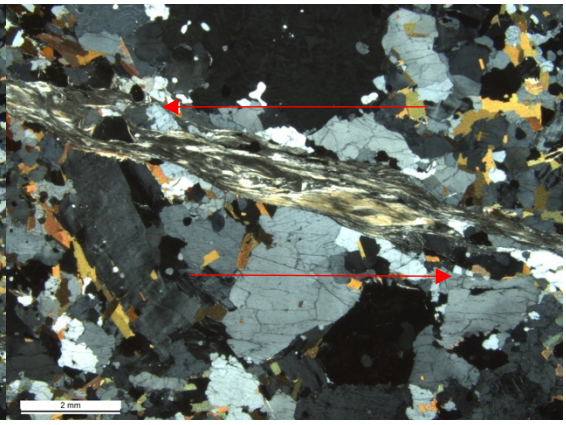


Image 28

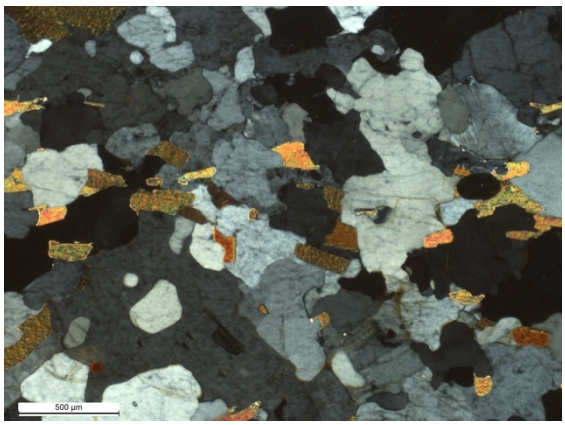


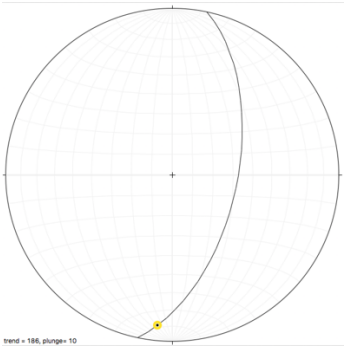
Image 29

Lineation orientation: top right

Sample:	**17N 4c**	Map label: 9	Foliation: 012,58
Location:	Pangboche trail, closest to corner		Rake: 12S
GPS:	27.846196/86.762198		Lineation: 10,186
Notes:			

Thin Section Description:

Rock Type:	Biotite gneiss
Mineralogy:	biotite, quartz, albite, orthoclase
Microstructure:	Equigranular texture, highly recrystallized quartz
Shear Sense:	None
LPO:	No distinguishable LPO
Qtz. grains:	Fully recrystallized quartz, almost no deformation lamellae, subgrains, etc., high temperature grain boundary migration recrystallization (Image 31)



Type of Lineation:
Weak ductile stretching lineation

Sense of Shear:
N./A.

Metamorphic grade:
Sillimanite grade, GMB recrystallization

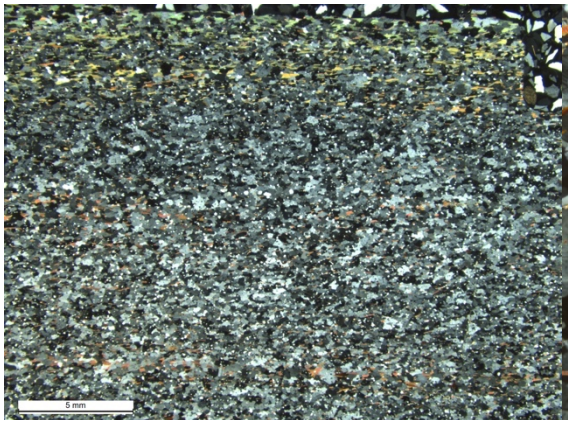


Image 30

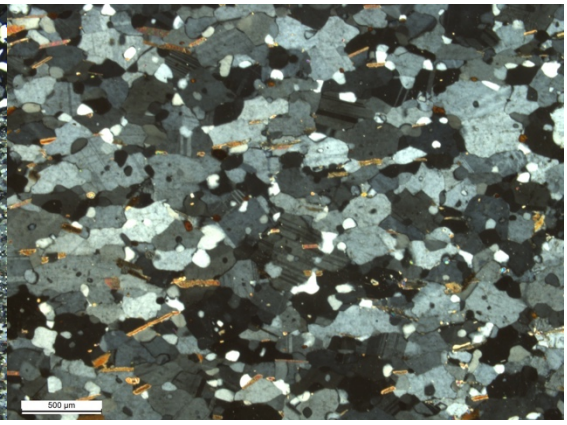


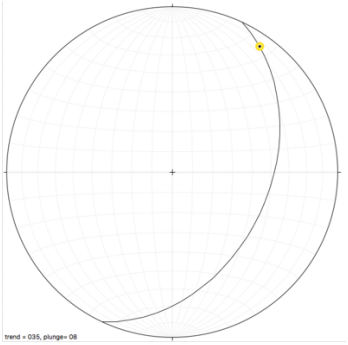
Image 31

Lineation orientation: top right

Sample:	**17N 4d**	Map label: 10	Foliation: 025,41
Location:	Pangboche trail between corner and Phortse		Rake: 13NE
GPS:	27.846755/86.761269		Lineation: 08,035
Notes:	Augen gneiss present		

Thin Section Description:

Rock Type:	Biotite gneiss
Mineralogy:	Biotite, quartz, albite, orthoclase, microcline, white mica (sericite)
Microstructure:	Orthoclase porphyroblasts surrounded by equigranular texture, high amount of quartz recrystallization, feldspars show perthitic texture, some sericitization of feldspars occurring
Shear Sense:	None
LPO:	No distinguishable LPO
Qtz. grains:	Subgrain rotation recrystallization, as well as high temperature grain boundary migration recrystallization (Image 33), quartz shows undulose extinction, subgrains exhibiting polygonal texture, however, there are also some completely recrystallized grains



Type of Lineation:
Weak ductile stretching lineation

Sense of Shear:
N./A.

Metamorphic grade:
Sillimanite grade, SGR and GBM recrystallization

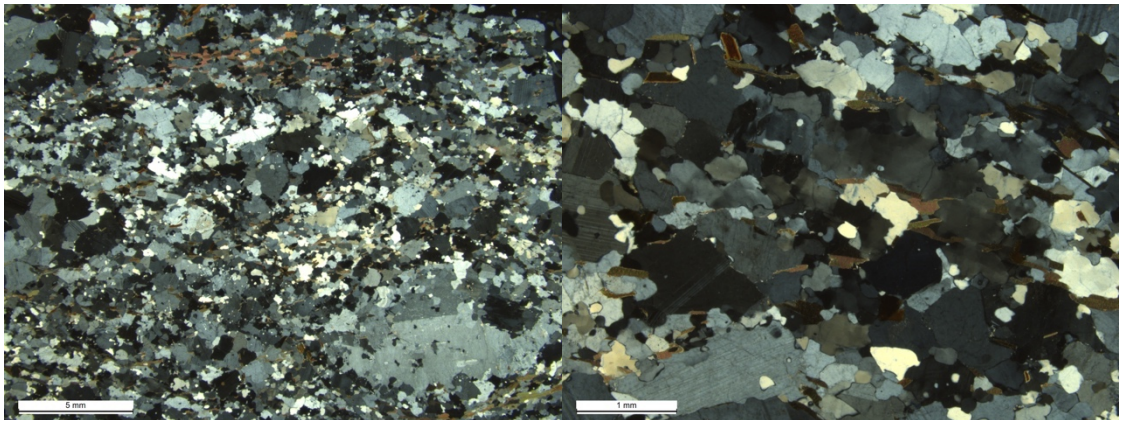


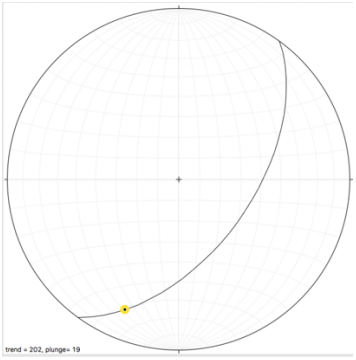
Image 32 Image 33

Lineation orientation: top right

Sample:	**17N 4e**	Map label:	11	Foliation:	036,55
Location:	Pangboche, close to 17N 4d			Rake:	23SW
GPS:	27.846851/86.760756			Lineation:	19,202
Notes:	Lineation visible				

Thin Section Description:

Rock Type:	Biotite gneiss
Mineralogy:	Biotite, quartz, orthoclase, albite
Microstructure:	Equigranular, mainly quartz, mostly recrystallized by quartz, almost looks igneous
Shear Sense:	None
LPO:	No distinguishable LPO
Qtz. grains:	Fully recrystallized quartz, almost no deformation lamellae, subgrains, etc., high temperature grain boundary migration recrystallization (Image 35)



Type of Lineation:
Very weak ductile stretching lineation

Sense of Shear:
N./A.

Metamorphic grade:
Sillimanite grade, GMB recrystallization

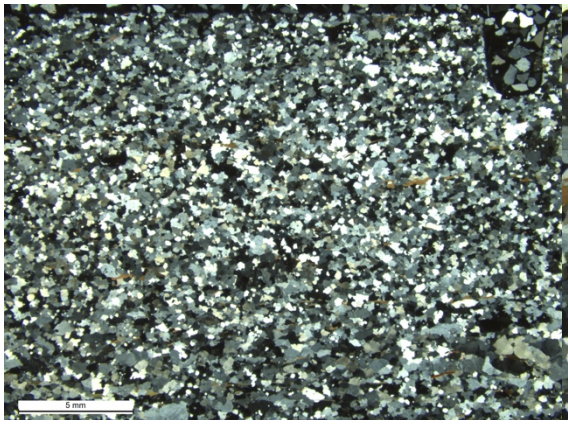


Image 34

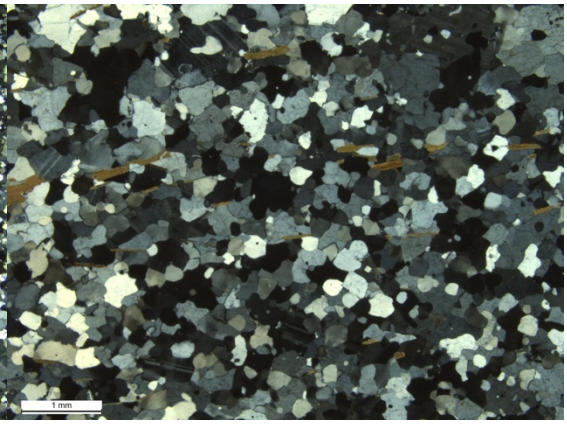


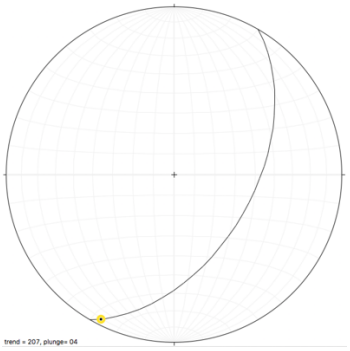
Image 35

Lineation orientation: top right

Sample:	**17N 4f**	Map label: 12	Foliation: 030,51
Location:	Pangboche climbing wall		Rake: 5SW
GPS:	27.847298/86.756366		Lineation: 04,207
Notes:	green color, lineation nicely visible (marked)		

Thin Section Description:

Rock Type:	Biotite, sillimanite gneiss
Mineralogy:	Biotite, muscovite, sillimanite, chlorite, quartz, orthoclase, albite, white mica (sericite)
Microstructure:	Equigranular texture, sheared sillimanite and muscovite banding (Image 37), some sericitization of feldspars
Shear Sense:	Mica fish within sillimanite bands showing top to the right (Image 38), weakly developed shear bands, suggesting left-lateral with low confidence
LPO:	No distinguishable LPO
Qtz. grains:	Subgrain rotation recrystallization, quartz grains show individual subgrains with a polygonal texture (Image 39)



Type of Lineation:
Strong ductile stretching lineation

Sense of Shear:
Left-lateral

Metamorphic grade:
Sillimanite grade, SGR recrystallization

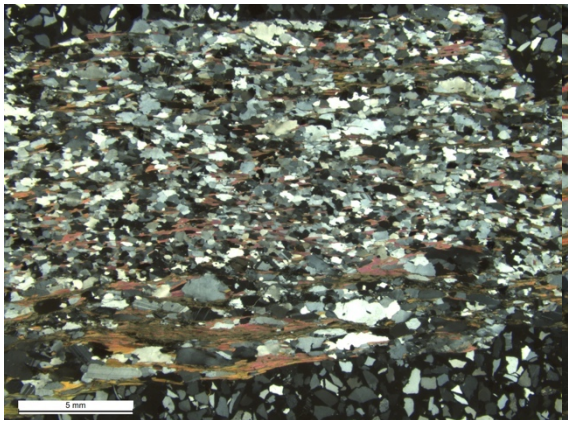


Image 36

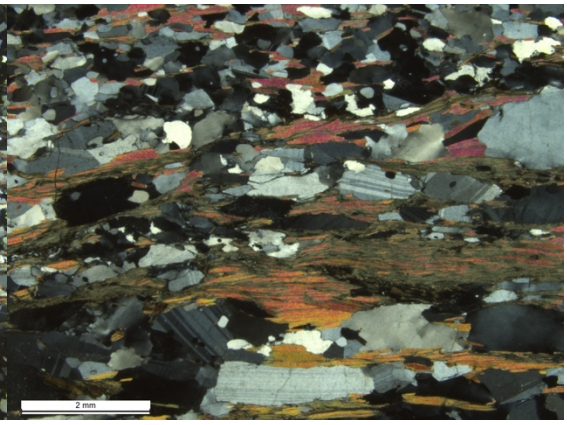


Image 37

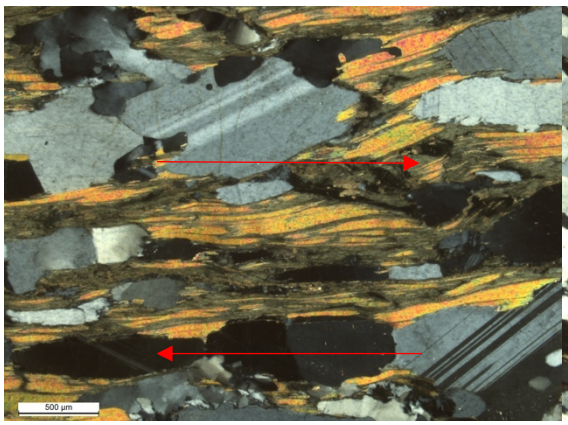


Image 38

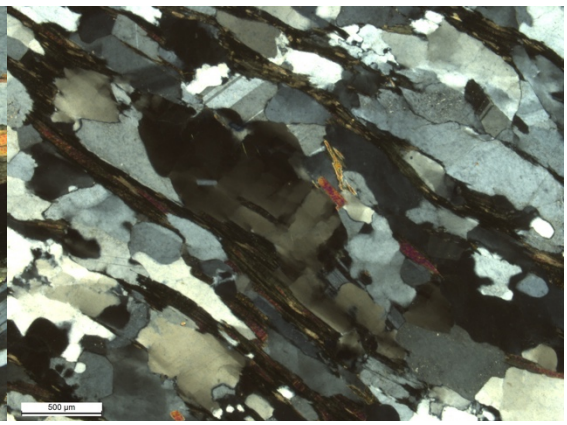


Image 39

Lineation orientation: top right

Sample:	**17N 5a** Map label: 13	Orientation: N./A.
Location:	Last outcrop before Pangboche	
GPS:	27.853317/86.778245	
Notes:	Unoriented sample for lithology. Possible east side of fault zone, anastomosing shear zone of several lithologies: granite, mafic?, calc-silicate	
	Thin Section Description:	Metamorphic grade: Sillimanite grade, GMB recrystallization
Rock Type:	Muscovite, sillimanite gneiss	
Mineralogy:	Orthoclase, sillimanite, muscovite, quartz, albite, sericite, phlogopite?	
Microstructure:	Orthoclase porphyroblasts on one side, the other shows equigranular quartz, muscovite, and sillimanite. Muscovite, sillimanite organized along random fabric, fluid metasomatism reaction visible and highly sericitized feldspars. This is a hydrothermally altered gneiss	
Shear Sense:	None	
LPO:	No distinguishable LPO	
Qtz. grains:	Fully recrystallized quartz, almost no deformation lamellae, subgrains, etc., high temperature grain boundary migration recrystallization (Image 41)	

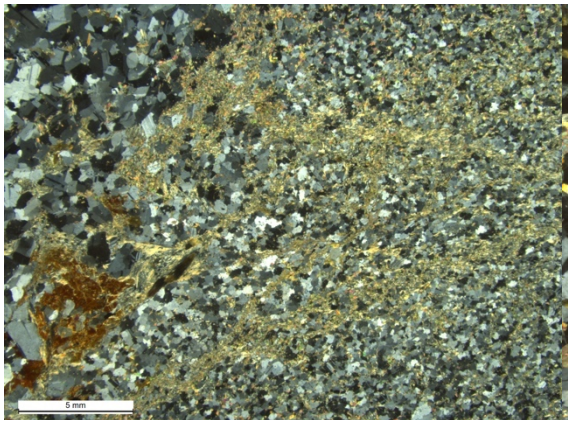


Image 40

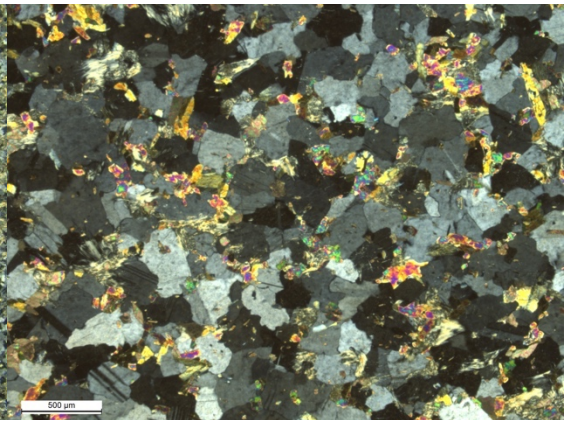


Image 41

Sample:	**17N 5b** Map label: 14	Orientation: N./A.
Location:	Last outcrop before Pangboche	
GPS:	27.853317/86.778245	
Notes:	Unoriented sample for lithology. Possible east side of fault zone, anastomosing shear zone of several lithologies: granite, mafic?, calc-silicate	
	Thin Section Description:	Metamorphic grade: Sillimanite grade, GMB recrystallization
Rock Type:	Calc-silicate	
Mineralogy:	Quartz, plagioclase, calcite, k-feldspar, muscovite	
Microstructure:	Equigranular texture, secondary alteration minerals present, difficult to determine	
Shear Sense:	None	
LPO:	No distinguishable LPO	
Qtz. grains:	Fully recrystallized quartz, almost no deformation lamellae, subgrains, etc., high temperature grain boundary migration recrystallization (Image 43)	

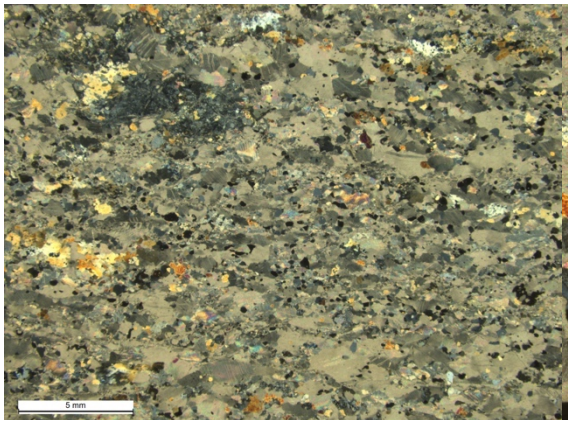


Image 42

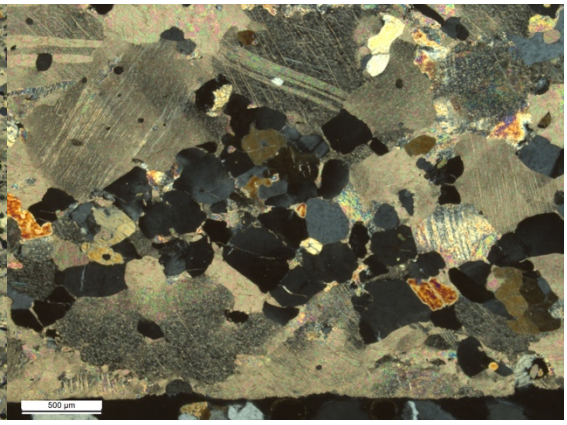
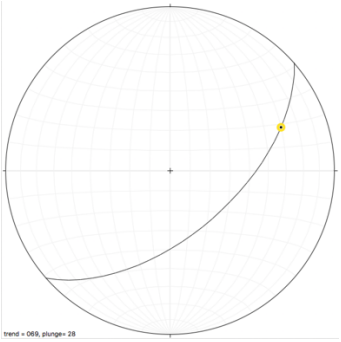


Image 43

Sample:	**17N 6a**	Map label: 15	Foliation: 049,58
Location:	Highest elevation up Tukla beyond Everest Memorial site		Rake: 34NE
			Lineation: 28,069
GPS:	27.938664/86.801524		
Notes:	Overturned. Heavily deformed layers of mylonite, biotite rich, plus pegmatite inclusions		

Thin Section Description:

Rock Type:	Biotite gneiss
Mineralogy:	Muscovite, biotite, orthoclase, albite, sericite, sillimanite
Microstructure:	Equigranular texture, some course-grained orthoclase, euhedral micas which are aligned along foliation. Micas have been extremely stretched. Sericitized feldspars common (Image 45)
Shear Sense:	Micas and sillimanite bands have been sheared but show no obvious sense of shear
LPO:	No distinguishable LPO
Qtz. grains:	Fully recrystallized quartz, almost no deformation lamellae, subgrains, etc., high temperature grain boundary migration recrystallization (Image 46)



Type of Lineation:
Ductile stretching lineation

Sense of Shear:
N./A.

Metamorphic grade:
Sillimanite grade, GMB recrystallization

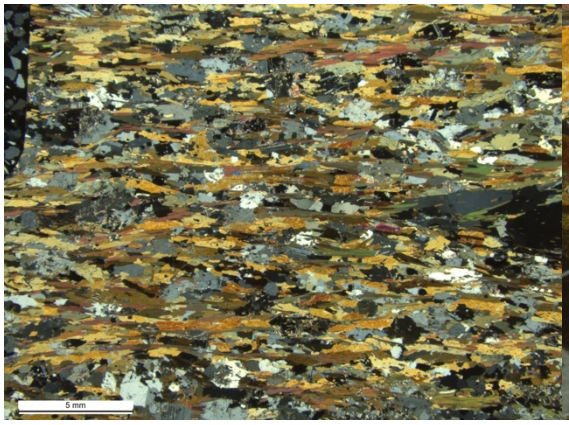


Image 44

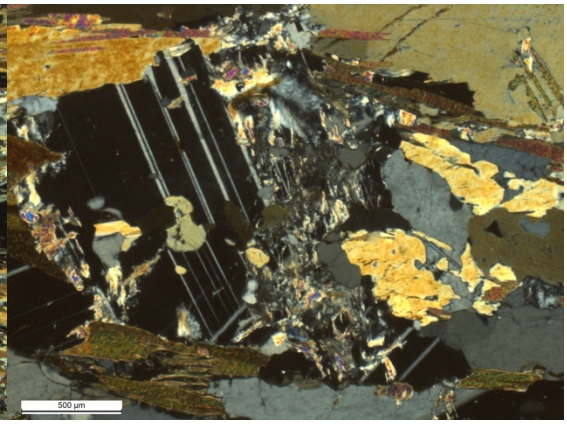


Image 55

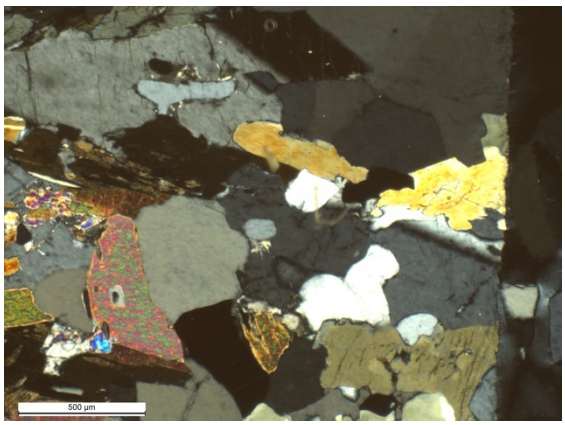


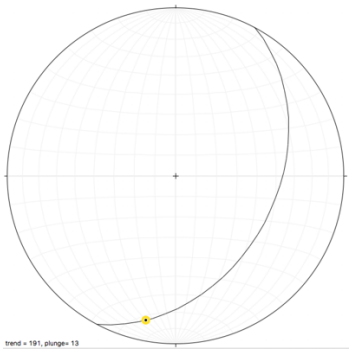
Image 56

Lineation orientation: top left

Sample:	**17N 8a**	Map label:	16	Foliation:	028,40
Location:	Walk up to Sanasa			Rake:	21SW
GPS:	27.827784/86.736216			Lineation:	13,191
Notes:	Stretched quartz grain fabric, beautiful horizontal lineation				

Thin Section Description:

Rock Type:	Biotite, garnet gneiss
Mineralogy:	Biotite, garnet, muscovite, orthoclase, quartz, sillimanite, sericite
Microstructure:	Equigranular, course-grained texture, micas surrounding orthoclase and quartz, no obvious pattern to their distribution, feldspars show sericitization and perthitic texture
Shear Sense:	Difficult to distinguish (Image 58)
LPO:	Weak quartz LPO
Qtz. grains:	Subgrain rotation recrystallization, as well as high temperature grain boundary migration recrystallization (Image 56 and 57), quartz shows undulose extinction, subgrains exhibiting polygonal texture, however, there are also some completely recrystallized grains



Type of Lineation:
Strong brittle-ductile mineral lineation

Sense of Shear:
N./A.

Metamorphic grade:
Sillimanite grade, SGR and GBM recrystallization

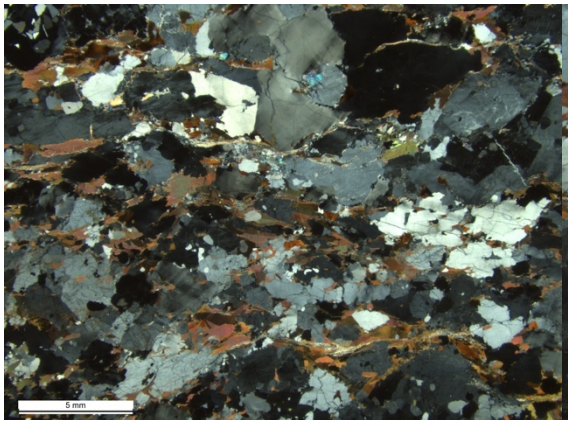


Image 57

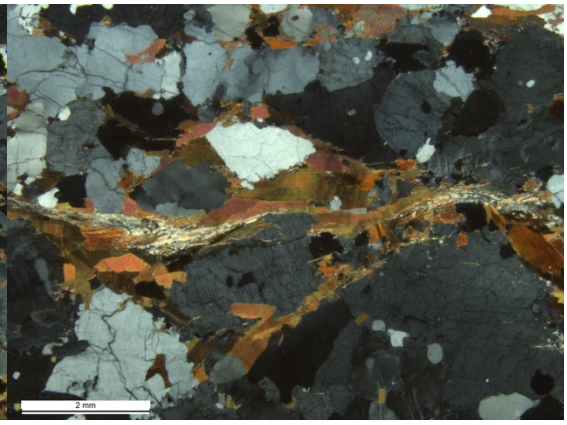


Image 58

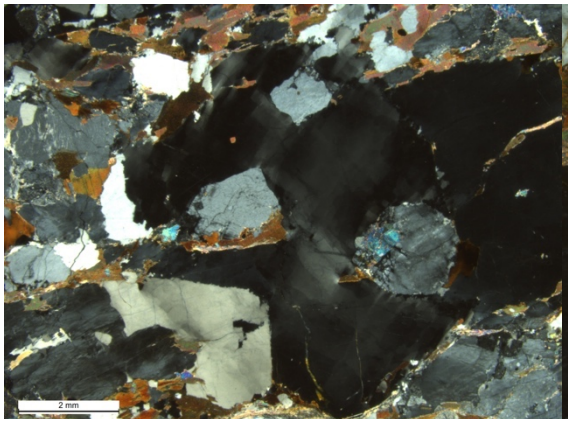


Image 59

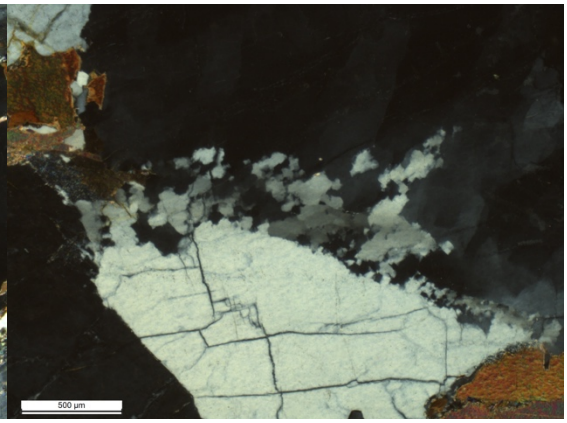


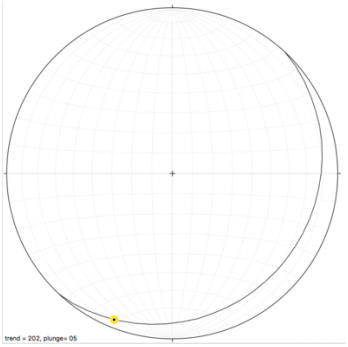
Image 60

Lineation orientation: top left

Sample:	**17N 8b**	Map label: 17	Foliation: 043,15
Location:	Before Sanasa lookout, close to 17N 8a		Rake: 22SW
GPS:	27.826264/86.735439		Lineation: 05,202
Notes:	Beautiful sillimanite lineation		

Thin Section Description:

Rock Type:	Biotite, sillimanite gneiss
Mineralogy:	Sillimanite, biotite, quartz, garnet, k-feldspar
Microstructure:	Layers of course-grained quartz, separated by sillimanite and biotite layers, strong apparent strain variation, garnets show strain shadows (Image 62)
Shear Sense:	Overall foliation fish pattern indicates top to the right (Image 63), sillimanite accommodated a fair bit of strain (Image 64), possible shear bands, garnet strain shadows indicate top to the right
LPO:	Moderate quartz LPO
Qtz. grains:	Subgrain rotation recrystallization, quartz grains show individual subgrains with a polygonal texture (Image 65)



Type of Lineation:
Very strong ductile sillimanite stretching lineation

Sense of Shear:
Normal, right-lateral

Metamorphic grade:
Sillimanite grade, SGR recrystallization

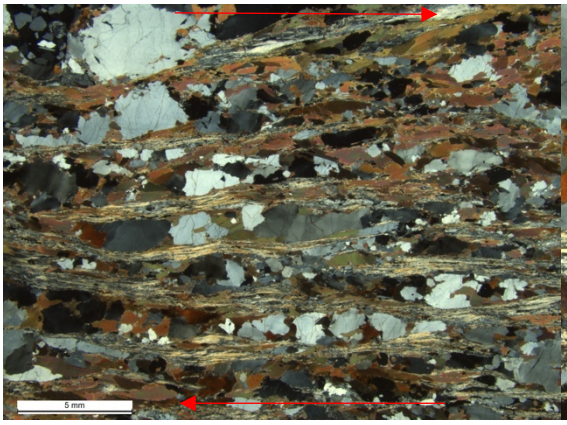


Image 61

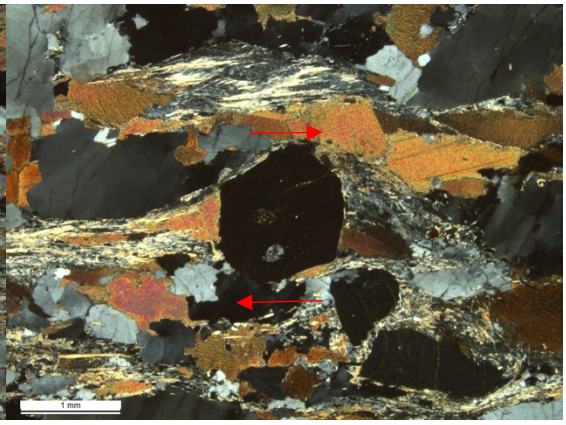


Image 62

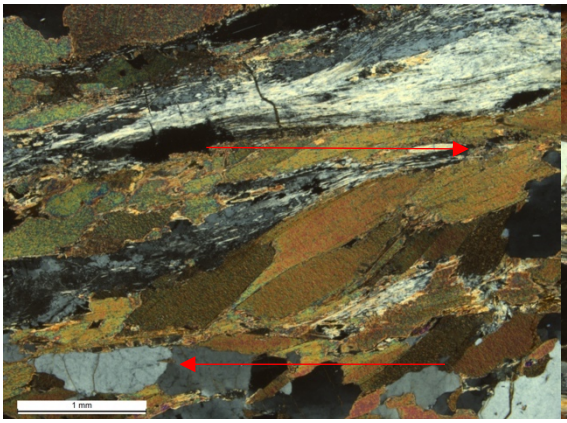


Image 63

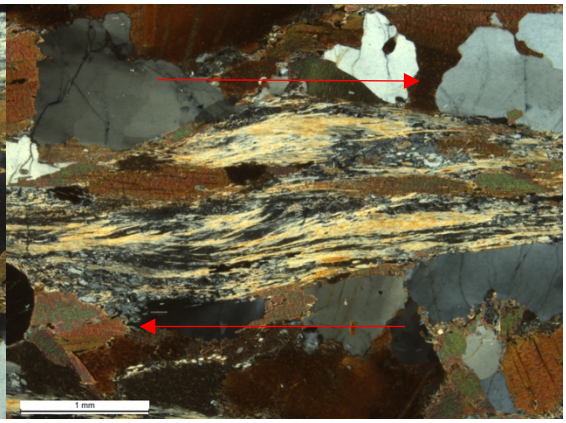


Image 64

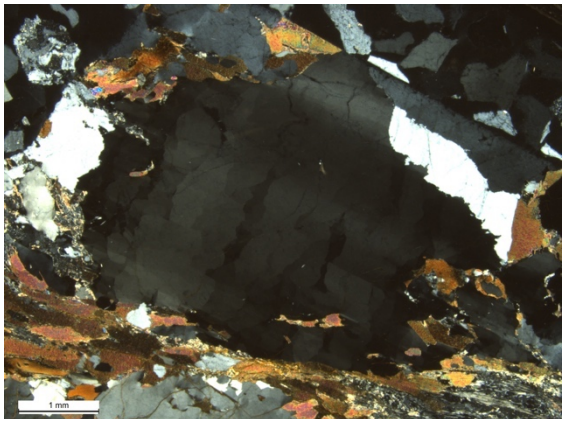
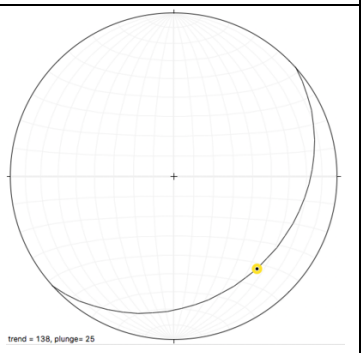


Image 65

Lineation orientation: top left

Sample:	**17N 8c**	Map label: 18	Foliation: 048,25
Location:	Before Sanasa lookout, close to 17N 8a		Rake: 90
GPS:	27.826264/86.735439		Lineation: 25,138
Notes:	Small grained biotite gneiss with surface lineation down-dip		

	Thin Section Description:
Rock Type:	Biotite, sillimanite gneiss
Mineralogy:	Quartz, biotite, sillimanite, sericite, garnet
Microstructure:	Some porphyroblasts of quartz and biotite surrounded by fine-grained quartz, biotite matrix, some course-grained biotite clusters, seemingly random. Sillimanite are oriented along foliation, feldspars are highly sericitized (Image 67), sillimanite is replacing biotite (Image 68)
Shear Sense:	None obvious
LPO:	No distinguishable LPO
Qtz. grains:	Subgrain rotation recrystallization, quartz grains show individual subgrains with a polygonal texture (Image 69)



Type of Lineation:
Strong brittle-ductile mineral lineation

Sense of Shear:
N./A.

Metamorphic grade:
Sillimanite grade, SGR recrystallization

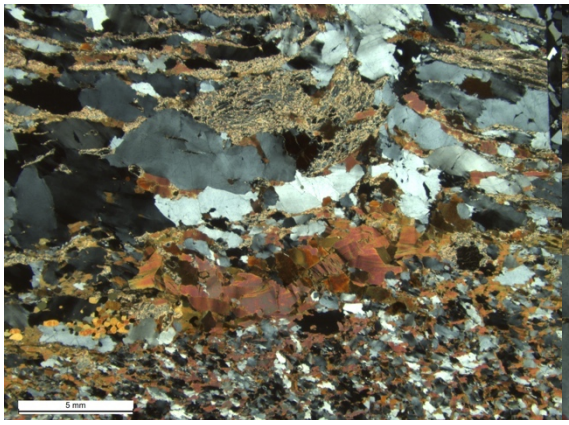


Image 66

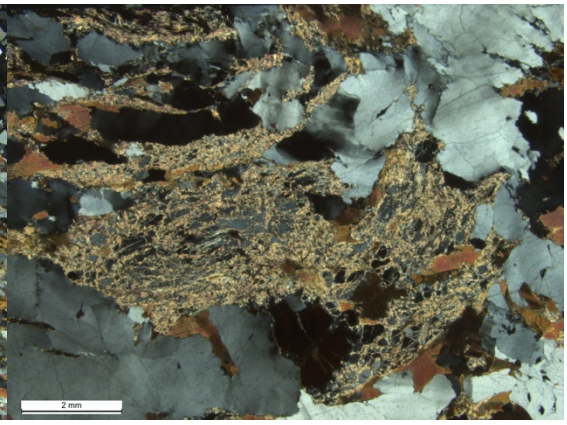


Image 67

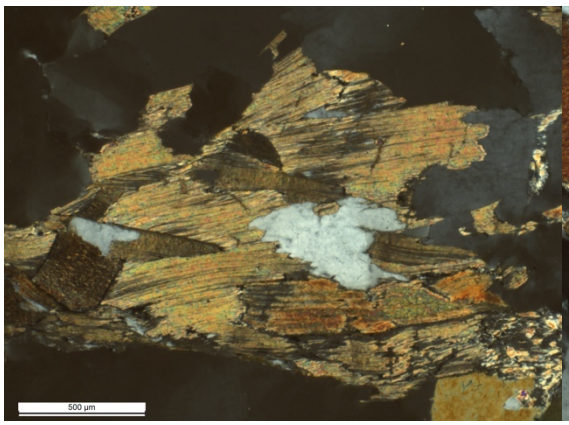


Image 68

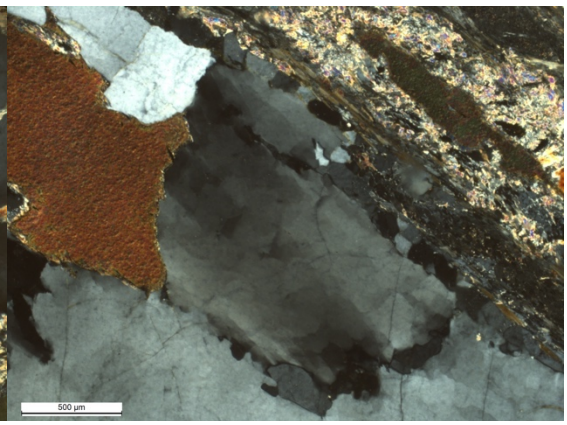


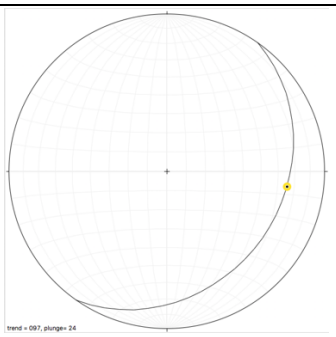
Image 69

Lineation orientation: top right

Sample:	**17N 9a**	Map label: 19	Foliation: 035,27
Location:	Walking out of Benkar, past waterfall		Rake: 65NE
GPS:	27.761194/86.712256		Lineation: 24,097
Notes:	Biotite gneiss with foliation down-dip. Interesting intersection of foliation and lineation		

Thin Section Description:

Rock Type:	Biotite gneiss
Mineralogy:	Biotite, quartz, muscovite, orthoclase, albite, sericite
Microstructure:	Equigranular texture, obvious alignment of micas along foliation, feldspars show myrmekitic texture (Image 71), perthitic texture, and sericitization
Shear Sense:	None obvious
LPO:	No distinguishable LPO
Qtz. grains:	Subgrain rotation recrystallization, quartz grains show individual subgrains with a polygonal texture (Image 72)



Type of Lineation:
Strong ductile stretching lineation

Sense of Shear:
N./A.

Metamorphic grade:
Sillimanite grade, SGR recrystallization

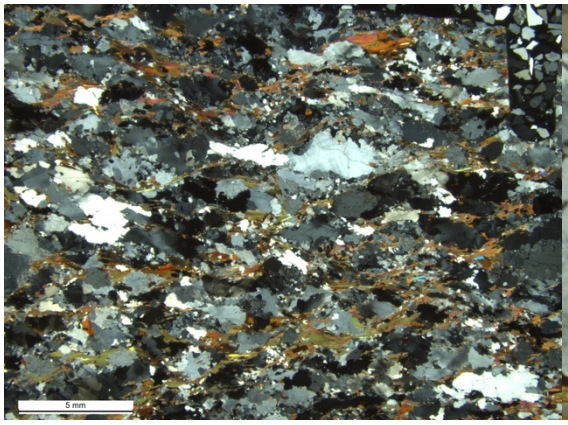


Image 70

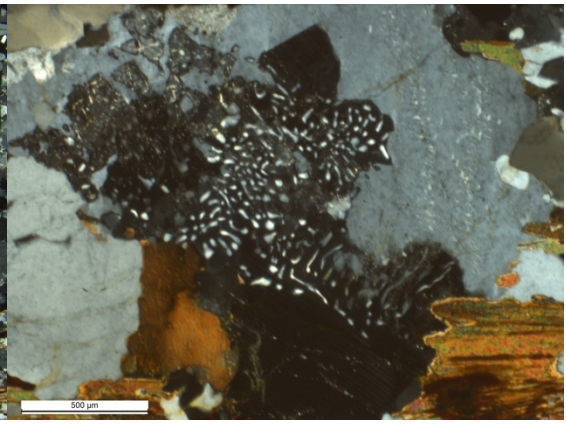


Image 71

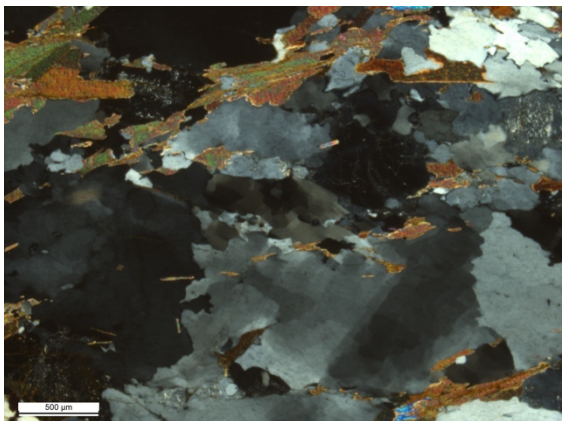


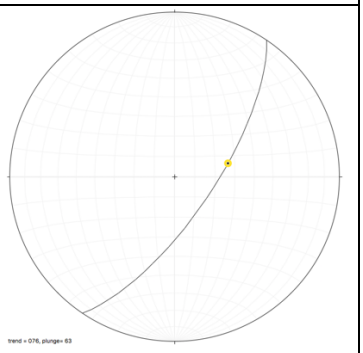
Image 72

Lineation orientation: top right

Sample:	**18N 2c**	Map label: 20	Orientation: 034,71
Location:	Valley towards Kongde Ri from Phakding		Foliation: 252,38
			Rake: ≈ 70 NE
GPS:	27.736557/86.698692		Lineation: ≈ 63,076
Notes:	Measurement on sample is a fracture, fracture seems to cut the ductile foliation, notch in reference to foliation surface, rake is approximate		

Thin Section Description:

Rock Type:	Quartzofeldspathic gneiss
Mineralogy:	Biotite, muscovite, quartz, orthoclase, sillimanite, microcline, albite
Microstructure:	Mostly equigranular texture, micas aligned along foliation, micas show shear, feldspars do not, apparent strain variation
Shear Sense:	Mica fish, small shear band (Image 74) indicating normal right-lateral sense of shear
LPO:	Shows distinct quartz LPO in quartz rich zones
Qtz. grains:	Subgrain rotation recrystallization, quartz grains show individual subgrains with a polygonal texture



Type of Lineation:
Ductile stretching lineation

Sense of Shear:
Normal

Metamorphic grade:
Sillimanite grade, SGR recrystallization

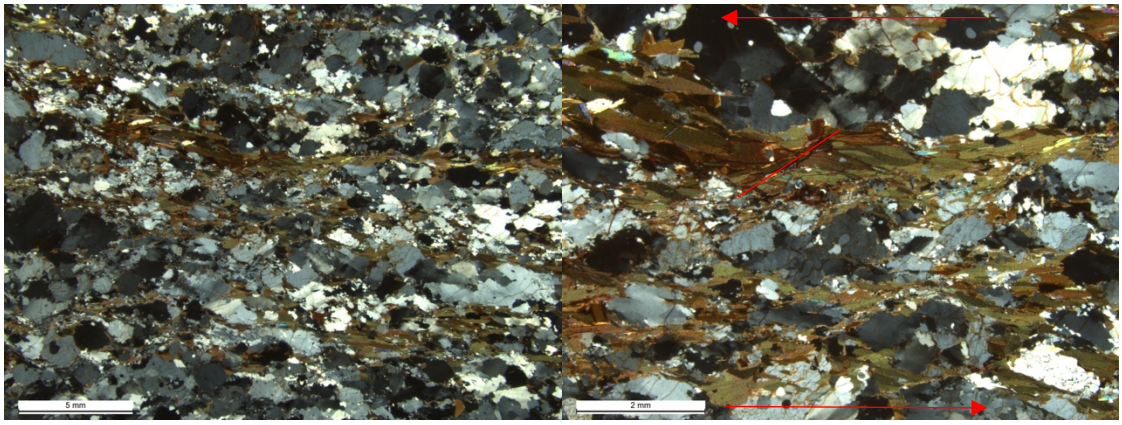


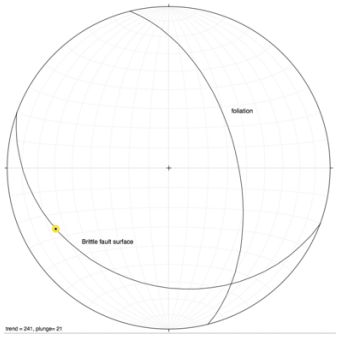
Image 73 Image 74

Lineation orientation: top right

Sample:	**18N 3a**	Map label: 21	Orientation: 110,28
Location:	1st sample towards Thamserku		Foliation: 346,55
GPS:	27.772457/86.730643		Rake: 52 NW
Notes:	Brittle slickenlines showing normal right-lateral sense of shear		Lineation: 22,242

Thin Section Description:

Rock Type:	Quartzofeldspathic gneiss
Mineralogy:	Quartz, biotite, muscovite, orthoclase, microcline, sillimanite, albite
Microstructure:	Equigranular fabric, foliation is crosscut by ductile/brittle surface rich in sillimanite, muscovite, and recrystallized quartz, evidence for brittle faulting
Shear Sense:	Ductile/brittle layer shows micas and sillimanite clasts leaning over towards the sense of shear (Image 76) indicating normal right-lateral sense of shear for the brittle/ductile surface
LPO:	Shows distinct quartz LPO in quartz rich zones
Qtz. grains:	Subgrain rotation recrystallization (Image 77), quartz grains show individual subgrains with a polygonal texture as well as distinct undulose extinction and deformation lamellae



Type of Lineation:
Brittle fault surface, slickenline striations

Sense of Shear:
Normal right-lateral

Metamorphic grade:
Sillimanite grade, SGR recrystallization

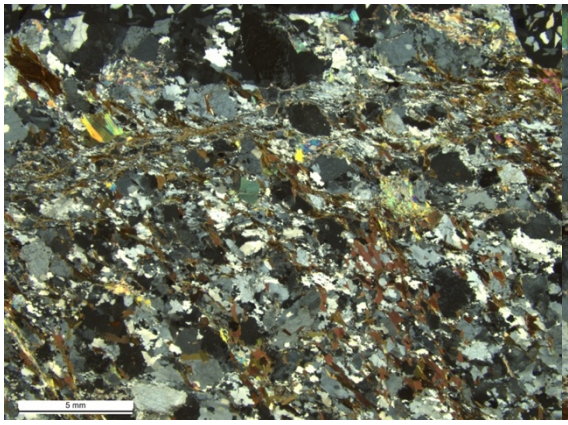


Image 75

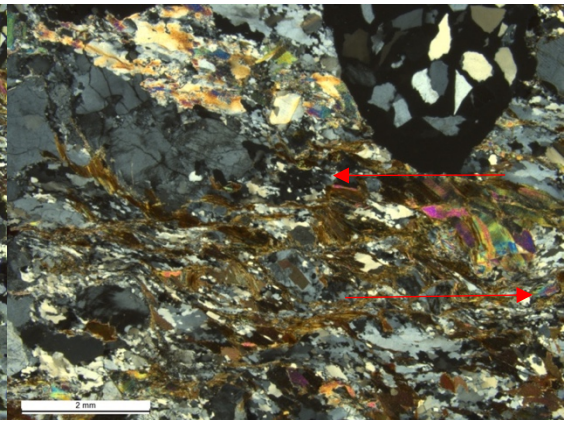


Image 76

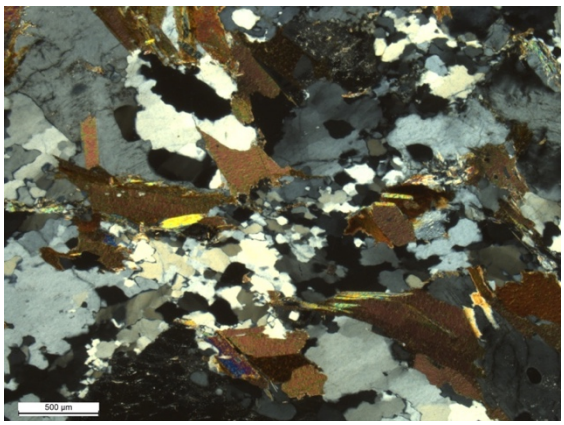


Image 77



Image 78

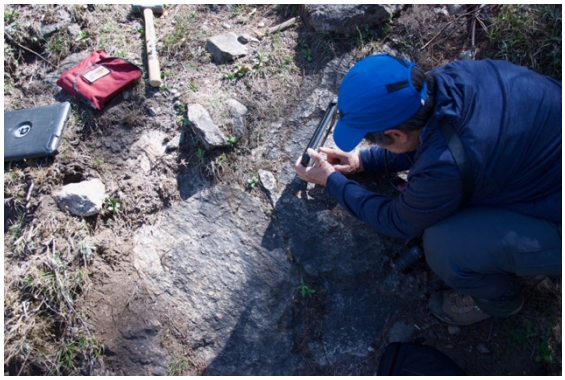


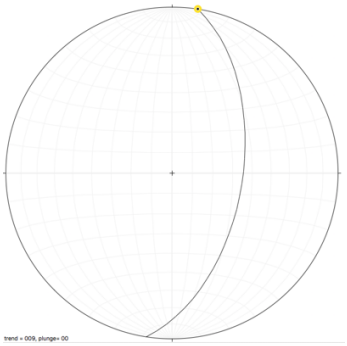
Image 79

Lineation orientation: top right

Sample:	**18N 3c**	Map label: 22	Foliation: 009,55
Location:	2nd sample towards Thamserku		Rake: 0
GPS:	27.773984/86.739224		Lineation: 00,009
Notes:	Overturned, notch on NE side of strike		

Thin Section Description:

Rock Type:	Quartzofeldspathic gneiss
Mineralogy:	Orthoclase, biotite, muscovite, garnet, albite, sillimanite, microcline
Microstructure:	Inequigranular texture, larger orthoclase porphyroblasts surrounded by quartz and mica matrix, highly fractured and recrystallized garnet replaced by micas (Image 81)
Shear Sense:	No fabric asymmetries visible
LPO:	No distinguishable LPO
Qtz. grains:	Fully recrystallized quartz, no deformation lamellae, subgrains, etc., (image 82), high temperature grain boundary migration recrystallization



Type of Lineation:
Ductile stretching lineation

Sense of Shear:
N./A.

Metamorphic grade:
Sillimanite grade, GMB recrystallization

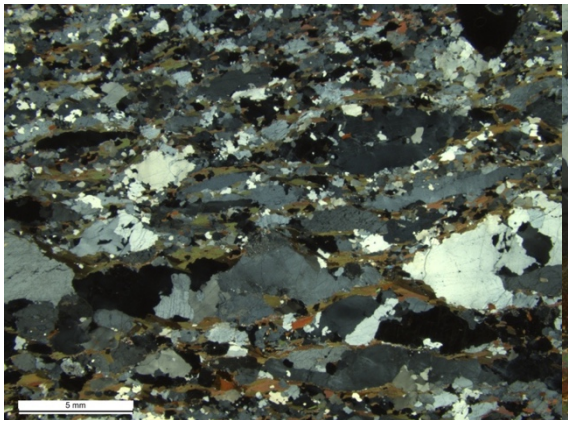


Image 80

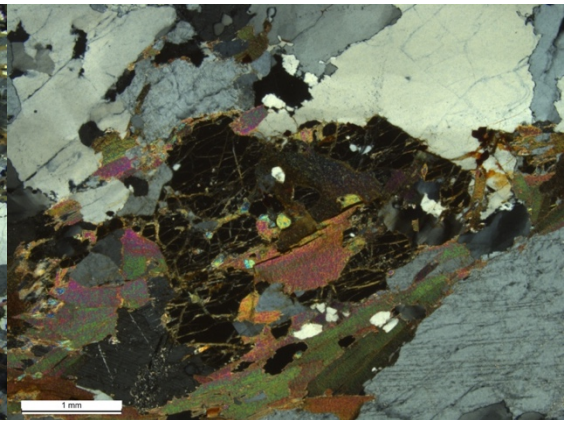


Image 81

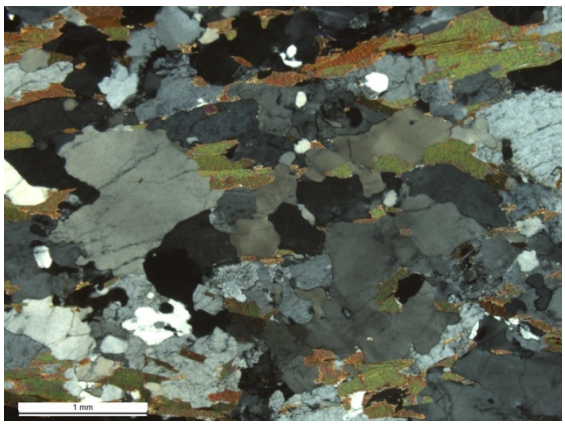


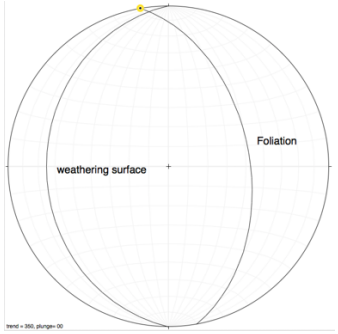
Image 82

Lineation orientation: top right

Sample:	**18N 3g**	Map label: 23	Orientation: 180,25
Location:	3rd sample towards Thamserku		Foliation: 350,48
GPS:	27.773484/86.740815		Rake: ≈ 0
Notes:	Measurement of weathering surface, sample for geochronology, notch on N side of strike line for foliation, rake is approximate		Lineation: ≈ 00,350

Thin Section Description:

Rock Type:	Quartzofeldspathic gneiss
Mineralogy:	Orthoclase, quartz, biotite, sillimanite, garnet
Microstructure:	Mostly equigranular texture with one area of orthoclase porphyroblasts, sillimanite organized in distinct bands, some feldspars show exsolution lamellae
Shear Sense:	Sillimanite bands leaning over in the direction of sense of shear (Image 84) suggests right-lateral sense of shear
LPO:	No distinguishable LPO
Qtz. grains:	Fully recrystallized quartz, no deformation lamellae, subgrains, etc., (Image 85), high temperature grain boundary migration recrystallization



Type of Lineation:
Ductile mineral stretching lineation

Sense of Shear:
Right-lateral

Metamorphic grade:
Sillimanite grade, GMB recrystallization

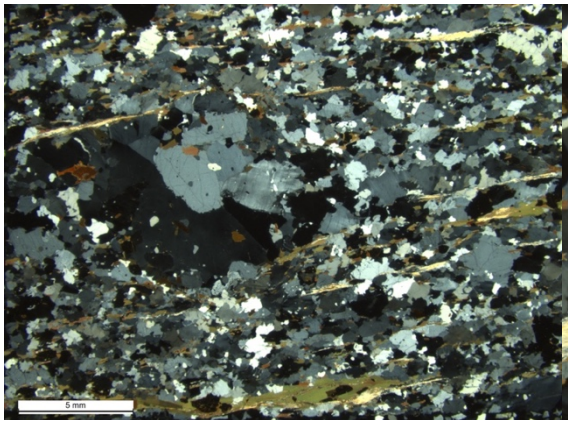


Image 83

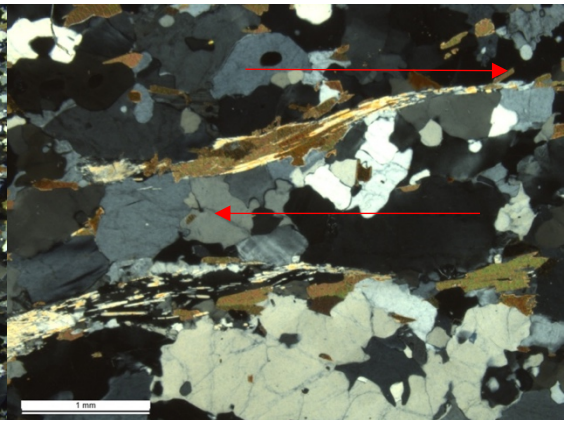


Image 84

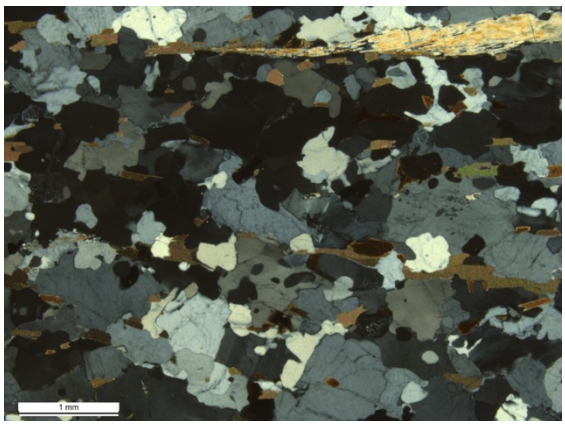


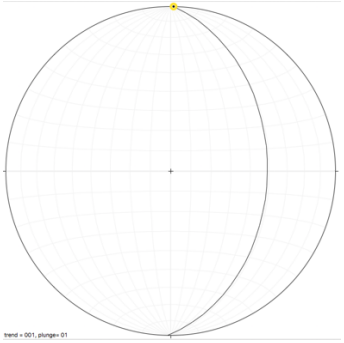
Image 85

Lineation orientation: top left

Sample:	**18N 4b**	Map label:	24	Foliation:	001,41
Location:	Before Namche hill			Rake:	0
GPS:	27.783777/86.722562			Lineation:	01,001
Notes:	Overturned sample, notch on NE side				

Thin Section Description:

Rock Type:	Biotite gneiss
Mineralogy:	Orthoclase, albite, quartz, biotite, garnet, sillimanite
Microstructure:	Fine grained equigranular texture, evidence for brittle fracturing (Image 87), highly replaced garnets, sillimanite rich zone perpendicular to foliation
Shear Sense:	No fabric asymmetries visible
LPO:	Slight LPO visible in quartz groupings
Qtz. Grains:	Subgrain rotation recrystallization (Image 88), quartz shows deformation lamellae and subgrains



Type of Lineation:
Ductile stretching lineation

Sense of Shear:
N./A.

Metamorphic grade:
Sillimanite grade, SGR recrystallization

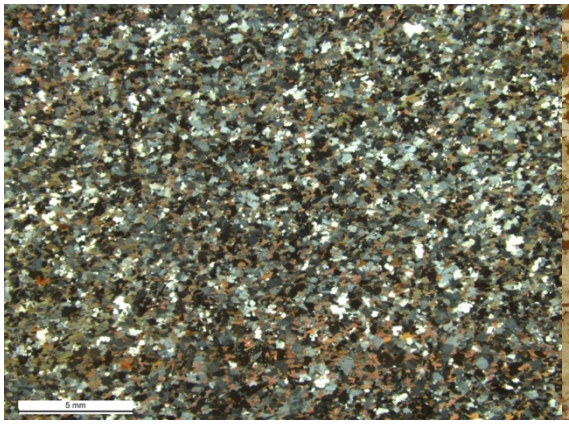


Image 86

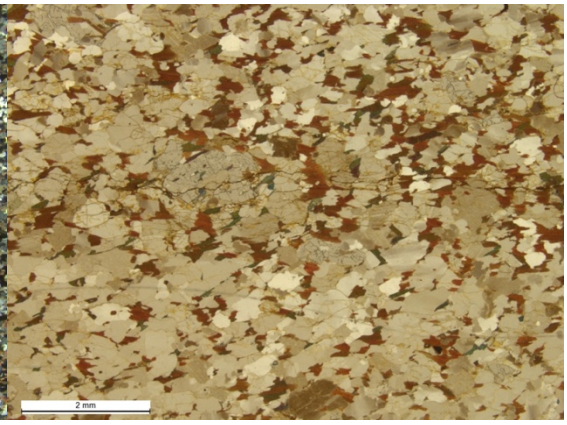


Image 87 (plane polarized light)

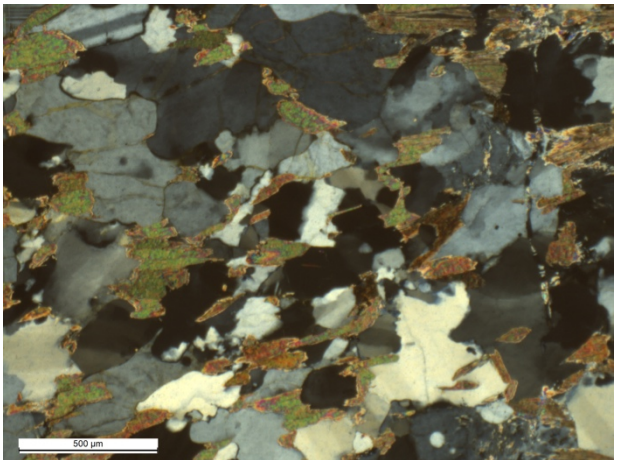


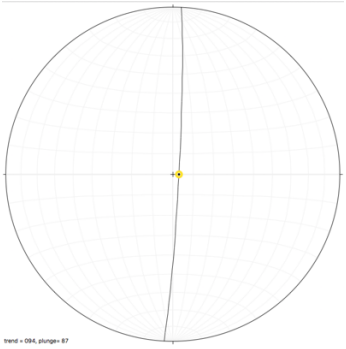
Image 88

Lineation orientation: top left

Sample:	**18N 5a**	Map label: 25	Foliation: 003,87
Location:	1st sample from Namche to Thame		Rake: 90
GPS:	27.809558/86.899688		Lineation: 87,090
Notes:	Thin laminae with pegmatites, lineation looks downdip on sample but is actually oblique to foliation, brittle slickenlines show normal right-lateral sense of shear		

Thin Section Description:

Rock Type:	Quartzofeldspathic gneiss
Mineralogy:	Orthoclase, albite, microcline, quartz, biotite, muscovite, sillimanite
Microstructure:	Inequigranular texture, larger feldspar porphyroblasts separated by finer grained biotite, quartz, and sillimanite rich bands, some feldspars show exsolution lamellae
Shear Sense:	Mica fish (Image 90) suggests normal sense of shear in this sample and normal right-lateral in outcrop
LPO:	Distinct LPO where quartz is organized in thin bands
Qtz. grains:	Subgrain rotation recrystallization (Image 91), quartz shows deformation lamellae, bulging at grain boundaries and subgrains exhibiting polygonal texture



Type of Lineation:
Brittle slickenlines

Sense of Shear:
Normal

Metamorphic grade:
Sillimanite grade, SGR recrystallization

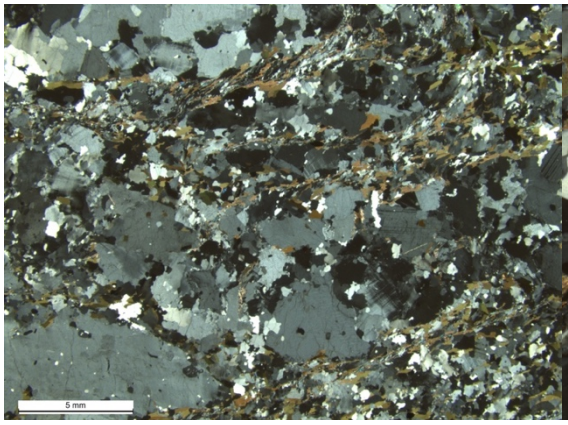


Image 89

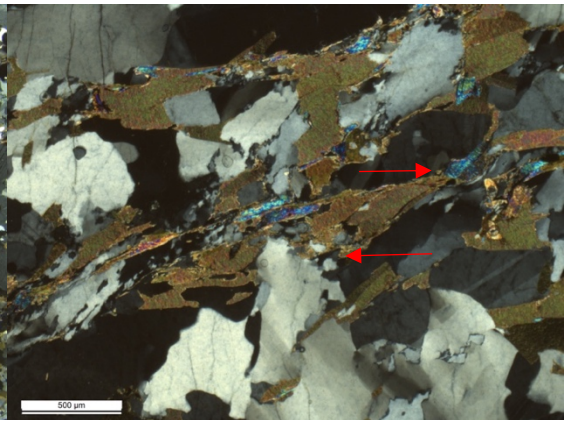


Image 90

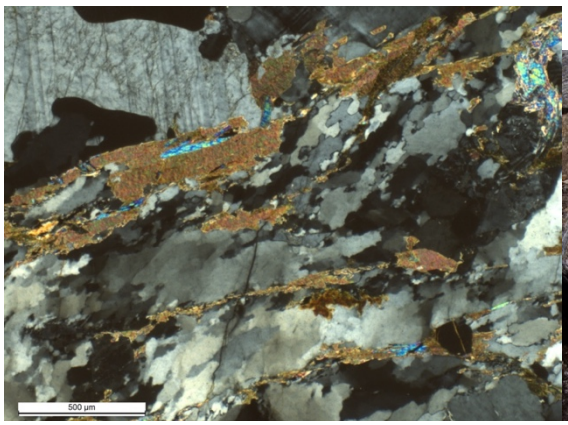


Image 91



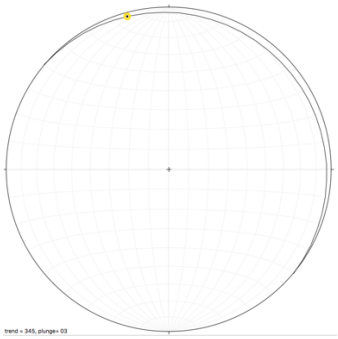
Image 92

Lineation orientation: top left

Sample:	**18N 5c**	Map label: 26	Foliation: 310,05
Location:	2nd sample from Namche to Thame		Rake: 35 NW
GPS:	27.811464/86.696218		Lineation: 03,345
Notes:	Augen gneiss		

Thin Section Description:

Rock Type:	Quartzofeldspathic gneiss
Mineralogy:	Orthoclase, microcline, quartz, biotite, muscovite, sillimanite
Microstructure:	Equigranular texture, some feldspars show exsolution lamellae, Myrmekite texture visible (Image 94)
Shear Sense:	No fabric asymmetries visible
LPO:	No distinguishable LPO
Qtz. grains:	Subgrain rotation recrystallization (Image 95), quartz shows undulose extinction and subgrains exhibiting polygonal texture



Type of Lineation:
Ductile stretching lineation

Sense of Shear:
N./A.

Metamorphic grade:
Sillimanite grade, SGR recrystallization

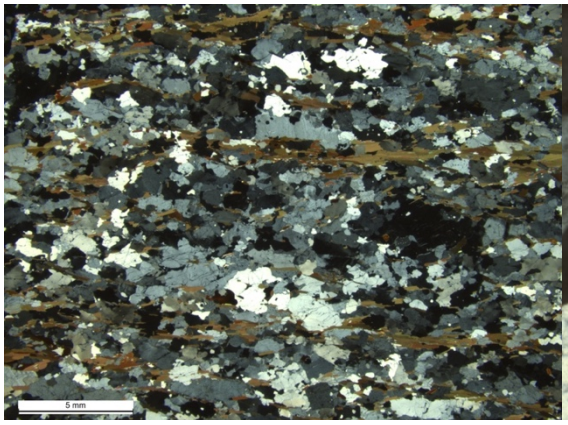


Image 93

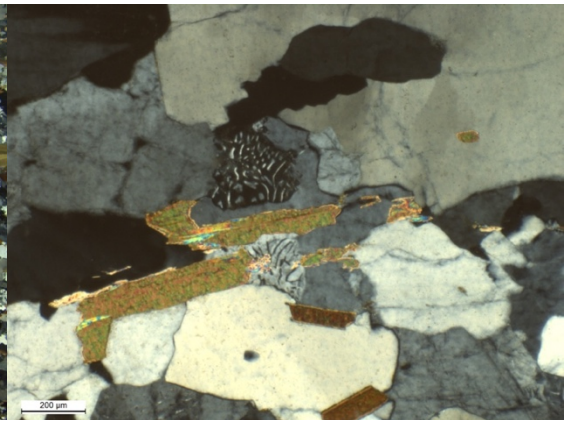


Image 94

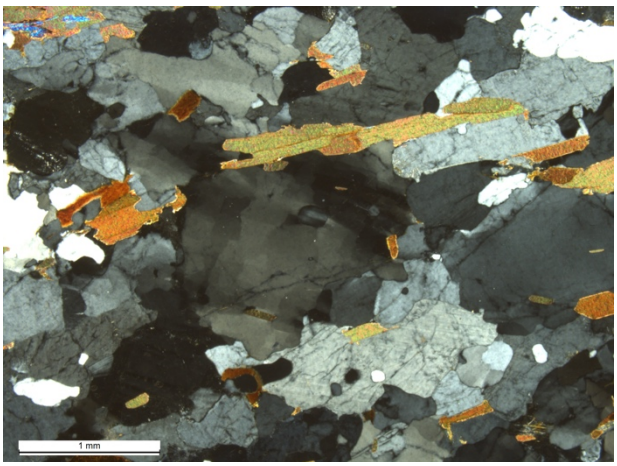


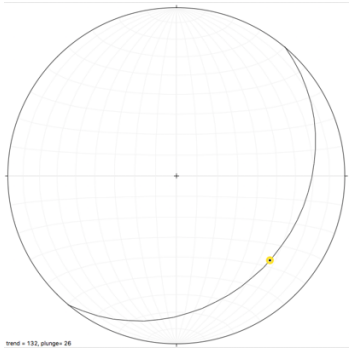
Image 95

Lineation orientation: top left

Sample:	**18N 5d**	Map label: 27	Foliation: 040,26
Location:	3rd sample from Namche to Thame		Rake: 88 SW
GPS:	27.820272/86.682378		Lineation: 26,132
Notes:	Sample taken for lithology		

Thin Section Description:

Rock Type:	Quartzite
Mineralogy:	Quartz, muscovite, biotite, albite, orthoclase, sillimanite
Microstructure:	Equigranular texture, feldspars are being replaced by muscovite and sillimanite (Image 97)
Shear Sense:	No fabric asymmetries visible
LPO:	Distinct LPO throughout
Qtz. grains:	Subgrain rotation recrystallization (Image 98), quartz shows undulose extinction and subgrains exhibiting polygonal texture



Type of Lineation:
Ductile stretching lineation

Sense of Shear:
N./A.

Metamorphic grade:
Sillimanite grade, SGR recrystallization

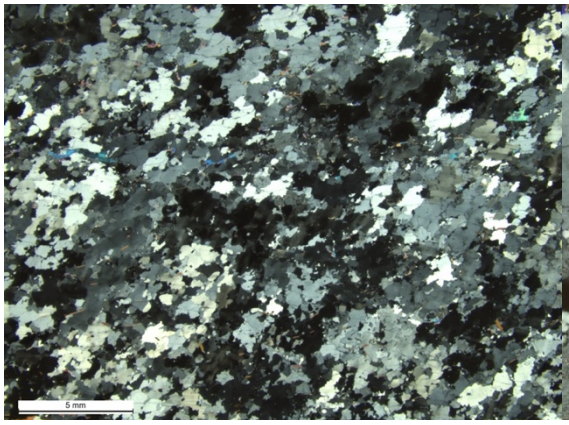


Image 96

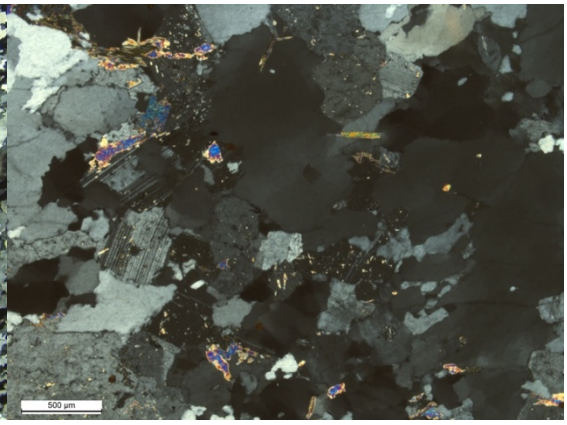


Image 97

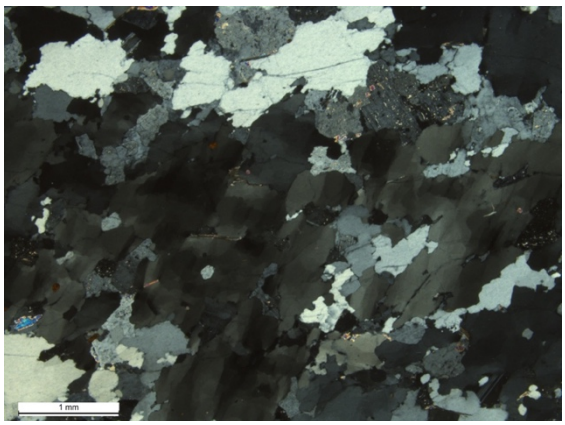


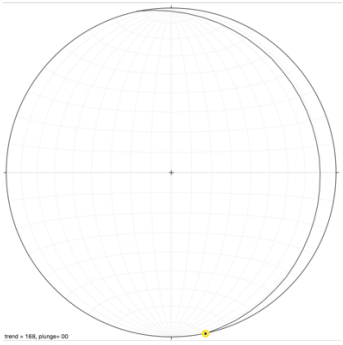
Image 98

Lineation orientation: top left

Sample:	**18N 7b** Map label: 28	Foliation: 348,11
Location:	Waterfall next to Hotel by Kongde Ri	Rake: 0
GPS:	27.782746/86.691529	Lineation: 00,168
Notes:	Biotite gneiss with gentle folding, notch on SE side	

Thin Section Description:

Rock Type:	Biotite gneiss
Mineralogy:	Quartz, muscovite, biotite, sillimanite, orthoclase
Microstructure:	Equigranular texture, very rich in micas, which are stretched and oriented along foliation
Shear Sense:	Micas are clearly stretched but do not indicate a sense of shear, they are very symmetrical (Image 100)
LPO:	Quartz shows LPO
Qtz. grains:	Subgrain rotation recrystallization (Image 101), quartz shows undulose extinction, subgrains exhibiting polygonal texture, and very strong deformation lamellae



Type of Lineation:
Ductile stretching lineation

Sense of Shear:
N./A.

Metamorphic grade:
Sillimanite grade, SGR recrystallization

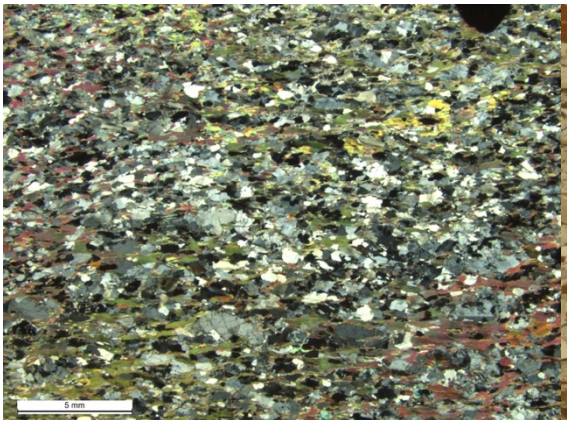


Image 99

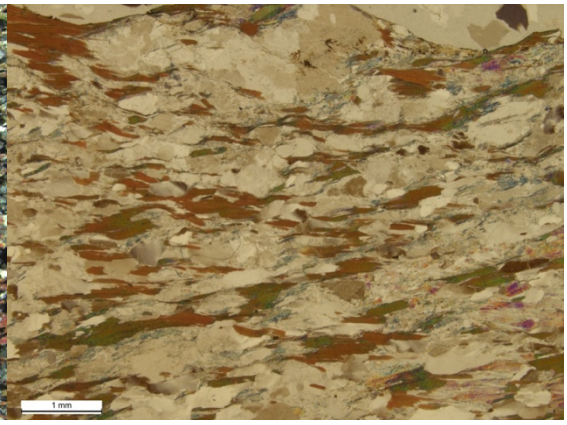


Image 100 (plane polarized light)

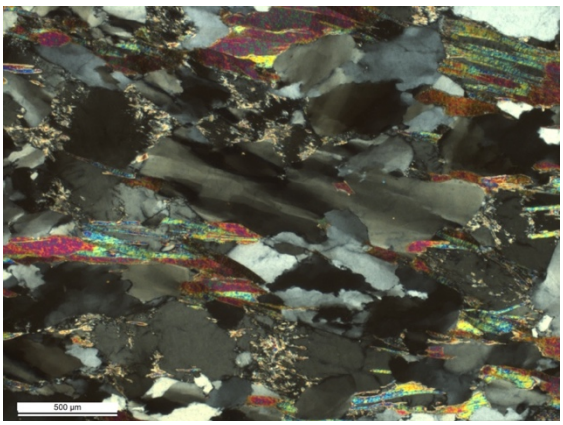


Image 101



Image 102

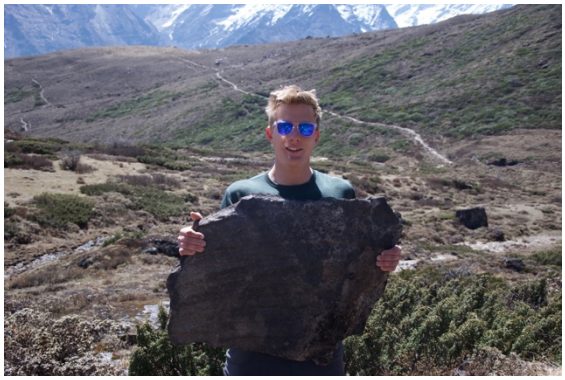


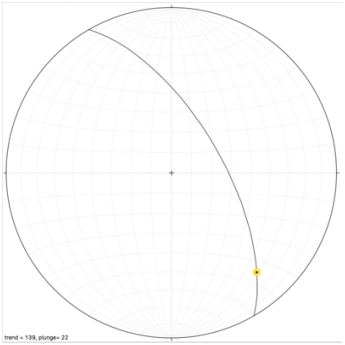
Image 103

Lineation orientation: top right

Sample:	**18N 8a**	Map label: 29	Foliation: 330,65
Location:	1st sample walking from Hotel to Toktok		Rake: 24 SE
			Lineation: 22,139
GPS:	27.776480/86.709542		
Notes:	Overturned sample		

Thin Section Description:

Rock Type:	Biotite gneiss
Mineralogy:	Quartz, biotite, muscovite, orthoclase, albite
Microstructure:	Mostly equigranular texture with some larger orthoclase porphyroblasts, some feldspars show exsolution lamellae
Shear Sense:	No fabric asymmetries visible
LPO:	No distinguishable LPO
Qtz. grains:	Subgrain rotation recrystallization (Image 105), as well as high temperature grain boundary migration recrystallization (Image 106), quartz shows undulose extinction, subgrains exhibiting polygonal texture, however, there are also some completely recrystallized grains



Type of Lineation:
Ductile stretching lineation

Sense of Shear:
N./A.

Metamorphic grade:
Sillimanite grade, SGR and GBM recrystallization

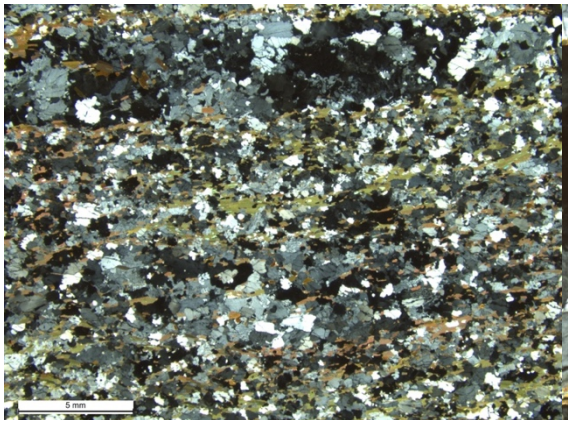


Image 104

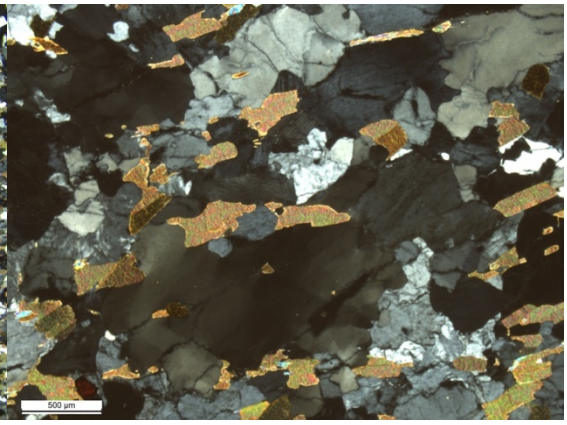


Image 105

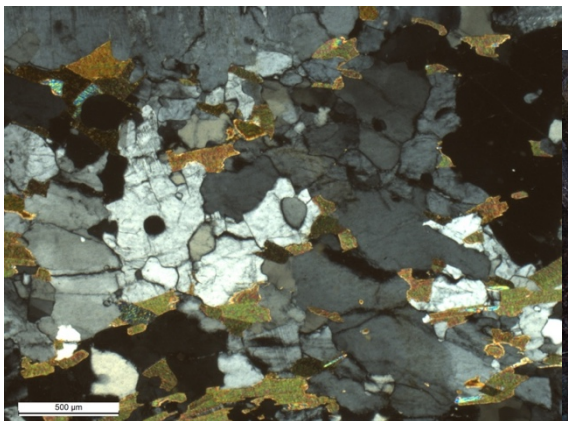


Image 106



Image 107



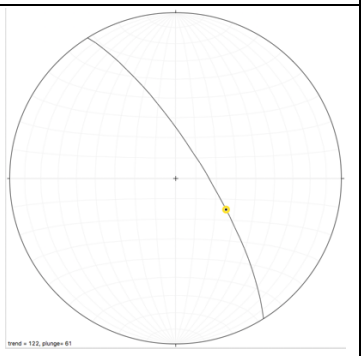
Image 108

Lineation orientation: top right

Sample:	**18N 8f**	Map label: 30	Foliation: 328,76
Location:	2nd sample walking from Hotel to Toktok		Rake: 64 SE
			Lineation: 61,122
GPS:	27.767844/86.708366		
Notes:	brittle fault surface that stretched foliation from flat to vertical, brittle slickenlines show normal sense of shear, foliation otherwise is 008,15		

Thin Section Description:

Rock Type:	Quartzofeldspathic gneiss
Mineralogy:	Quartz, biotite, muscovite, orthoclase, albite, sillimanite
Microstructure:	Inequigranular texture, larger orthoclase porphyroblasts surrounded by finer grained quartz, mica, sillimanite matrix that is organized along thin bands, apparent strain variation, highly deformed and sheared fabric, mylonitic texture, some feldspars show exsolution lamellae
Shear Sense:	Mica fish (Image 110 and 111), orientation of shear bands (Image 109), suggests normal right-lateral sense of shear with very strong confidence
LPO:	Very strong quartz LPO
Qtz. grains:	High temperature grain boundary migration recrystallization (Image 112), quartz grains are completely recrystallized, no deformation lamellae or undulose extinction visible, grains have lobate and straight grain boundaries



Type of Lineation:
Ductile stretching lineation

Sense of Shear:
Normal right-lateral

Metamorphic grade:
Sillimanite grade, GBM recrystallization

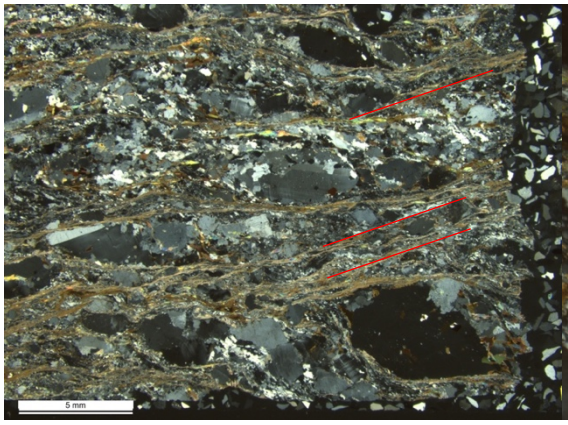


Image 109

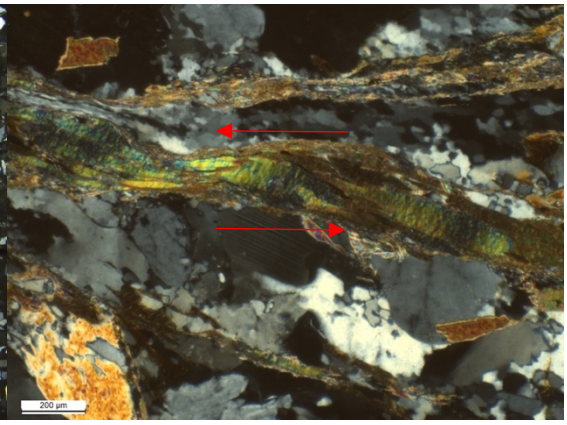


Image 110

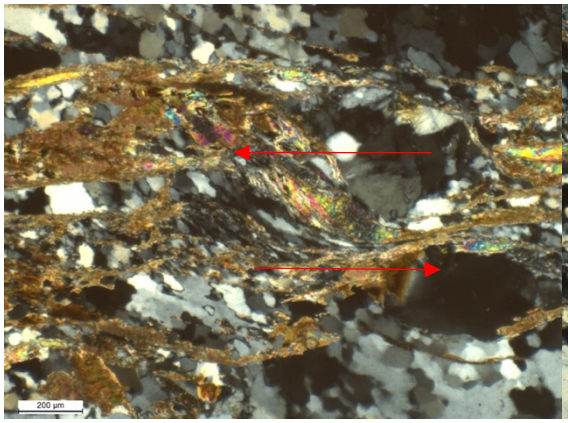


Image 111

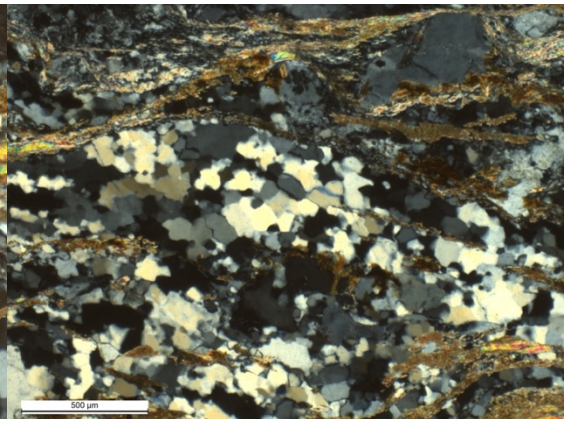


Image 112



Image 113



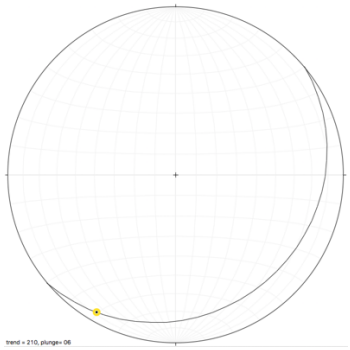
Image 114

Lineation orientation: top right

Sample:	**18N 10a**	Map label: 31	Foliation: 050,18
Location:	Namche to Phortse trail		Rake: 21SW
GPS:	27.826559/86.731789		Lineation: 06,210
Notes:	Beautiful steps and lineation visible suggesting normal right-lateral sense of shear		

Thin Section Description:

Rock Type:	Quartzofeldspathic gneiss
Mineralogy:	Quartz, biotite, muscovite, orthoclase, sillimanite, garnet
Microstructure:	Inequigranular texture, larger orthoclase porphyroblasts surrounded by finer grained mica and sillimanite matrix that is organized along thin bands, apparent strain variation, highly deformed and sheared fabric, highly fractured and replaced garnets (Image 116)
Shear Sense:	Delta clasts (Image 117) and overall orientation of sillimanite bands (Image 118) suggests normal right-lateral sense of shear with strong confidence
LPO:	Weak quartz LPO, due to the scattered appearance of quartz
Qtz. grains:	Subgrain rotation recrystallization (Image 119), as well as high temperature grain boundary migration recrystallization (Image 119), quartz shows undulose extinction, subgrains exhibiting polygonal texture, however, there are also some completely recrystallized grains, evidence for strain variation



Type of Lineation:
Brittle slickenlines and ductile mineral stretching lineation

Sense of Shear:
Normal right-lateral

Metamorphic grade:
Sillimanite grade, SGR and GBM recrystallization

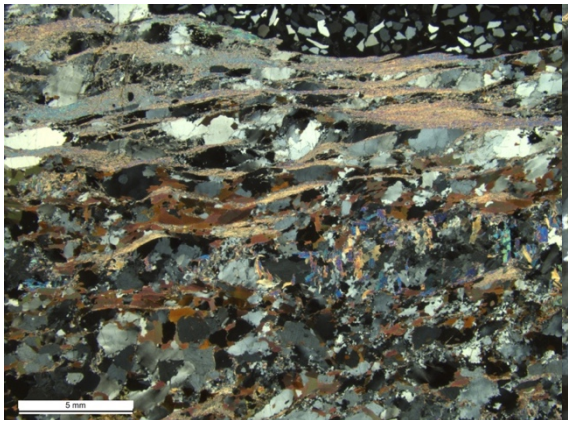


Image 115

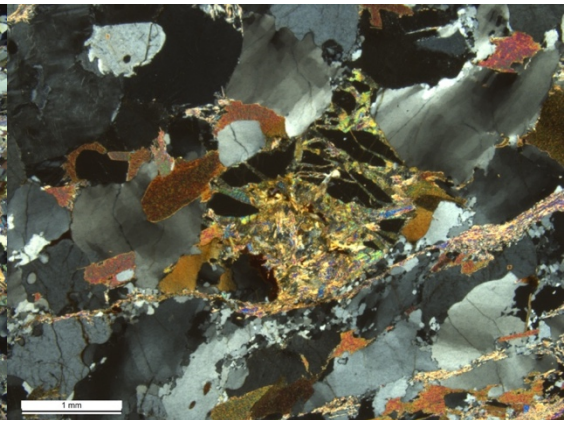


Image 116

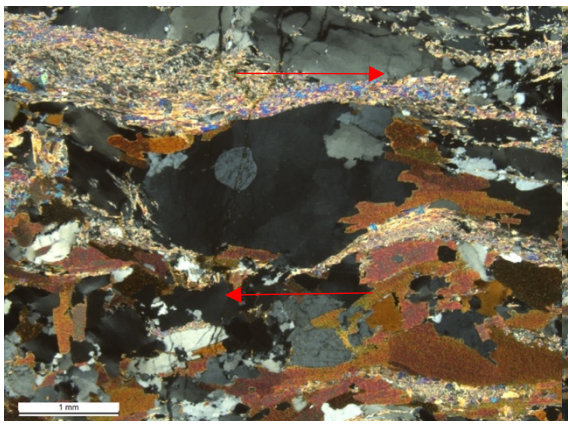


Image 117

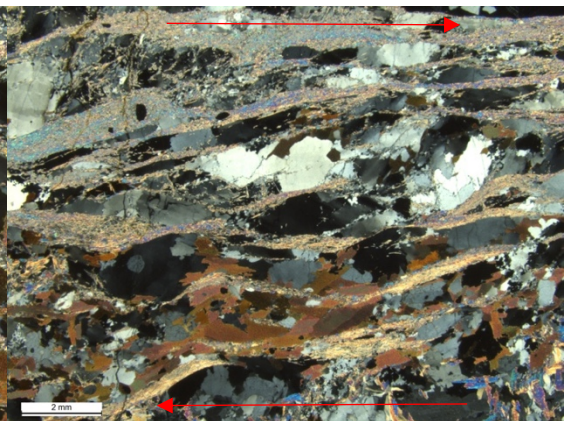


Image 118

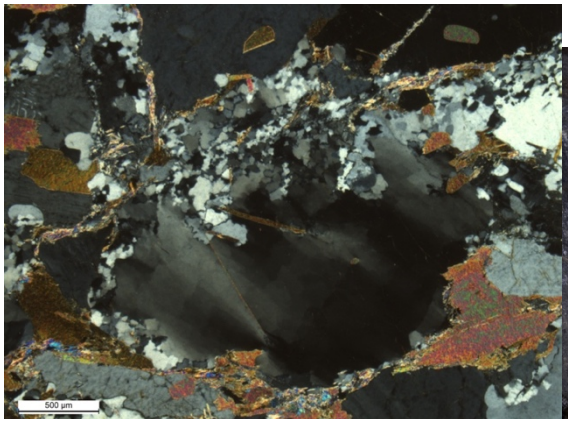


Image 119



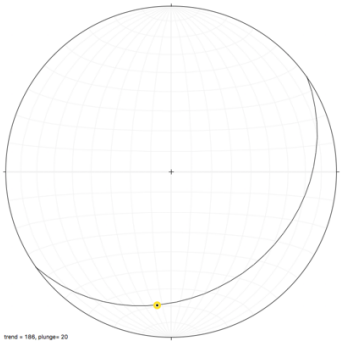
Image 120

Lineation orientation: top left

Sample:	**18N 11e**	Map label: 32	Orientation: 055,26
Location:	Phortse trail towards Pheriche		Foliation: 027,50
GPS:	27.853078/86.781540		Rake: 52SW
Notes:	Shows beautiful mineral stretching lineation indicating right-lateral sense of shear		Lineation: 20,186

<u>Thin Section Description:</u>

Rock Type:	Biotite gneiss
Mineralogy:	Quartz, biotite, muscovite, orthoclase, sillimanite, garnet, hornblende (Image 123), albite
Microstructure:	Inequigranular texture, larger orthoclase porphyroblasts surrounded by finer grained mica and quartz matrix, apparent strain variation
Shear Sense:	Orientation of mica fish (Image 122) suggests normal right-lateral sense of shear with medium confidence
LPO:	Weak to no quartz LPO
Qtz. grains:	Subgrain rotation recrystallization (Image 124), quartz shows undulose extinction, subgrains exhibiting polygonal texture



<u>Type of Lineation:</u>
Ductile stretching lineation

<u>Sense of Shear:</u>
Normal right-lateral

<u>Metamorphic grade:</u>
Sillimanite grade, SGR recrystallization

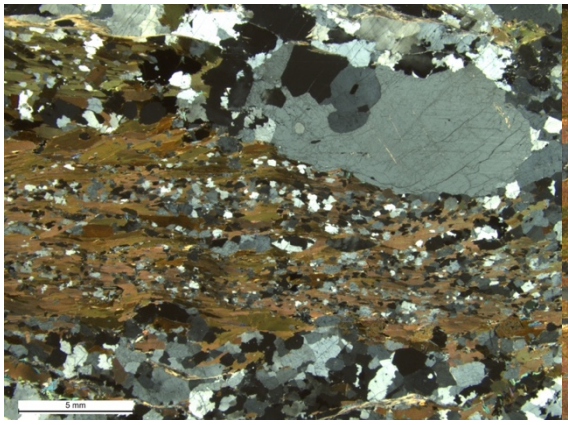


Image 121

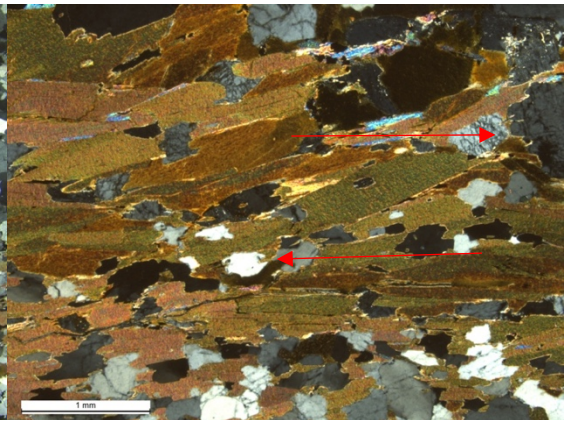


Image 122

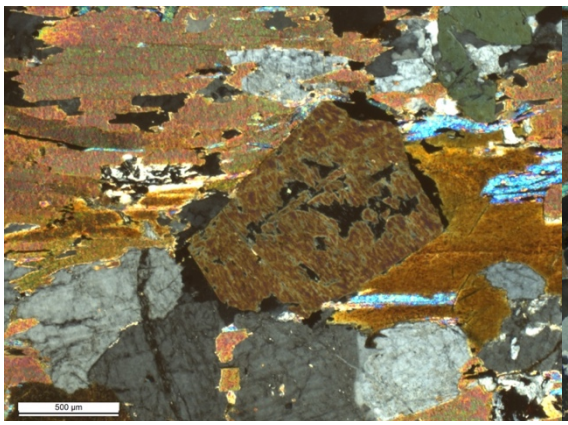


Image 123

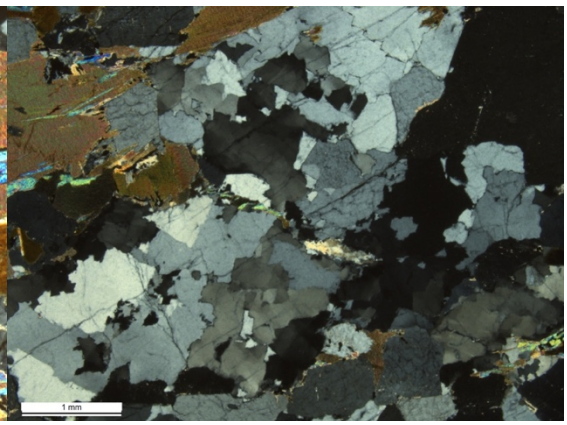


Image 124



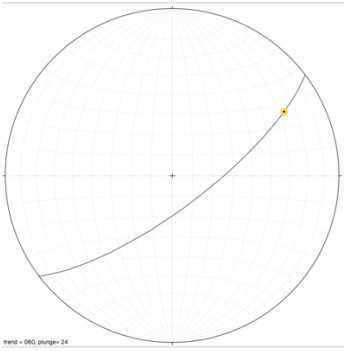
Image 125

Lineation orientation: top left

Sample:	**18N 11h**	Map label: 33	Foliation: 053,74
Location:	Opposite of Pheriche, across the river		Rake: 25 NE
GPS:	27.890971/86.816150		Lineation: 24,060
Notes:	Biotite gneiss with sillimanite clots		

Thin Section Description:

Rock Type:	Biotite gneiss
Mineralogy:	Quartz, biotite, muscovite, orthoclase, albite, sillimanite
Microstructure:	Inequigranular texture, larger sillimanite clots surrounded by mica, quartz, and orthoclase matrix
Shear Sense:	micas show no fish structures and sillimanite clots are very symmetrical (Image 127), sense of shear is indistinguishable
LPO:	Quartz shows LPO
Qtz. grains:	High temperature grain boundary migration recrystallization (Image 128), quartz grains are completely recrystallized, no deformation lamellae or undulose extinction visible, grains have lobate and straight grain boundaries



Type of Lineation:
Ductile stretching lineation

Sense of Shear:
N./A.

Metamorphic grade:
Sillimanite grade, SGR recrystallization

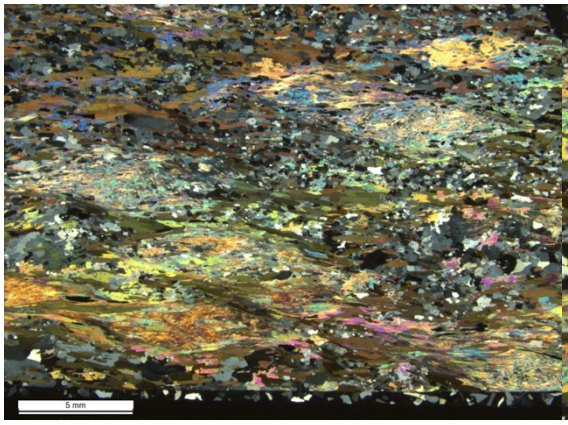


Image 126

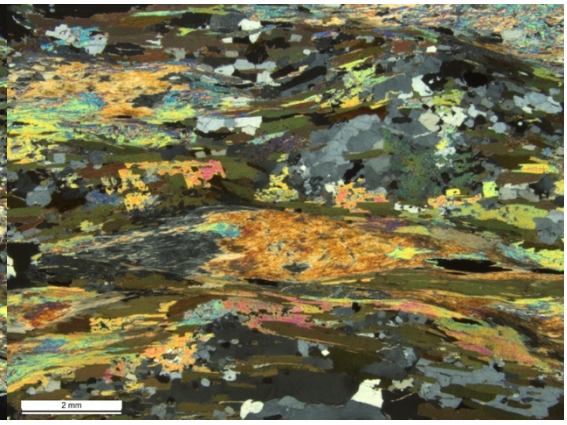


Image 127

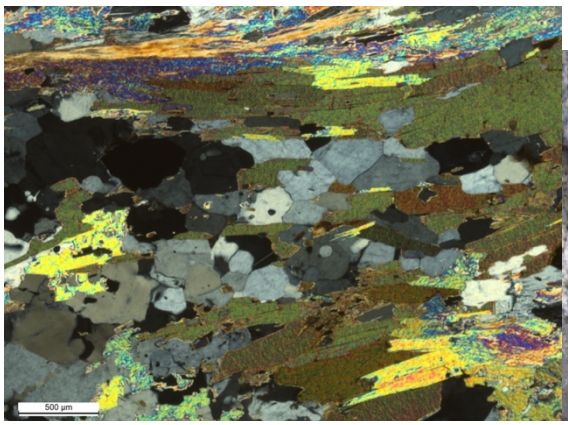


Image 128



Image 129



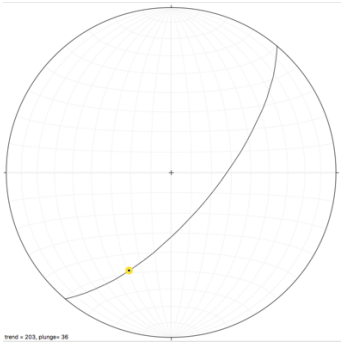
Image 130

Lineation orientation: top right

Sample:	**18N 12a**	Map label: 34	Foliation: 040,68
Location:	2nd sample opposite Pheriche		Rake: 39 SW
GPS:	27.901382/86.807099		Lineation: 36,203
Notes:	Notch has not been preserved during thin section making, however, orientation on sample is correct		

Thin Section Description:

Rock Type:	Biotite gneiss
Mineralogy:	Quartz, biotite, muscovite, orthoclase, albite, sillimanite, chlorite (Image 132)
Microstructure:	Inequigranular texture, orthoclase porphyroblasts surrounded by mica and quartz matrix, distinct bands of chlorite and sillimanite, in spots sillimanite is replacing orthoclase (Image 133)
Shear Sense:	No fabric asymmetries visible
LPO:	No distinguishable quartz LPO
Qtz. grains:	High temperature grain boundary migration recrystallization (Image 134), quartz grains are completely recrystallized, no deformation lamellae or undulose extinction visible, grains have lobate and straight grain boundaries



Type of Lineation:
Ductile stretching lineation

Sense of Shear:
N./A.

Metamorphic grade:
Sillimanite grade, SGR recrystallization

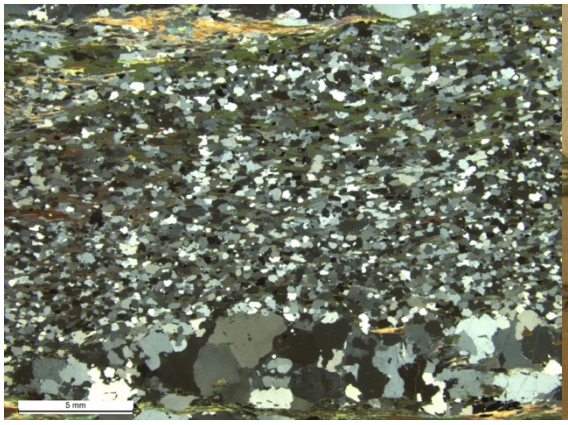


Image 131

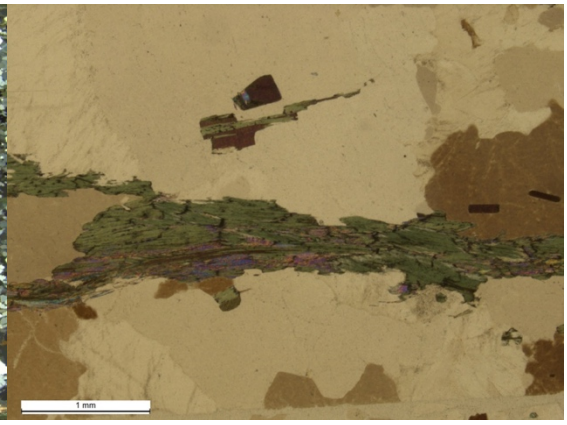


Image 132 (plane polarized light)

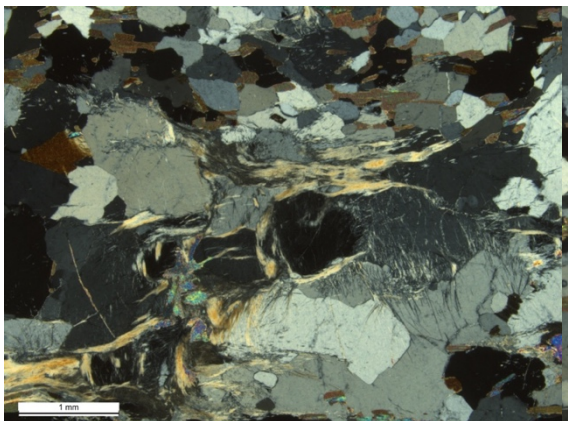


Image 133

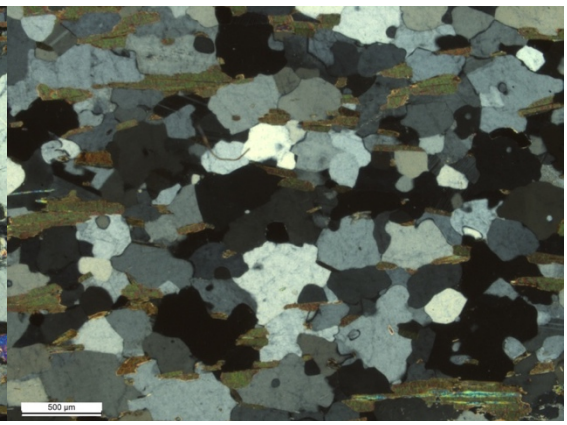


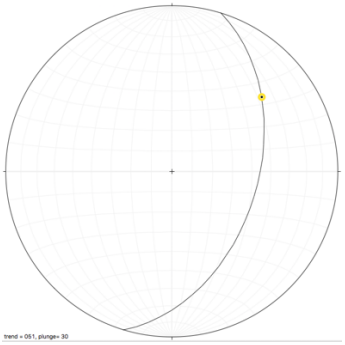
Image 134

Lineation orientation: top right

Sample:	**18N 13a**	Map label:	35	Foliation:	017,47
Location:	Top of Kala Pathar			Rake:	44 NE
GPS:	27.994638/86.828330			Lineation:	30,051
Notes:	Augen gneiss in outcrop				

Thin Section Description:

Rock Type:	Quartzofeldspathic gneiss
Mineralogy:	Quartz, biotite, muscovite, orthoclase, albite
Microstructure:	Mostly equigranular texture, minerals weakly aligned along foliation, some feldspars show exsolution lamellae
Shear Sense:	No fabric asymmetries visible
LPO:	No distinguishable quartz LPO
Qtz. grains:	High temperature grain boundary migration recrystallization (Image 135), quartz grains are completely recrystallized, no deformation lamellae or undulose extinction visible, grains have lobate and straight grain boundaries



Type of Lineation:
Ductile stretching lineation

Sense of Shear:
N./A.

Metamorphic grade:
Sillimanite grade, SGR recrystallization

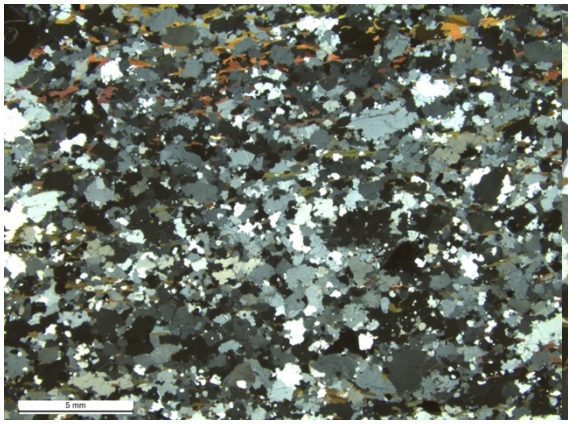


Image 135

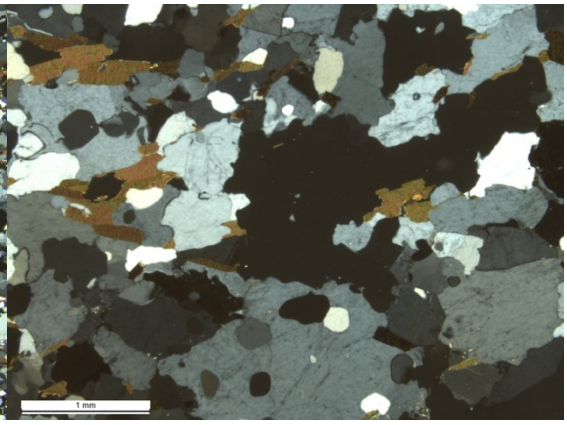


Image 136



Image 137



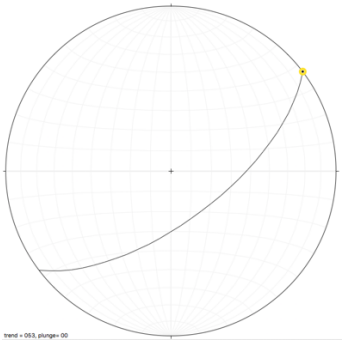
Image 137

Lineation orientation: top left

Sample:	**18N 13b**	Map label: 36	Foliation: 053,65
Location:	NE of Dughla, Lobuche basecamp		Rake: 0
GPS:	27.933871/86.794075		Lineation: 00,053
Notes:	Notch on NE side of strike line		

Thin Section Description:

Rock Type:	Biotite gneiss
Mineralogy:	Quartz, biotite, muscovite, orthoclase, albite, sillimanite
Microstructure:	Mostly equigranular texture, biotite grouped and aligned along foliation, high amount of shear visible
Shear Sense:	Mica fish (Image 139, 140), delta clasts (Image 141) indicate right-lateral sense of shear
LPO:	Weak quartz LPO
Qtz. grains:	Subgrain rotation recrystallization (Image 142), as well as high temperature grain boundary migration recrystallization (Image 143), quartz shows undulose extinction, subgrains exhibiting polygonal texture, however, there are also some completely recrystallized grains



Type of Lineation:
Ductile stretching lineation

Sense of Shear:
Right-lateral

Metamorphic grade:
Sillimanite grade, SGR and GBM recrystallization

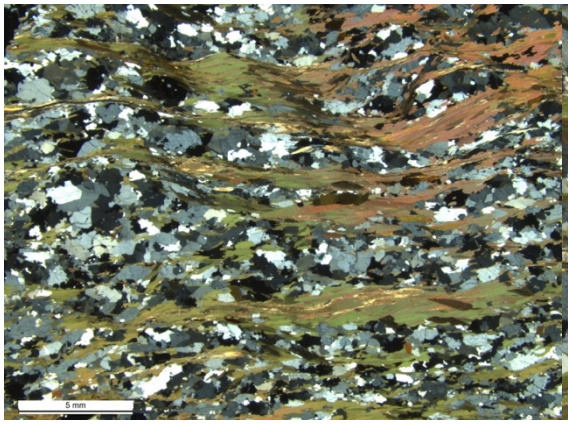


Image 138

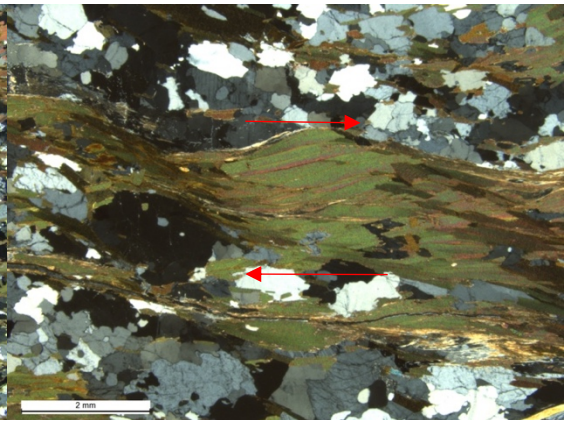


Image 139

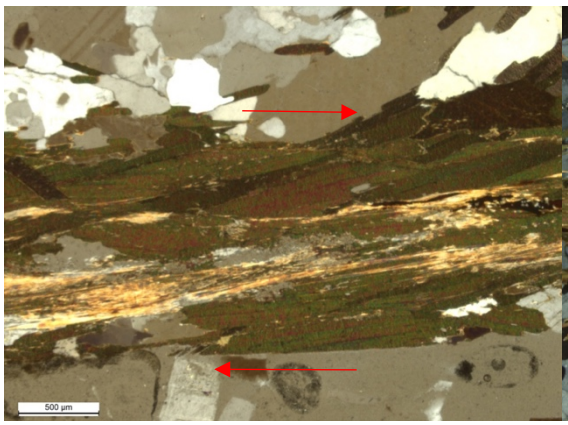


Image 140

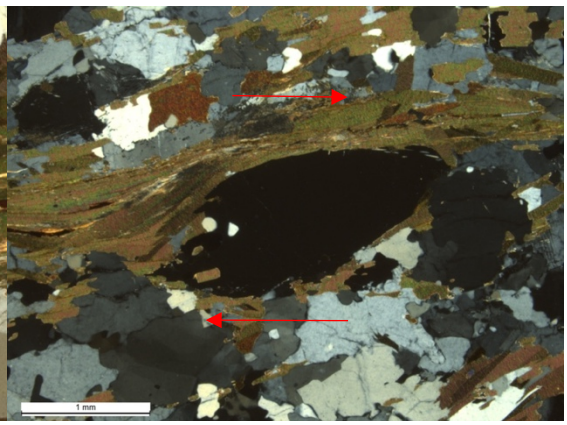


Image 141

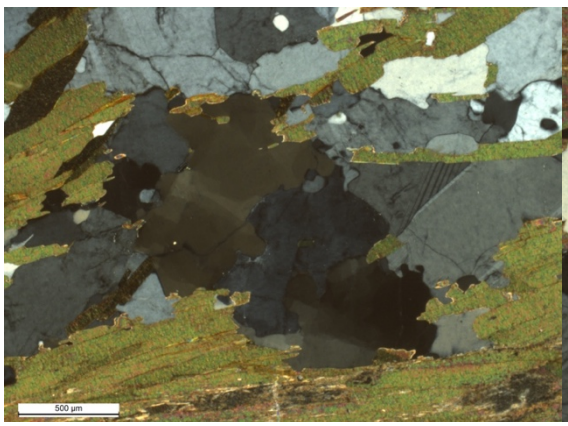


Image 142

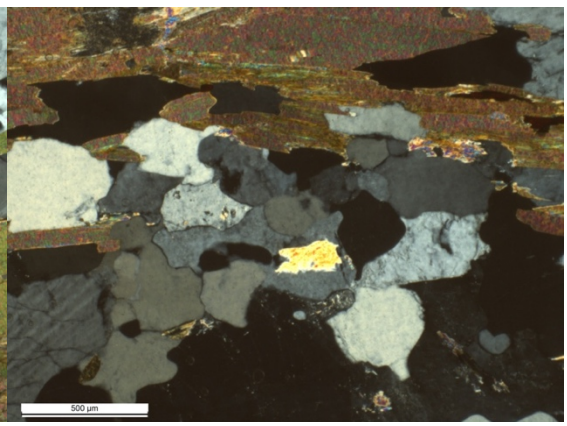


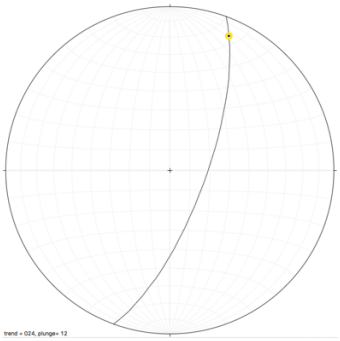
Image 143

Lineation orientation: top left

Sample:	**18N 14a**	Map label:	37	Foliation:	020,72
Location:	1st sample Chola pass			Rake:	12 NE
GPS:	27.952359/86.765226			Lineation:	12,024
Notes:					

Thin Section Description:

Rock Type:	Biotite gneiss
Mineralogy:	Quartz, biotite, orthoclase, albite, sillimanite, chlorite
Microstructure:	Mostly equigranular texture, biotite organized along one thicker band, sillimanite replaced orthoclase (Image 145)
Shear Sense:	No fabric asymmetries visible
LPO:	No distinguishable quartz LPO
Qtz. grains:	High temperature grain boundary migration recrystallization (Image 146), quartz grains are completely recrystallized, no deformation lamellae or undulose extinction visible, grains have lobate and straight grain boundaries



Type of Lineation:
Ductile stretching lineation

Sense of Shear:
N./A.

Metamorphic grade:
Sillimanite grade, GBM recrystallization

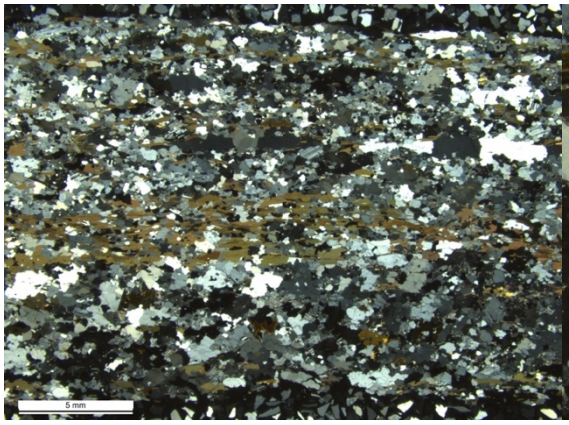


Image 144

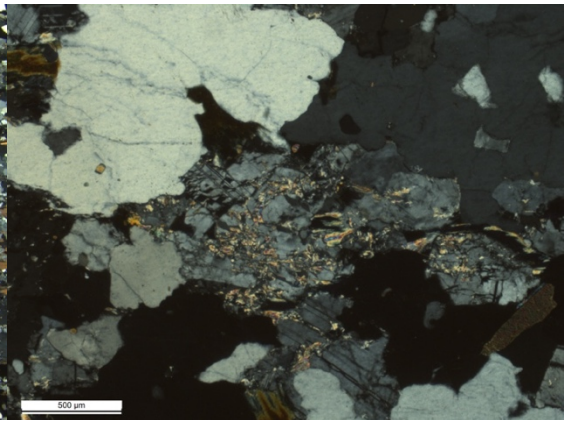


Image 145

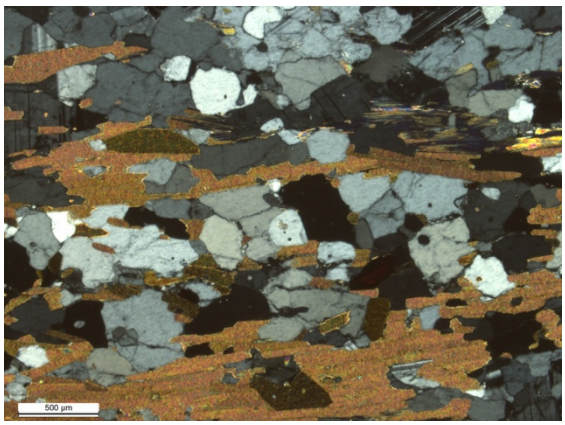


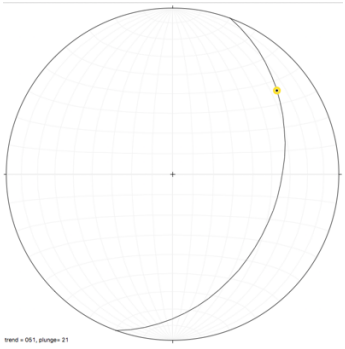
Image 146

Lineation orientation: top right

Sample:	**18N 14c**	Map label: 38	Foliation: 020,36
Location:	2nd sample Chola pass		Rake: 37 NE
GPS:	27.958424/86.758810		Lineation: 21,051
Notes:	Biotite gneiss with sillimanite clots		

Thin Section Description:

Rock Type:	Biotite gneiss
Mineralogy:	Quartz, biotite, orthoclase, sillimanite
Microstructure:	Mostly equigranular texture, sillimanite organized in clots surrounded by a biotite, quartz, orthoclase matrix
Shear Sense:	No fabric asymmetries visible, sillimanite clots are symmetrical, biotite shows no shear
LPO:	No distinguishable quartz LPO
Qtz. grains:	High temperature grain boundary migration recrystallization (Image 148), quartz grains are completely recrystallized, no deformation lamellae or undulose extinction visible, grains have lobate and straight grain boundaries



Type of Lineation:
Ductile stretching lineation

Sense of Shear:
N./A.

Metamorphic grade:
Sillimanite grade, GBM recrystallization

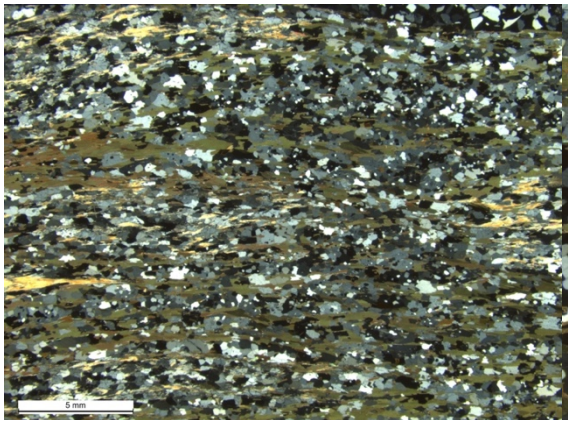


Image 147

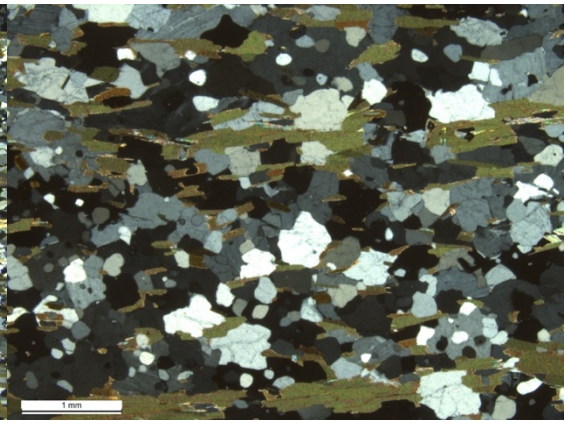


Image 148



Image 149

Lineation orientation: top right